AN INTERDISCIPLINARY GEOLOGICAL AND GEOMORPHIC CHARACTERIZATION AND LANDSLIDE INVESTIGATION IN RED BUTTE CANYON, UTAH

by

James William Schloss

A thesis submitted to the faculty of
The University of Utah
in partial fulfillment of the requirements for the degree of

Master of Science

in

Geological Engineering

Department of Geology and Geophysics

The University of Utah

August 2013

The University of Utah Graduate School

STATEMENT OF THESIS APPROVAL

The thesis of **James William Schloss**

has been approved by the following supervisory committee members:

Paul W. Jewell	, Chair	**3/19/2013** Date Approved
Aurelian C. Trandafir	, Member	**3/13/2013** Date Approved
D. Kip Solomon	, Member	**3/19/2013** Date Approved

and by **D. Kip Solomon** , Chair of

the Department of **Geology and Geophysics**

and by Donna M. White, Interim Dean of The Graduate School.

ABSTRACT

Red Butte Canyon is a federally protected research area located outside Salt Lake City, Utah east of the University of Utah. The Wasatch Fault Zone, an active fault capable of producing magnitude 7.0 earthquakes, is also located less than one mile west of Red Butte Canyon. A series of geomorphic features exist in Red Butte Canyon including landslides, rock falls, creep, and steep slopes within both the primary Red Butte Creek channel and the secondary Parleys Fork channel. Possible paleochannels exist adjacent to a mapped landslide at Red Butte Creek and Parleys Fork. A detailed geologic and engineering investigation was executed to address these unusual geomorphic features. Research objectives included detailed geologic mapping in the study area to better evaluate geologic characteristics and determine the characteristics of subsurface sediments. Additional objectives included performing a groundwater and slope stability evaluation within selected areas of the study area. Methods included drilling and sampling, seismic refraction, groundwater measurements, geotechnical engineering testing, slope stability modeling, and radiocarbon dating to evaluate the geological and geotechnical characteristics of geomorphic features. A combination of sediment type, grain size distributions of soils and radiocarbon dating suggest that subsurface sediments closest to the landslide area formed in an alluvial / lacustrine depositional environment suggesting a lake existed in Red Butte Canyon behind a landslide dam at some point in the past. Charcoal samples discovered in the subsurface yielded radiocarbon ages of

4,370 ± 30 years, in close agreement with independent paleoseismology studies for on the Wasatch Fault dated 4,000 ± 500 years ago, suggesting the lacustrine sediments formed in response to the earthquake and landslide.

Slope stability analysis investigated undrained and drained conditions and utilized the Pseudostatic Method. The results show that selected slopes within the field site were stable under drained conditions except when a high groundwater table exists. Slopes were also less stable under drained conditions, particularly when a peak horizontal ground acceleration exceeded $0.1\ g - 0.15\ g$. The reduced stability of slopes under seismic loading conditions also suggests that the landslide was triggered by an earthquake in the aforementioned time frame.

TABLE OF CONTENTS

LIST OF FIGURES

LIST OF TABLES

ACKNOWLEDGEMENTS

This interdisciplinary thesis project could not have been completed without the support and assistance from a great many people. My thanks and gratitude cannot be emphasized enough to all of the people who helped me with this project would like to first thank my supervisory committee for their support and guidance. Thanks to Dr. Kip Solomon for having a conceptual project in mind, and one that was conveniently located in our school's own back yard, Red Butte Canyon. Thanks to Dr. Aurel Trandafir for providing guidance on Geotechnical Engineering testing and analysis even after he moved to Houston, TX. A special thanks to my adviser Dr. Paul Jewell for providing financial support and guidance throughout the project, and having an open door policy to ask questions or talk in general whenever I needed to.

Tremendous thanks to our geophysics department! I want to thank Dr. Mike Thorne for coming with me in the field and making recommendations on acquiring shallow seismic data appropriate for the site conditions. A special thanks to Paul Gettings for showing me how to use our department's seismograph and writing code to extract and process my seismic data. I'd also like to thank Mason Edwards and Kevin Kwon for helping acquire the seismic data in the field. Lastly, a tremendous thanks to my friend Oner Sufri who volunteered to help me with every aspect of the seismic work including acquiring data, processing the data, and helping to analyze the data as he worked on his Ph.D.

I also need to thank my friends, fiancée, my uncle, Dr. Gerry Kuecher, and my brother, John. John Boswell and Becky Holingshaus worked patiently with me and collected cone penetrometer data on some cold November days in Red Butte Canyon. My fiancée, Beth helped me with field work on several occasions as well! Thanks to my uncle for the advice on the geological characterization and editing. Monumental thanks to my brother John for helping with field work and drilling. John stayed with me for an entire month in Salt Lake City as he finished a temporary job in the Uinta Basin and searched for a career job in fall 2011. He was my personal field assistant. I could never have done this without him!

I'd also like to thank Quintin Sahratian, Dan Seeley, and two of my students. Quintin helped me gather lab equipment for the specific gravity tests and grain size distribution tests and was always helpful as he was bombarded with his own work and other students requesting lab assistance. A special thanks to Dan Seeley for guidance on geotechnical engineering lab testing. I also want to thank Eric Thomas and Chris Tingey for helping me with the Geotechnical Engineering lab testing among their very busy schedules as I was their T.A. for Structural Geology.

I would also like to thank all of the drillers I worked with in the past as a geotechnical engineer and exploration geologist. I learned about the principles and mechanics of drilling by working side by side with them and with drilling rigs. I was only able to successfully hand drill and collect samples through what I observed and learned from them in the field.

CHAPTER 1

INTRODUCTION

Overview of Project Area

Red Butte Canyon is a federally protected research area and pristine watershed isolated from human development located outside of Salt Lake City, UT directly east of the University of Utah. Red Butte Canyon has a unique and long human history. Red Butte Canyon acted as the watershed for U.S. Army Post Fort Douglas built in 1862 and was also mined for red sandstone used as some of the construction materials of the original Salt Lake City (Ehleringer, 2009). The canyon was closed entirely to the public in 1969 when the USDA Forest Service designated Red Butte Canyon as Research Natural Area (RNA), setting aside the site for significant ecological research to follow (Ehleringer et al., 1992). The goals of RNAs are: 1) to protect the RNAs as examples of baseline undisturbed ecosystems and 2) to study their ecological component parts, including terrestrial and aquatic ecosystems.

A large volume of ecological and biological research occurred after the canyon was classified as an RNA and continues today as Red Butte Canyon has been designated as a National Ecological Observatory Network (NEON) Site. Today, as part of NEON its goals are understanding and forecasting the impacts of climate change, land-use change and invasive species on continental-scale ecology by providing infrastructure and

consistent methodologies to support research and education in these areas (Neon.org, 2012). Most previous research in Red Butte Canyon has focused on biological, ecological, and hydrological systems. The hydrological studies that have taken place in Red Butte Canyon have provided important results supporting the RNA objectives, but there are remaining mysteries about the hydrological systems. One of the goals of this study is to address the underlying geological systems of the site as well as the geomorphic evolution of the canyon and how these may play a part in the overall hydrological system as well as to follow the goals of both the National Ecological Observatory Network and Research Natural Area by complementing previous hydrological research.

Although the overall geology for Red Butte Canyon is well understood, it is incomplete (Crittenden & Van Horn, 1987). Most previous research in Red Butte Canyon is related to biological and ecological relationships and has not focused on geology or geomorphology. Research directed by Dr. Kip Solomon focusing on hydrological systems has led to further questions on understanding groundwater flow toward Red Butte Creek with Hill (2006) and groundwater flow through the hyphoreic zone of Red Butte Creek as described by studies with Stolpe (2011) and Hollingshaus (2012). Questions addressed in this research may lead to understanding the slope stability and perhaps the climate as well.

Research Objectives

A detailed site investigation took place within Red Butte Canyon from summer 2011 – summer 2012. The site is outlined on Figure 1.1 and described in greater detail in

the next section. The motivation for this study was addressing unusual geological and geomorphic features within this study area, in particular, the peculiar features associated with a known landslide at the intersection of Red Butte Canyon and Parleys Fork. In addition, there are several steep slopes that abruptly rise within an otherwise flat stream bed that defines Parleys Fork.

The research objectives of this study are two-fold. The first is to perform more detailed geologic mapping in order to evaluate unusual geologic and geomorphic characteristics within the study area and determine the nature of the related sediments and how they may have formed. The second objective is to characterize the behavior of groundwater in the study area and determine whether or not sloped features and hill slopes within the study area are stable or not, and what sort of geological or other climatic mechanisms could cause these features to lose stability and fail.

Red Butte Canyon

Topography

Figure 1.1 shows a Digital Elevation Model (D.E.M.) of Red Butte Canyon and dramatic elevation change from 4665 ft. to 8335 ft. between its highest and lowest points as well dramatic changes in slope from a gently sloped valley floor of approximately 1° to hill slopes ranging between 10° to 80°.

Hydrologic characteristics and climate

Red Butte Canyon is one of several canyons on the Wasatch Front. Geographic Information System (*G*.I.S.) analysis shows that the drainage area is 22.7 km^2 (5609

Acres) (Figure 1.1), which is in agreement with existing literature (Ehleringer et al., 1992). The average precipitation varies in the canyon as a function of elevation. Most precipitation is in the form of snow in the winter and spring that ranges from 50 cm/year at lower elevations to 90 cm/year at higher elevations (Erhelinger et al., 1992). Average discharge rates of Red Butte Creek vary with base flow of 0.058 m^3/s in September and a maximum of 0.416 m^3/s in May (Ehleringer, 2009). Temperature varies with elevation but the canyon sees an annual average low in of -2°C and an annual average high of 23°C (Utah Field Stations, 2009).

Geology

Geologic Units

The underlying geology of Red Butte Canyon is a package of carbonate and clastic rocks spanning the Pennsylvanian Period, approximately 360 Ma, to the Middle Jurassic Period, approximately 161 Ma (Crittenden & Van Horn, 1987). Erosive forces have led to the formation of flood plain deposits, landslides, debris flows, and soils within the stream channels and hill slopes of Red Butte Canyon, which are a result of the uplift of Wasatch Fault beginning in the Miocene (Figures 1.2 –1.3). (Crittenden & Van Horn, 1987).

From south to north in the canyon the geologic units go from stratigraphically youngest to oldest. The geologic formations are Twin Creek Formation (Middle Jurassic), Nugget Sandstone (Jurassic/Triassic), Ankareh Formation (Triassic), Thaynes Formation (Lower Triassic), Woodside Shale Formation (Lower Triassic), Park City Formation (Permian), and Weber Quartzite Formation (Pennsylvanian) (Crittenden & Van Horn, 1987). Only the Twin Creek Limestone, Nugget Sandstone, Ankareh

Formation, and Thaynes Formation are within the field site for this project. A stratigraphic column with a brief description of the geologic units summarizes the geologic formations within Red Butte Canyon (Table1.1).

Faults and Folds

A series of normal faults are found in the study area. The Wasatch Fault, an extensive and active normal fault running parallel to the Wasatch Mountains, lies within close proximity of Red Butte Canyon. Specifically, the East Bench Fault of the Wasatch Fault is 0.9 miles southwest of Red Butte Canyon. The faults are particularly identifiable within the Ankareh Formation, Gartra Grit member near the field site because of the unit's resistance to erosion and competence. These faults are not a part of the Wasatch Fault Zone, but are believed to have formed as a consequence of the normal faulting in the Wasatch Fault Zone.

The northern boundary of Red Butte Canyon displays the Black Mountain Thrust Fault that places the older Humbug Formation (Mississippian) adjacent to the younger Weber Quartzite (Pennsylvanian) and cuts out the Round Valley Limestone (Lower Pennsylvanian), Doughnut Formation (Upper Mississippian), and Great Blue Formation (Upper Mississippian) from the stratigraphic sequence (Crittenden & Van Horn, 1987).

The attitude of all geologic formations within Red Butte Canyon is controlled by the structure of a syncline which trends northeast and whose fold axis is located within Emigration Canyon, immediately south of Red Butte Canyon (Crittenden & Van Horn, 1987). These units strike northeast and dip southeast (Figure 1.4).

Seismic Hazards

The Wasatch fault is a large 240 mile long normal fault stretching from Fayette, UT to Malad City, ID and is broken into several fault segments, approximately 25 miles in length each (Utah Geological Survey, 1996: 2). This has been described as one of the longest and most active normal faults in the world (Utah Geological Survey, 1996: 2). The fault formed as a consequence of the interaction between the relatively thin crust of the Basin and Range province to the east juxtaposed against the thicker and more stable crust of the Rocky Mountains and Colorado Plateau to the east (Utah Geological Survey, 1996). The fault dips toward the west under the Salt Lake Valley.

The Wasatch Fault has a history of earthquake activity that has varied by fault segment over at least the past 6,000 years. The Utah Geological Survey has investigated fault scarps along the Wasatch fault and determined the recurrence interval of earthquakes by radiocarbon dating, mostly of charcoal (Utah Geological Survey, 1996: 6). Over the entire fault segment, geologists have determined that an earthquake occurs approximately every 350 years, but the last major earthquake along the Salt Lake City segment occurred approximately 1,200 years ago (Utah Geological Survey, 1996: 6).

Several published reports evaluated the ground shaking and horizontal ground accelerations along the Wasatch fault (Wong et al., 2002; Christenson, 1994). During an earthquake, seismic waves are generated, propagate outward, and oscillate both horizontally and vertically, resulting in ground shaking, typically measured as a function of gravity (Christenson, 1994: 2).

The Utah Geological Survey in conjunction with URS Corporation, Pacific Engineering and Analysis, and the University of Utah Seismograph Stations evaluated

ground shaking along the Wasatch fault (Wong et al., 2002). Red Butte Canyon is subjected to magnitudes of 0.5 *g* – 0.6 *g* peak horizontal acceleration during a magnitude 7.0 earthquake (Figure 1.5).

Geomorphic Characteristics

Several landslide and earth flow deposits are identified within Red Butte Canyon. Multiple Holocene and Pleistocene age landslides and earthflows are mapped on the southern side of the Red Butte Canyon (Crittenden & Van Horn, 1987). The largest of these features is approximately 12 acres in area with an estimated depth of 33 ft., located at the intersection of Red Butte Creek and Parleys Fork (Crittenden & Van Horn, 1987).

In addition, several other landslides have been identified in Red Butte Canyon by other studies through digital mapping techniques such as identification of curvilinear slopes (Elliott et al., 2010). These features have been included in the new geologic map of Red Butte Canyon. Lastly, rockfalls are evident in Red Butte Canyon, particularly on the south canyon walls. Landslides and rockfalls standout where no vegetation exists. Steep slopes are covered with debris and boulders.

Hydrogeology

Hill (2006) evaluated the major ion composition of groundwater in Red Butte Canyon and delineated groundwater flow paths. The work was based on numerous springs and seeps in addition to several wells installed within Red Butte Canyon. His results showed that groundwater flows toward Red Butte Creek from both the north and south.

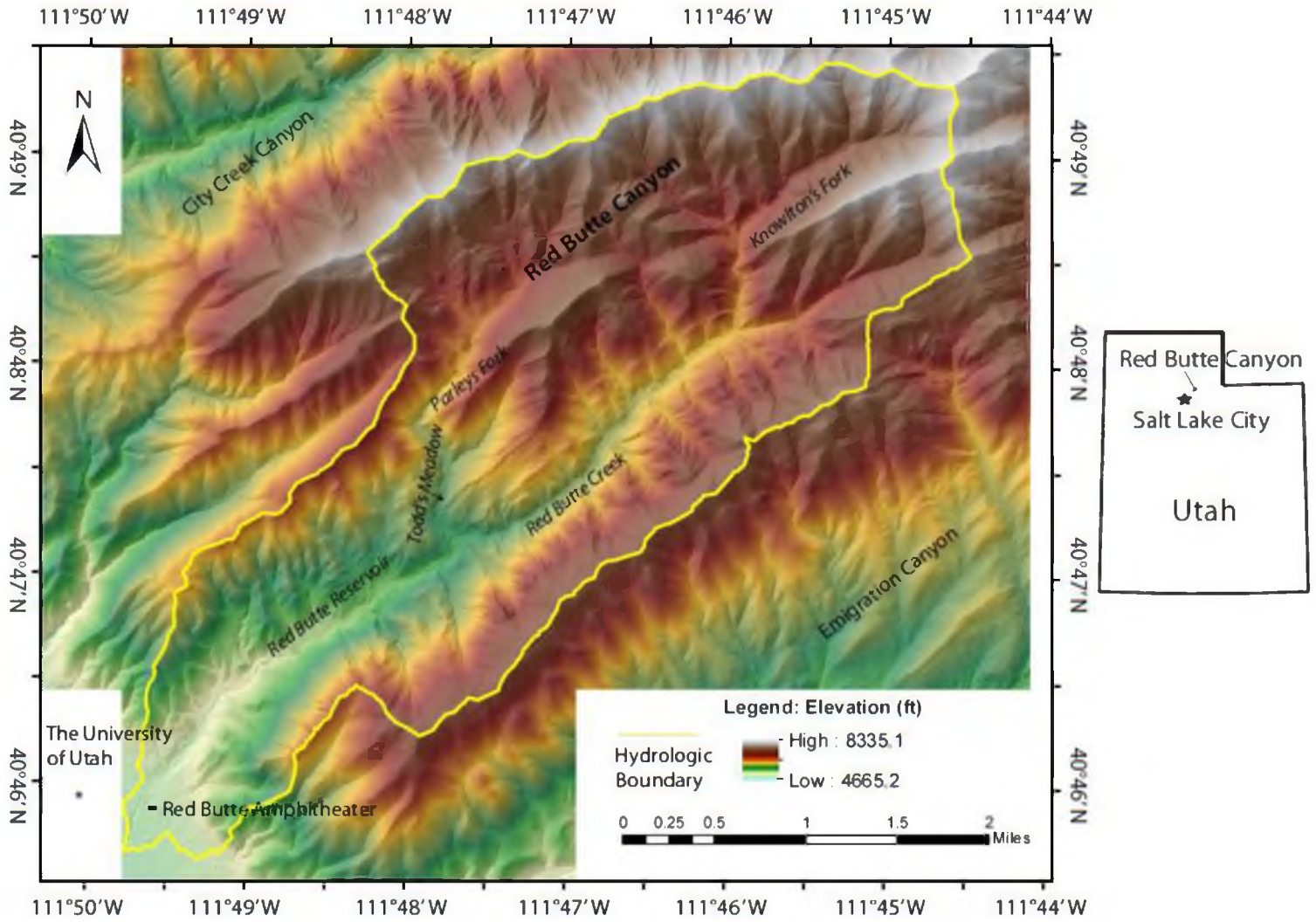

Figure 1.1, Red Butte Canyon, D.E.M. and hydrologic basin boundary

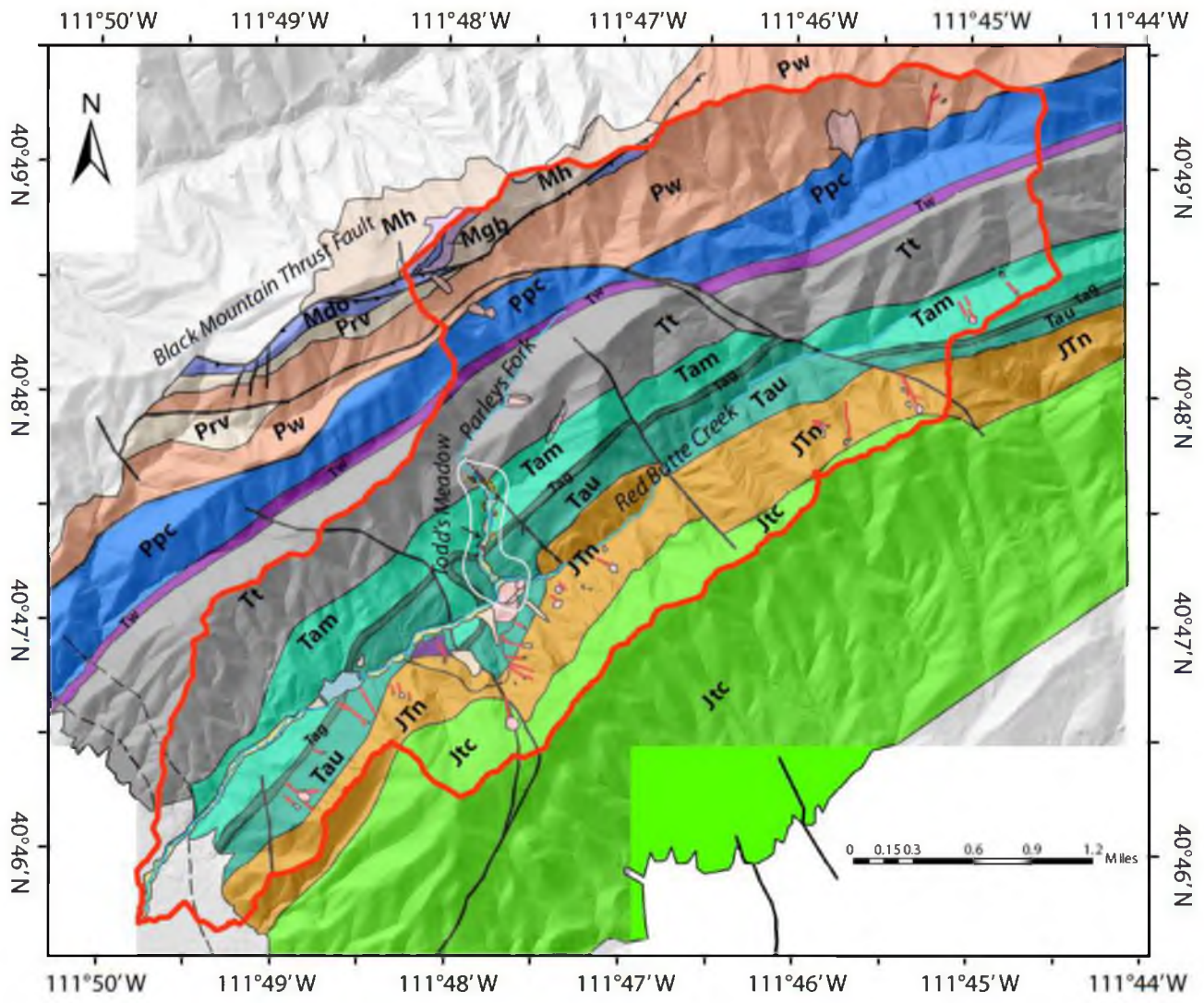

Figure 1.2, Overall geologic map of Red Butte Canyon. (Adapted from Crittenden & Van Horn, 1987)

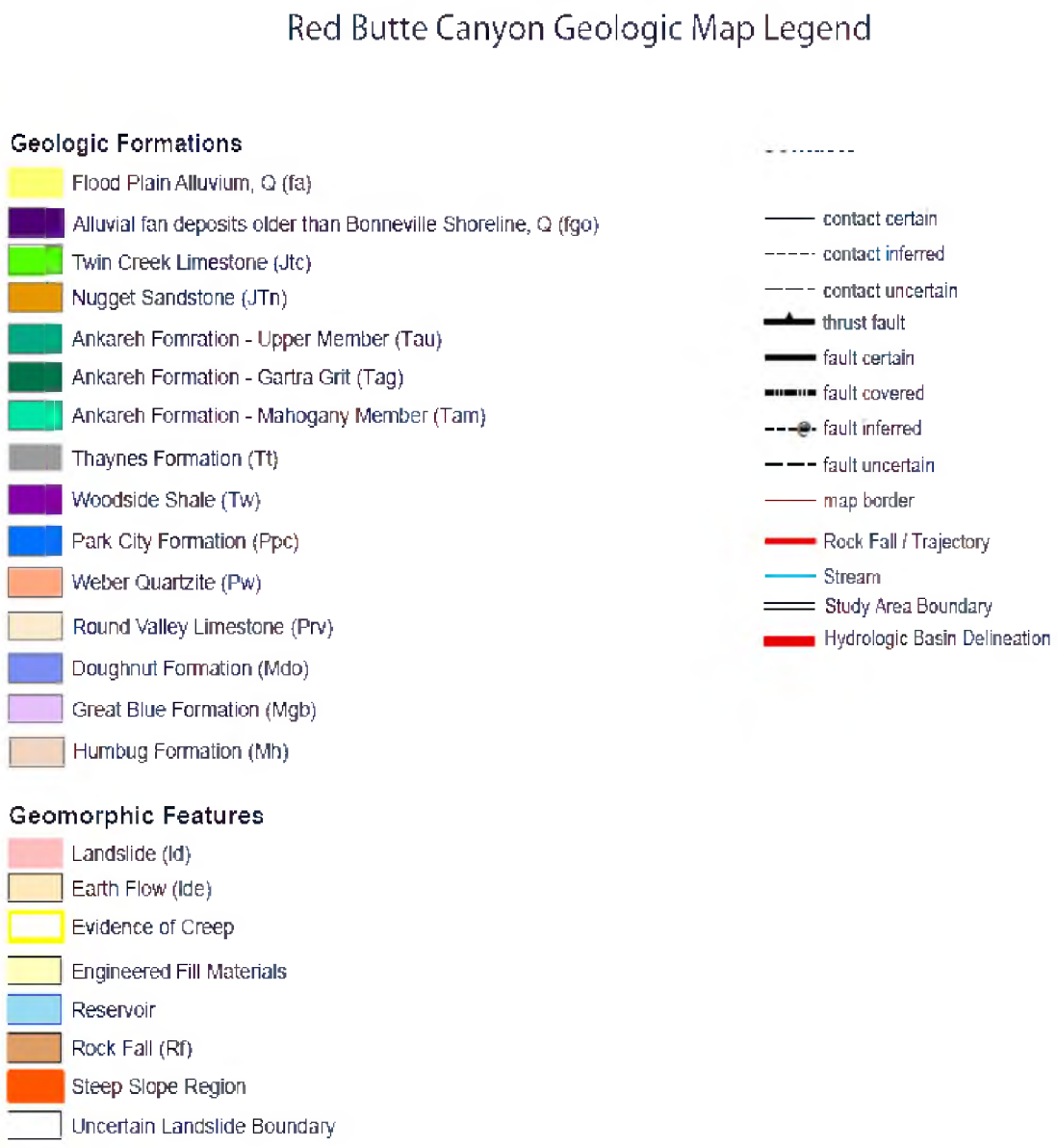

Figure 1.3, Overall Red Butte Canyon geologic map legend

Table 1.1, Geologic units within Red Butte Canyon

Geologic Unit (Abbreviation)	Age	Description
Flood Plain Alluvium (Fa)	Quaternary	Gray to brown sand. Cobbly to silty.
Undifferentiated fan deposits older than Bonneville shoreline (fgo)	Quaternary	Very well developed pre-Alpine formed on alluvial fan deposits
Twin Creek Limestone (Jtc)	Middle Jurassic	Brownish gray and pale gray to pale yellowish gray silty limestone, intercalated with greenish gray shale.
Nugget Sandstone (JTn)	Jurassic? And Triassic?	Pale pinkish buff, fine- to medium-grained, well-sorted sandstone that weathers orange-brown. Massive outcrops form the ridge called Red Butte.
Ankareh Formation, Upper Member (Tau)	Triassic	Reddish brown, reddish purple, grayish red, or bright red shale, siltstone, and sandstone.
Ankareh Formation, Gartra Grit Member (Tag)		White to pale purple, thick-bedded, crossbedded, pebbly quartzite. Forms a prominent white ledge for long distances.
Ankareh Formation, Mahogany Member (Tau)		Reddish brown, reddish purple, grayish red, or bright red shale, siltstone, and sandstone.
Thaynes Formation (Tt)	Lower Triassic	Medium to light gray, fossiliferous, locally nodular limestone, limy siltstone, and sandstone.
Woodside Shale Formation (Tw)	Lower Triassic	Grayish red, grayish purple, or reddish shale and siltstone. Abrupt contact with Thaynes Formation.
Park City Formation (Ppc)	Permian	Fossiliferous sandy limestone, calcareous sandstone, and medial phosphatic shale.
Weber Quartzite Formation (Pw)	Pennsylvanian	Tan to white fine to medium gravel and quartzite.
Round Valley Limestone Formation (Prv)	Lower Pennsylvanian	Pale gray limestone with pale gray siltstone partings.
Doughnut Formation (Mdo)	Upper Mississippian	Thin bedded limestone with black/gray chert and brachiopods.
Doughnut Formation, Shale Unit (Mdos)	Upper Mississippian	Thick zone of of splintery-weathering black, greenish, or locally reddish shale.
Great Blue Formation (Mgb)	Upper Mississippian	Thick bedded, cliff forming, pale-gray, fine grained limestone.
Humbug Formation (Mh)	Mississippian	Alternating, tan-weathering sandstone and limestone or dolomite.

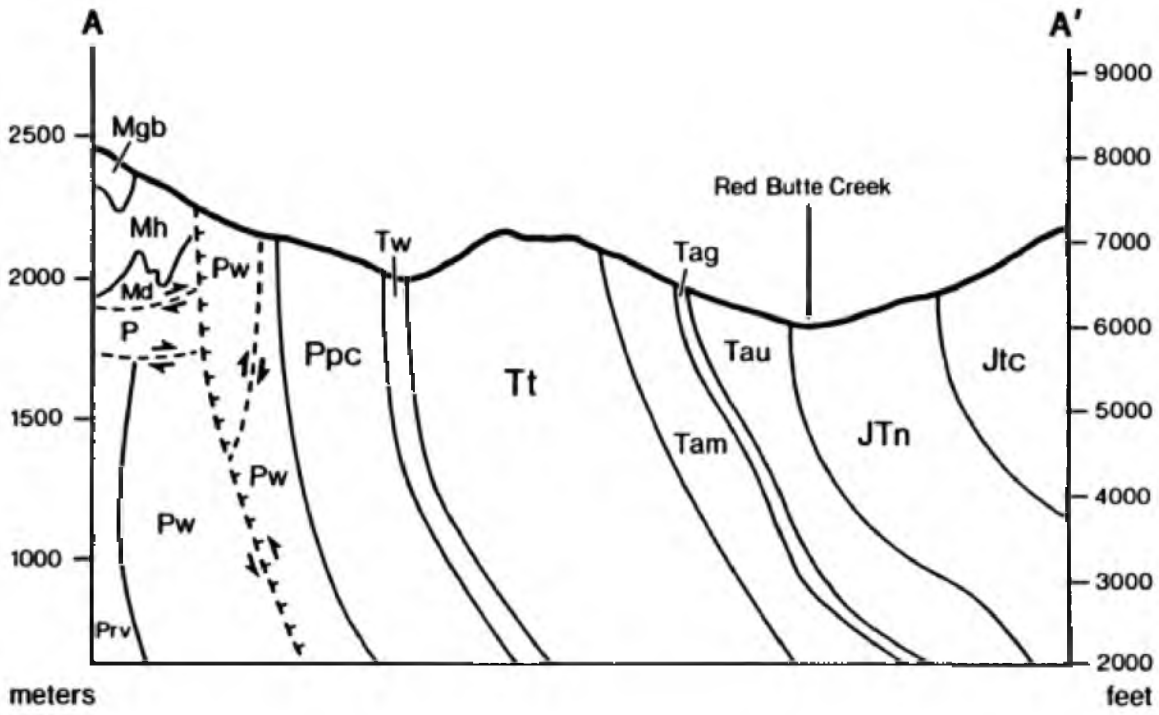

Figure 1.4, Generalized cross-section of Red Butte Canyon (Adapted from Crittenden & Van Horn, 1987)

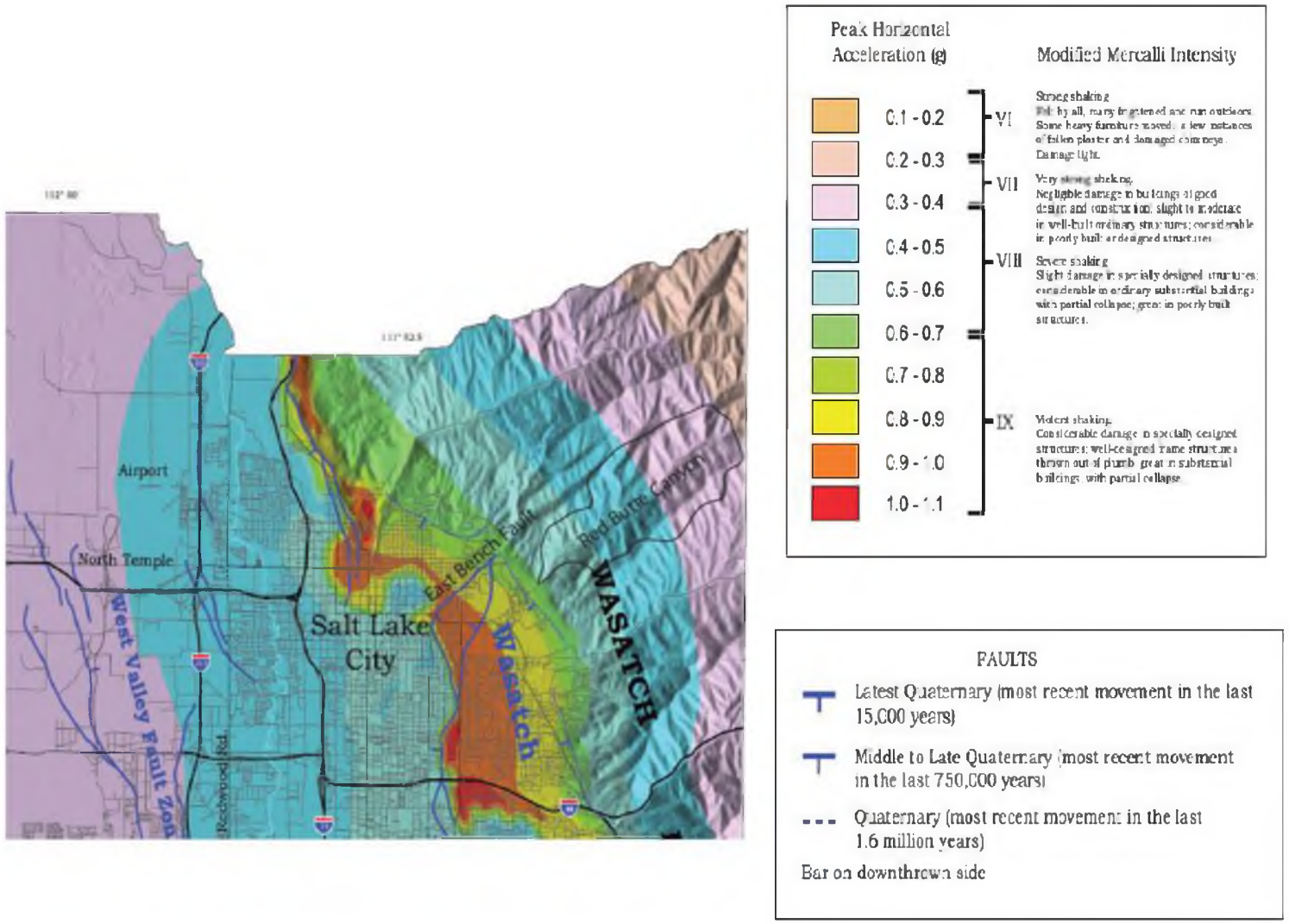

Figure 1.5, Peak horizontal acceleration map along Wasatch Fault (Wong et al., 2002)

CHAPTER 2

METHODS

Surface Mapping and Investigation

ArcGIS Maps and Digital Mapping

ArcGIS was used extensively in this project in order to efficiently map the study area and identify key geologic and geomorphic features. ArcGIS maps were constructed using high resolution digital elevation data acquired from airborne-based Light Detection and Ranging (LIDAR) data from the Utah Automated Geographic Reference Center (AGRC).

A series of 14 LIDAR-based files from the Red Butte Canyon area were downloaded from the AGRC data server in order to construct the series of ArcGIS maps used in this project. The data have 2 m horizontal resolution LIDAR in ASCII file format covering a 400 m × 400 m surface land area (AGRC, 2011).

Field Mapping and Geologic Mapping

The purpose of geologic field mapping was to find geologic contacts of the Nugget Sandstone, Ankareh Formation, and Thaynes Formation as well as to identify key geomorphic features that may have not been addressed in Van Horn and Crittenden's (1987) geologic map. A combination of dense vegetation, steep terrain, and a lack of

exposed rock outcrops made field mapping extremely challenging. For these conditions, the best field mapping method was a combination of a hand-held GPS unit and ArcGIS maps.

LIDAR-based ArcGIS maps made for the field site included both contours and slopes for more readily identifying features while working in dense vegetation. Graticules on field maps were used so that the precise geographic location was included on the contour maps and slope maps in coordination with field mapping with the GPS unit. A Garmin GPSMAP® 60CSx unit was used to aid in the mapping process. This device has some unique features including display of contour maps, storing waypoints, and also tracking paths taken while in the field. Each of these data types are stored in the unit's internal memory card and can be downloaded and accessed for later analysis via computer. All features such as borings, piezometers, outcrops, strikes and dips, and geomorphic features were stored as waypoints for future use and used in the construction of the geologic map.

A Brunton compass was used for mapping existing geologic units whenever they were encountered in the field. Strike and dip measurements were recorded according to the right hand rule and later incorporated in the new geologic map. Rock outcroppings were sparse due to the lack of competency in the Ankareh Formation and thick covering of top soil on the hillsides. However, some units such as the Gartra Grit Member of the Ankareh Formation, Thaynes Limestone, and Nugget Sandstone are more competent units and could be mapped more easily in the field.

Geologic Cross-Sections

A series of geologic cross-sections were created with no vertical exaggeration to show the subsurface geometry. All geologic cross-sections were constructed using the information from field mapping and from Crittenden and Van Horn (1987). The surface elevation of each cross-section was determined using interpolations of the surface D.E.M.s in ArcMap.

Photography

Hundreds of pictures were taken throughout all stages of the field investigation. A digital camera was used to take pictures of terrain, boring logs, soil cuttings, and all features associated with the field investigation. One unique feature of the photography was the camera's GPS logger (built in) so that picture data showed the features precise latitude and longitude.

Subsurface Investigations

Drilling and Sampling Program

A total of 8 borings were successfully drilled by hand in the field site within the flood plain alluvium and landslide features. Figure 2.1 shows the field site the location of borings, piezometers, and hill slopes shown in slope angle. An AMS, Inc. 2.25 in. diameter hand drilling set was purchased for this operation. An AMS 2 in. split spoon sampler was also used in order to obtain undisturbed soil samples (Figure 2.2).

The auger head was 8 in. in length, so soil samples were drilled, extracted, collected, and logged at 8 in. intervals, continuously for all borings. Samples were then

placed in Ziploc® bags and labeled at the appropriate depth for geotechnical engineering testing.

Undisturbed samples were collected simultaneously at 4.0 ft. intervals with the split spoon sampler by first placing standard 6.0 in. × 2.0 in. brass liners in the sampler and then driving the sampler into the formation using an axial hammer. Samples were recovered, capped, and labeled for future geotechnical testing. Two consecutive samples constituting a complete 1.0 ft. undisturbed samples were collected.

Sampling and Drilling Limitations

Although drilling in the field site was surprisingly amenable to hand augering, two limitations were commonly encountered. On several occasions neither the auger itself nor the split spoon sampler could recover soil samples while drilling through some groundwater saturated zones. The reason is believed to be a negative pressure or "suction" that developed between the walls of the auger and split spoon sampler while below the groundwater table. The second limitation was drilling into boulders in the landslide zone. It was impossible to drill through any materials larger than coarse grained sand/gravel. This difficulty was encountered in the landslide above Red Butte Creek and Parleys Fork. There was simply not enough downward pressure, torque, and strength of the auger to penetrate such materials with hand drilling.

Dynamic Cone Penetrometer

A Humboldt - Kessler Dynamic Cone Penetrometer (DCP) was also used in the field investigation. This device is typically used in geotechnical and civil engineering

industries to determine in situ shear soil strength based on empirical relations with the California Bearing Ratio (CBR), ultimate bearing capacity, q_c, and undrained shear strength, S_u (Kessler Soils Engineering Products, Inc., 2010; Duncan & Wright, 2005: 48). Briefly, the device works as an axial hammer dropped from the exact same height multiple times to drive a rod incrementally into the subsurface. The number of hammer blows per length increment has an empirical relationship to soil type and soil strength. The Kessler DCP can be used to estimate the strength characteristics of fine grained soils, granular construction materials and weak stabilized or modified materials (Kessler Soils Engineering Products, Inc., 2010). Figure 2.3 shows a schematic of the Kessler DCP.

The DCP subsurface data were also used to correlate specific zones with the boring logs. Regions of large incremental rod advancement (low blow count) at shallow depths are believed to be weaker zones, and represent top soil. Regions of low incremental rod advancement (high blow count) correlated with gravelly soils from debris flows and stream channels in addition to known tufa deposits.

The undrained shear strength of soils for Slope # 2 was obtained using the DCP data collected from Slope # 2. A series of empirical correlations and equations were used to translate the DCP into ultimate bearing capacity, and then from bearing capacity into undrained shear strength. These equations and methods are shown in Appendix B.

Seismic Refraction Survey

Seismic refraction surveys were performed in the field investigation within Todd's Meadow (Fig. 1.1) for a variety reasons. The depth to bedrock, or the most competent geologic unit, was needed for geotechnical modeling and geological

classification purposes. Hand augering was limited to depths of 22 ft. An actual drilling rig could not be used in Red Butte Canyon due to the environmental sensitivity of the site in addition to the off-road restrictions. A seismic survey solved this problem by determining the depth to bedrock.

The survey used 3.0 m spacing and 15 stacks (hammer blows). The energy source was a 10-lb. sledge hammer struck against a steel plate. A Bison 120-channel seismograph recorded the seismic data. Seismic processing was accomplished by coding with C++, Matlab, and other computer languages by University of Utah Ph.D. geophysics candidates Paul Gettings and Oner Sufri. Once the data were processed, seismograms were constructed using traditional first break analysis of the head wave.

Groundwater Monitoring and Measurements

Groundwater levels were recorded from borings drilled in this project as well as piezometers previously installed for research projects near the intersection of Red Butte Creek and Parleys Fork up through Todd's Meadow. When groundwater was encountered in drilling, the depth to groundwater was measured and recorded using a water level meter. The depth to groundwater below the ground surface elevation was measured in borings as well as previously installed piezometers infrequently throughout the project.

Geotechnical Testing

Since no prior geotechnical engineering testing has been completed within the study area a detailed investigation was executed to classify the geologic materials.

A large variety of geotechnical engineering tests were performed including natural moisture content, specific gravity tests, Atterberg Limits (liquid limit and plastic limit tests), grain size distribution, and undrained triaxial shear strength. These tests were necessary to determine the geotechnical properties of the soils used in slope stability modeling as well as better define the precise sedimentary features and grain sizes of the soils. Appendix A provides a detailed description of geotechnical testing and data.

Unified Soil Classification System

Geotechnical engineers commonly use one of several standardized index property tests to define a soil system. The most popular system is the Unified Soil Classification System, USCS (Coduto, 1997: 141). The USCS correlates important properties such as drained and undrained shear strength and angle of internal friction. The USCS also classifies soil types according to grain size distribution and behavior of Atterberg Limits Tests. All testing in this project was done according to the USCS. All tests were conducted at the University of Utah.

Some laboratory testing proved to be difficult because of the nature of the sandy clay soils in the field site. The problems encountered and solutions implemented were mostly with Atterberg Limit tests and grain size distribution tests as explained in the following sections.

Natural Moisture Content

Natural moisture content tests were conducted according to ASTM D 2216-90, Method of Laboratory Determination of Water (Moisture) Content of Soil, Rock, and

Soil-Aggregate Mixtures (Bardet, 1997: 2). A total of 125 soil samples were tested.

Atterberg Limit Tests

Atterberg limit tests were conducted according to ASTM D 4318-93, Test Method for liquid limit, plastic limit, and plasticity index of soils (Bardet, 1997: 2). A total of 27 Atterberg Limit tests were conducted on soils.

Soil samples were first prepared by passing the material through a #40 sieve as described in the test procedure. This proved to be challenging because of the nature of the sandy clay soils. Medium to coarse-grained sands and gravels needed to first be extracted from the clay before testing could begin. The most productive and least time consuming way to separate coarse grains from fine grains was to push the naturally wet clay through the #40 sieve. A summary of the liquid limit tests and plastic limit tests can be found in Appendix A.

Specific Gravity Tests

Specific Gravity tests were conducted according to ASTM D 854-92, Standard Test Method for Specific Gravity of Soils (Bardet, 1997: 2). A total of 29 specific gravity tests were conducted on soils.

Grain Size Distribution Tests

Grain size distribution tests were conducted according to ASTM D 422-63 and ASTM 2217-85, Test Method of Particle Size Analysis of Soil and Practice for Wet Preparation of Soil Samples for Particle-Size Analysis and Determination of Soil Constants (Bardet, 1997: 2). A total of 20 grain size distribution tests were performed on

the soil samples collected during the field program. All borings were tested with the exception of B – 3 due to sampling difficulties in the landslide material.

Grain size distribution tests also proved to be difficult due to the nature of the sandy clay soils. Coarser grains such as sands, gravels, and tufa were completely coated in clays and had to be fully washed, fluid separated from the clay, and then fully dried before sieve testing could occur.

Consolidated, Undrained Triaxial Tests (CU Tests)

Consolidated, undrained triaxial tests (CU tests) were attempted in the geological engineering laboratory, but after running into unresolved technical issues with the triaxial machine, samples were sent to Knight-Pièsold Consulting in Denver, CO. Each test was conducted according to ASTM D 4767-11, Test Method for Consolidated-Undrained Triaxial Compression Test for Cohesive Soils.

Drained and undrained soil shear strength conditions were evaluated for samples from B – 2, B – 6, and B – 8 from CU tests for Slope # 2, Slope # 3, and Slope # 4, respectively. Laboratory data for all CU tests can be found in Appendix G. No drained shear strengths were determined from soil samples from B – 2 for Slope # 1 due to sample disturbance, but undrained shear strengths were determined from the DCP data and empirical correlations. These DCP correlations and methodology are outlined later in the text.

The drained condition of a soil represents a scenario where water freely flows in and out of a volume of volume of soil in a length of time that the soil is subjected to a change in load, whereas the undrained condition of a soil represents a scenario in which

water is not permitted to flow in or out of a volume of soil in the period of time during the same changes (Duncan & Wright, 2005: 24). The undrained shear strength represents the typical stresses a soil is exposed to, where loads such as the accumulation of weight from snowpack in winter are gradual. On the other hand, possibilities for a short-term loading condition for the undrained shear strength would be an earthquake where dynamic loads are imparted on the soil for which there may not be enough time for water to flow out of soil and pore water pressures to dissipate.

Slope Stability Analysis

Methods for slope stability analysis come from standard geotechnical engineering practice. Slope stability models were constructed using a combination of surficial and subsurface data obtained during the study. Elevation profiles for slopes were determined using interpolation of D.E.M.s in ArcMap. The subsurface model was assembled using the knowledge of the geology and changes in stratigraphy from borings and included known groundwater elevations. DCP data from the slopes adjacent to Slope # 1, Slope # 2, and Slope # 3 were used primarily to determine the depth to groundwater, which is assumed to be located where very high blow counts occur at shallow depths.

Slope stability model parameters include the necessary geotechnical properties of stratigraphic/soil type changes, unit weight of soil, cohesive strength, friction angle, and depth to groundwater.

Several techniques are used for slope stability analysis including limit-equilibrium methods, equations, and modeling. An effective stresses analysis was performed for the slopes. Slope stability models for Slope # 1 through Slope # 3are performed using

Slope/W. Specific analysis is based on limit-equilibrium methods, specifically Bishop's Method (Duncan & Wright, 2005: 25). Slope stability analysis was also performed on the hill slope adjacent to B – 8, but using an infinite slope analysis. The infinite slope analysis method was used because soil creep was observed at this location and shallow modes of failure are often associated with thin soils with colluvium (Abramson et al., 2005: 653).

Slope stability was performed in a deterministic approach with stability reported as the factor of safety (*F.S.*). In the limit equilibrium method, the factor of safety is the ratio of total shear strength to the total shear stresses acting along the failure surface (Coduto, 1999: 528). Slopes with a $F.S. > 1.0$ are stable while slopes with a $F.S. < 1.0$ are unstable for static conditions (Coduto, 1999: 528).

Drained and undrained soil strength conditions are considered in the slope stability models. Drained conditions are employed in a model scenario representing the groundwater elevations observed during the investigation. Drained conditions are also represented in a model scenario with a high water table condition. High water table conditions can materialize from extreme rainfall events as well as excessive snow melt (Abramson et al., 2002: 649). High groundwater conditions occur over a period of time such that soil shear strength is still in the drained condition. Undrained soil conditions are represented in the shallow groundwater conditions and come into play with seismic loads generated from earthquakes.

The Pseudostatic Method

The pseudostatic method is a relatively simple method for evaluating slope stability in earthquake regions (Abramson et al., 2002: 394). The method is implemented by including the horizontal and static seismic forces used to simulate inertial forces due to ground accelerations from an earthquake where the seismic forces are assumed to be proportional to the weight of any potential sliding mass multiplied by horizontal and vertical seismic coefficients, k_v and k_h (Abramson et al., 2002: 394). The seismic coefficients are expressed as a percentage of the acceleration of gravity, g, and in most analyses $k_v = 0$ so the seismic force is assumed to act only in the horizontal direction, which ultimately induces an inertial force k_hW within the slope where W represents the weight of the potential sliding mass (Abramson et al., 2002: 394). Only horizontal seismic loads were considered in the slope stability models.

A range of horizontal seismic coefficients have been included in the models. Peak Ground Accelerations (PGA) vary from 0.1 g – 0.6 g within the boundaries of Red Butte Canyon and vary from 0.4 g – 0.5 g within the field site (Wong et al., 2002). A conservative approach is to use the maximum seismic coefficient/peak ground acceleration (Duncan & Wright, 2005: 165). However, a more realistic approach for the value of the seismic coefficient comes from conventional analysis and design approach. Table 2.1 summarizes typical seismic coefficients and factors of safety appropriate for the pseudostatic method. Marcuson and Franklin (1983) suggested an appropriate seismic coefficient of 1/3 – 1/2 × PGA and $F.S. > 1.0$ for the Pseudostatic Method (Abramson et al., 2002: 395). Using PGA = 0.5 g, the maximum seismic coefficient within the field site for the Pseudostatic Method should be: 1/3 – 1/2 × (0.5g) = 0.08 g, or

0.10 *g* to be conservative. The U.S. Army Corps of Engineers also recommends a seismic coefficient of 0.10 *g* (Abramson et al., 2002: 395).

Radiocarbon Dating

Charcoal was found in all borings intermittently at depth as will be discussed in the results section. C-14 dating was used to date the age of charcoal to better determine the geomorphic relationships of some of the features found in the field. Charcoal samples were prepared and sent to Beta Analytic in Miami, FL for C-14 analysis.

In summary, three model types were constructed using Slope/W and are outlined with the following considerations: 1) drained shear strength of soils for slopes under shallow groundwater elevations; 2) drained shear strength of soils under fully saturated slope conditions; 3) undrained shear strength of soils under shallow groundwater conditions with and without horizontal seismic loads.

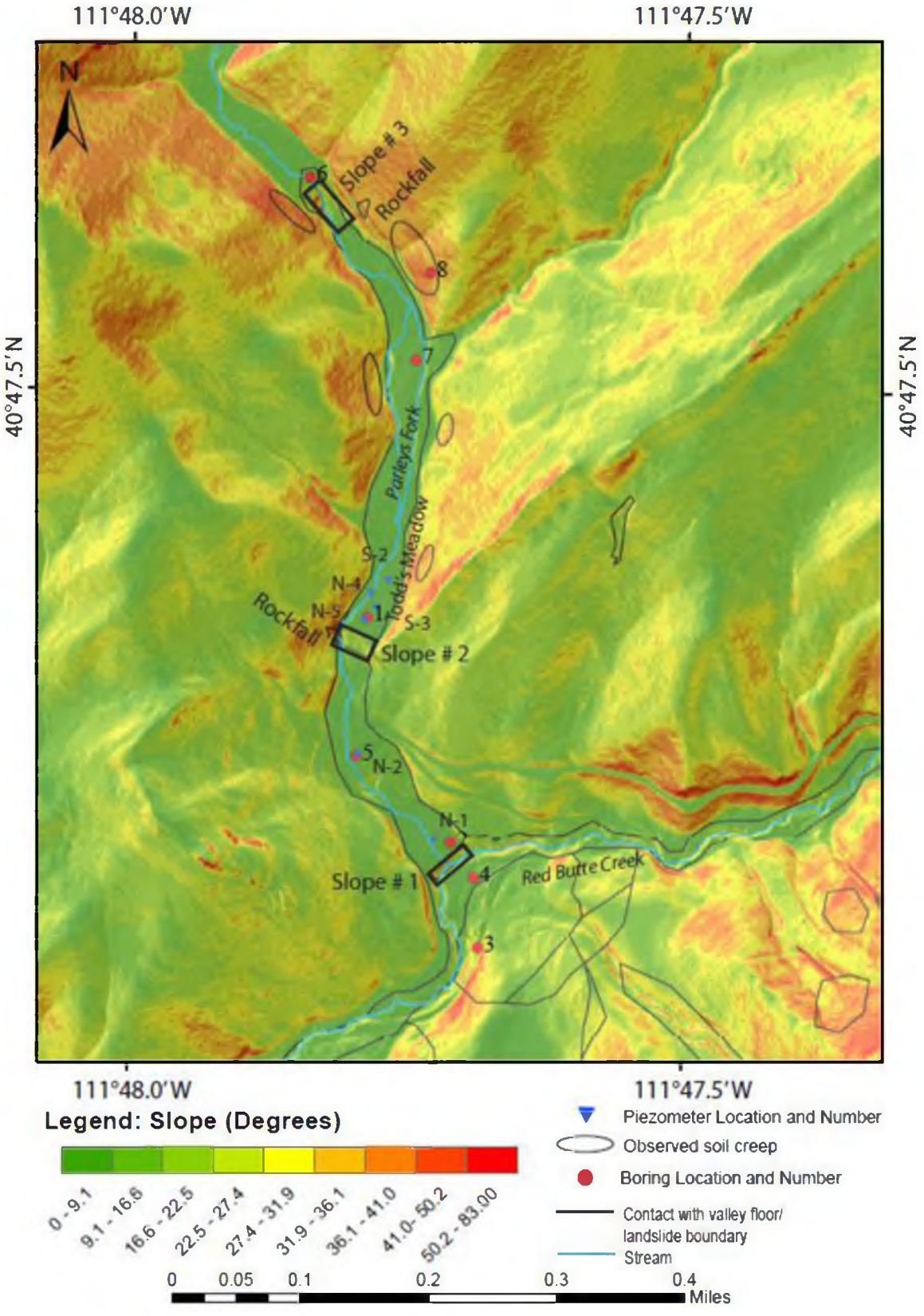

Figure 2.1, Site location and features

Figure 2.2, AMS, Inc. drill set and split spoon sampler (www.ams-samplers.com, 2011)

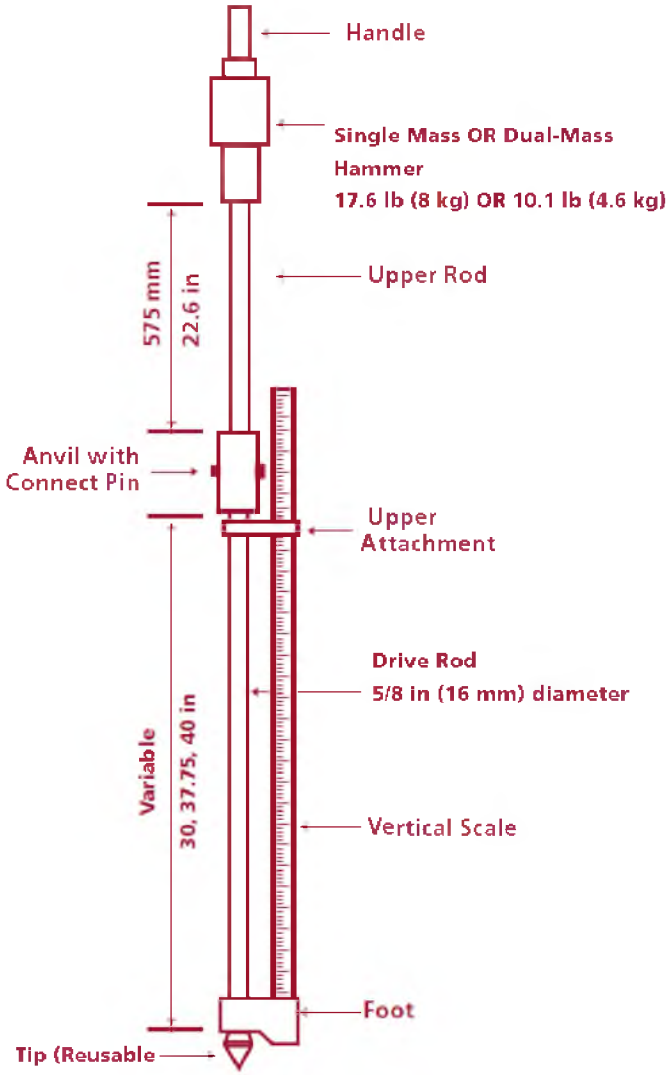

Figure 2.3, Kessler dynamic cone penetrometer (Kessler Soils Engineering Products, Inc., 2010)

Table 2.1, Seismic coefficients and *F.S.* for pseudostatic method

Seismic Coefficient	Remarks
0.10	Major earthquake, F.S. > 1.0 (Corps of Engineers, 1982)
0.15	Great earthquake, F.S. > 1.0 (Corps of Engineers, 1982)
0.15-0.25	Japan, F.S. > 1.0
0.05-0.15	State of California
0.15	Seed (1979) with F.S. > 1.15 and 20% strength reduction
1/3 - 1/2 * PGA	Marcuson and Franklin(1983), F.S. > 1.0
1/2 * PGA	Hynes-Griffin and Franklin(1984), F.S. > 1.0 and 20% strength reduction

CHAPTER 3

RESULTS

Surface Geology and Geomorphology

Geologic Mapping

The map published by Crittenden and Van Horn (1987) used as a base geologic map for the field investigation. Field mapping confirmed that their geologic contacts and attitudes are accurate. Overall, the attitude of all geologic units encountered was in agreement with Crittenden and Van Horn (1987). Many additional geomorphic features were mapped that were not present in Crittenden and Van Horn (1987) as discussed below (Figures 3.1 – 3.2).

Geomorphology

Landslide at Red Butte Creek and Parleys Fork

The landslide of Crittenden and Van Horn (1987) is accurately mapped, but the field investigation found this feature to be much larger than previously mapped. The original size of the mapped landslide was 10 acres (Crittenden & Van Horn, 1987). This investigation found the feature to be 16 acres due to angular boulders from the Nugget Sandstone extensively littering the hill slopes to the east. There may actually be two landslides, labeled as Id 1 and Id2 in Figure 3.1. Elliot et al. (2006) show this landslide

maybe even larger (100 acres). However, neither this study nor the study by Elliot et al. (2006) actually has mapped this feature in the field, rather it was interpreted through ArcGIS through curvature maps and other surface analysis tools.

Geomorphic Features of the Landslide at Red Butte Creek

There are two unusual characteristics of the landslide at Red Butte Creek. First, the Red Butte Creek channel seems to have been deflected by the landslide. Second, there appear to be distinct channel features within the landslide zone that parallel the direction of Red Butte Creek, which appear as lineations (Figure 3.3).

Stream Channel Slope Changes

A pattern of abrupt changes in slope were noticed within the stream channels of both Parleys Fork and Red Butte Creek. Figures 3.4 – 3.5 show the slope degrees of the slopes in question. These patterns were mapped using the interpolated surface from the 3DAnalyst in ArcGIS. Elevation profiles (Figures 3.6- 3.8) show this trend. Three slopes are particularly noticeable. Slope # 1 occurs at the intersection of Red Butte Creek and Parleys Fork. Slope # 2 occurs within Parleys Fork and starts at the base of Todd's Meadow (Figure 3.6). Slope # 3 is found approximately 2,000 ft. north of Slope # 2. Elevation profiles of both Parleys Fork and Red Butte Creek (Figures 3.7 and Figure 3.8) show the outline of geomorphic features such as landslide boundaries, earthflows, and evidence of soil creep.

Rockfalls

Numerous locations show evidence of rockfalls in the study area. Angular boulders are seen on the majority of the hill slopes and within the edges of the valley floor closest to the hill slopes. One noteworthy example involved downhill movements from the Ankareh Formation, Gartra Grit Member (Tag). The Gartra Grit member is a quartzite and is particularly resistant to erosion (Crittenden & Van Horn, 1987). The competence of this unit allows it to clearly standout on the hill slopes within the study area. Figures 3.9 and 3.10 show rock fall behavior of this formation on the steep slopes as well as into the valley floor.

Two rockfalls were discovered immediately downstream of Slopes # 2 and # 3. Slope # 2 appears to be the older feature because it is covered with soil and plant detritus and was initially hard to detect. Slope # 3 is a more recent feature because it is not covered in soil and actually blocks the forest road, making it completely inaccessible now (Figures 3.11 - 3.12).

Soil Creep

Several locations in the study area show evidence of pronounced creep. Creep is defined as "the slow downslope transport of soil or regolith by bulk motion under the influence of gravity" (Anderson, 2010: 320). Creep was readily identifiable because groupings of trees are bent over as the subsurface was very slowly transported downhill. Areas of creep observed in the field are included in the geologic map. These areas tend to occur in regions of steep slopes as indicated on the slope maps of the study area (Figure 3.4). Active creep occurs next to boring B – 8 and B – 1 (Figures 3.13 - 3.14).

Tufa Deposits

Tufa is an "[…] an inorganic limestone precipitated from solution in the water of a continental spring, lake, or from percolating groundwater" (Carlson et al., 2002: 276). There are many tufa deposits within both Parleys Fork and Red Butte Creek that form stair-stepped patterns in the creeks themselves. Figure 3.15 shows the behavior of the stair-stepped tufa deposit at the junction of Red Butte Creek and Parleys Fork.

Slope Direction and Aspect Map

Aspect maps show the resultant of the direction of the slope. These maps illustrate the direction that soil, rock, or water would travel down slope. Figure 3.16 shows an aspect map demonstrating the flow direction vectors for where soil and rock could have flowed down the valley walls and slopes. Notice from the legend in Figure 3.16 that the bright pink color represents a flow direction ranging from 292.5° - 337.5° as shown with arrows on the figure. This concept of flow vectors applies to the other colors and directions represented in the legend and are applicable to subsurface geology findings and sediment composition discussed below.

Subsurface Geology

Borings B – 1 to B – 8 yielded three main subsurface components that were observed repeatedly: 1) organic soil horizons, 2) sandy clay unsaturated zones and 3) saturated sandy clay zones. Other soil constituents discovered in nearly all borings include: tufa, charcoal, freshwater mollusk and mussel shells, and angular to sub-rounded gravel from the surrounding geological formations Thaynes Formation, Ankareh Formation, and Nugget Sandstone.

Boring Logs

Logs for borings B – 1 to B – 8 (Figures 3.17 - 3.24) accurately represent the subsurface geology observed during drilling and corresponding geotechnical properties and Unified Soil Classification System (USCS) soil types.

Dynamic Cone Penetrometer Results

The Dynamic Cone Penetrometer (DCP) was used at all borings except for B – 4, B – 3, and B – 8 because of the fear of not being able to recover rods due to the presence of objects encountered while drilling. Penetration vs. depth has been plotted next to the boring logs (Figures 3.17 to 3.24). Notice the variation of blow count vs. depth such as boring B – 7 (Figure 3.18) where the blow count is less than 1 in. per blow. Since angular gravel of the Ankareh Formation and Thaynes Formation were observed in the field drilling as well as the grain size distribution from 9.5 – 10.0 ft. at this location, it is assumed that the low blow count represents layers of gravel at this location. Similar observations occur for a tufa layer or deposit encountered in B – 6 (Figure 3.17) from 12.5 - 13.0 ft.

The majority of the soils in the valley floor of the field site were classified according to the USCS as CL (Low Plasticity Clays) Sandy Lean Clays. Soils from B – 6 were classified as SC (Sandy Clays) Clayey Sands and soils from B – 8 were classified as CL – ML (Low Plasticity Clays to Low Plasticity Silts) Sandy Silty Clays.

Geotechnical Properties and Model Parameters

Atterberg Limit Test Results

The majority of soils have low plasticity (liquid limit < 50 %, index of plasticity ≈ 16%) (Figure 3.25). Upper soil horizons display a higher plasticity possibly due to organic content as explained in the geology section of this report (Figure 3.26). Lower portions of B – 2 are highly plastic (liquid limit > 50%). A complete listing of the Atterberg Limits for all soils is found in Appendix A.

Specific Gravity Tests

The specific gravity tests ranged from 2.165 to 2.738 with most values in the 2.60 – 2.70 range (Figure 3.27). Interpretation of these values is given in the Discussion section.

Grain Size Distribution Tests

Grain size distribution tests are plotted on grain size distribution curves for borings B – 8 – B – 1 and show changes in grain size over depth (Figure 3.28 – Figure 3.34). Notice the variation in grain size, indicative of poorly sorted (well graded) geologic materials.

Unit Weight of Soils

The unit weight of soils was based on laboratory results from Knight-Piésold as well as correlations for soil type based on the USCS and is summarized in Table 3.1.

Unit weights for B – 1, B – 8, and B – 6 were determined through laboratory testing. These unit weights are the most critical since they are used in slope stability models.

CU Test Interpretation

CU test results for soil samples from B – 1, B – 6, and B – 8 displayed behavior such that a cohesive strength and friction angles could not be directly taken from test results. For instance, each of the plots of the shear stress vs. normal stress in $\tau - \sigma$ space display unusual behavior for a typical CU test because Mohr circles did not plot favorably such that the circles plot tangentially to a defined failure envelope. Failure envelopes could be more readily identified using critical state soil mechanics where stress paths are linear and incremental changes in effective stress, p, and deviatoric stress, q, remain constant and plot on the x and y-axes in Cartesian coordinates (Abramson et al., 2002). In order to account for the true drained and undrained strength of the soils, CU test results were plotted in $p - q$ space because one does not have to fit the critical Mohr circles tangentially to the failure envelope (Abramson et al., 2002: 248).

Drained and Undrained Shear Strengths

The drained shear strength of the soils was identified through the effective stress paths in $p' - q$ space from CU tests. The drained shear strength is determined from the effective stress path where the point of maximum shear stresses occur, typically associated with the point of maximum stresses in $p' - q$ space (Abramson et al., 2002: 249). The critical failure line, *Kf*, is also determined from the point of maximum stress, where the drained shear friction angle corresponds to the angle ψ. Plots of the CU tests

in $p - q$ space as well as the relevant equations relating normal stress, shear stress, friction angles, and cohesive strength are shown in Appendix B.

The undrained shear strengths for the soils were determined from a normalized approach outlined in Appendix B. This normalized approach uses the concept that a hypothetical factor, N, relating the undrained shear strength to the initial confining stress used in the tests can be obtained for each CU test with B – 1, B – 6, and B – 8. This factor is plotted against the effective stress at depth in order to determine an appropriate undrained shear strength according to the Mohr-Coulomb strength criterion (Duncan & Wright, 2005: 22).

The drained and undrained shear strength of undisturbed soils was determined for samples from B – 1, B – 6, and B – 8 from CU tests. No drained shear strengths were determined from samples from B – 2 due to sample disturbance, but undrained shear strengths were determined from the DCP data and empirical correlations. Laboratory data for all CU tests can be found in Appendix B. Plots of the shear stress vs. normal stress in $\tau - \sigma$ space display unusual behavior in each of the CU tests because Mohr circles did not plot favorably such that the circles plot tangentially to a defined failure envelope.

The drained shear strength in terms of $p' - q$ space and ψ and a in addition to the equivalent shear strength in terms of $\sigma' - \tau$ space and c' and ϕ' are shown in Table 3.2. The undrained shear strength parameters are shown in Table 3.3. Refer to Appendix B for a detailed explanation of the derivation of the parameters.

Soil Types, Organic Materials, and Stratigraphy

Organic Materials in Soils

Black-colored soils were observed in all borings in the upper surface. The thickness of these soil horizons varied from 0 - 0.5 ft. to 0 - 2.8 ft. below the surface as shown in the boring logs. These zones typically had higher moisture content (16.8% - 26.6%) relative to the lower section of the soil borings and had a distinct humic odor that was easily identifiable in the field. Plant leaves, plant roots, and insect exoskeletons were commonly found in the organic soil horizons. Liquid limits greater than 50% were observed in the upper soil horizons, indicating high plasticity.

Unsaturated Zone and Saturated Zone Soil Types

Most soils within the flood plain alluvium and study area were classified geologically as poorly sorted sandy clays and often contained subrounded to angular sand and gravel that varied from location to location. The majority of soils appear to be CL Sandy Lean Clays under the USCS, but this varies by location.

The moisture content ranged from 11.2- 29.9% and increased drastically immediately above the saturated zone. The soil types within the saturated zone were the same as the unsaturated zone except that the moisture content was much higher ranging from 24-39%.

Landslide Materials

Landslide materials were encountered in borings B – 3 and B – 2. These materials were classified as very poorly sorted clay with angular boulders. A total depth

of only 0.8 ft. could be drilled at B – 3 because of large Nugget Sandstone boulders that the auger could not penetrate. Landslide materials were believed to have been contacted at a depth of 15.7 ft. at B – 2 since normal drilling could not go past this depth either. The split spoon sampler was used to recover Nugget Sandstone, charcoal, and splintered wood at 15.7 ft. in B – 2. The only other location where the Nugget Sandstone was encountered was on the hill slopes of the landslide and also in B – 3. Splintered wood was not encountered in any other boring.

Organic Materials: Charcoal and Wood

Charcoal was found intermittently at depth within all borings except for B – 8 and B – 3 and was interbedded and mixed in with the clay soils. The size of the charcoal varied from pieces as small as 0.5 mm to as large as 12 mm. Pieces of what appeared to be splintered wood were only found in B – 2 at a depth of 15.7 ft. The shape and size of these pieces were elongated and up to 2 cm in length as shown in Appendix E.

Radiocarbon Dating Results

Two charcoal samples analyzed for radiocarbon dating, B – 2 at 15.5 ft. and B – 5 at 14.5 ft., yielded precisely the same radiocarbon age as **4,370 ± 30 years** before present. Both samples ages were double-checked by Beta Analytic for accuracy who confirmed the same age.

Freshwater Mollusk Shells

Freshwater mollusk shells were found intermittently with depth in all borings except for B – 8 and B – 3. Clam shells were not as common being found in B – 1, B – 5, and B – 2 at intermittent depths. All mollusk shells were identified through a field guide on freshwater mollusks (Lysne, 2009) as the snail species *Gyraulus* and the *Pyrgulopsis*. There does not appear to be a specific depth where shells were most common. The size of the shells varies from 0.1 mm to 5 mm (Figure 3.35).

Tufa

Pieces of tufa were found in all borings except B – 3 and varied in size from fine-grained sand to coarse grained gravel. The tufa was found at all depths and was interbedded in clays and sands within the flood plain alluvium. The tufa grains constitute a major weight percentage of the overall grain size distribution as will be discussed in the geotechnical engineering properties section. In addition, there were a few locations where it is believed layers of tufa were drilled though such as in B – 6 from 12.5 -13.0 ft., B – 2 at multiple depths, and in B – 4 at 4.5 ft. These regions are assumed to be tufa zones because of drilling difficulties and breaking through with the split spoon sampler, which recovered tufa.

Gravel from surrounding Geologic Formations

Gravel was found within borings at irregular depths. B – 7 had by far the greatest amount of coarse sand and gravel of any boring. This subject will be examined further in the Discussion section.

Sedimentary Structures

The majority of soils and sediments were obtained by drilling and hence, were disturbed. Samples were brought to the surface and extruded from the auger head. In addition, drilling consequentially destroyed all remaining intact sedimentary structures. However, sedimentary structures remain preserved in undisturbed samples obtained with the split spoon sampler through extrusion from the 2.0 in. × 6.0 in. brass liners. Cross-bedding was seen in several undisturbed samples between clay layers with sand grains, shells, and charcoal pieces. In addition, fining-upward graded bedding was visible in some samples. However, the scale of such observations was limited to 6.0 in. sections. Figures 3.36 - 3.37 show examples of the sedimentary structures.

Groundwater and Aquifers

Historical Data in Todd's Meadow

Historical groundwater level data from Todd's Meadow acts as a framework for understanding the hydrogeology for the study area because previous records span two water years, whereas the groundwater data collected in this project was limited and only covered one water year (Table 3.4). Groundwater data for piezometers N – 5, N – 4, S – 3, and S – 2 from10/27/2000 to 4/17/2001 indicate the greatest depth to water occurs in the late fall and shallowest depth to water occur in the early spring months (Table 3.4) (Solomon, 2001).

Groundwater Data in Todd's Meadow

Todd's Meadow is relatively flat and only varies 2 -3 ft. in surface elevation. The depth to groundwater on the other hand varies from approximately from 15 ft. to 27 ft. (Table 3.4). Measurements from piezometer N-10 indicated that the depth to groundwater was shallower at approximately 15 ft. while the depth to groundwater at adjacent piezometers N-14 and N-15 was approximately 25 ft. (Table 3.4). A shallower depth to groundwater was also encountered 40 ft. to the north at boring B -1 where the depth to groundwater consistently remained at 16 ft. throughout the entire project duration (Table 3.4).

Groundwater Data in Lower Field Site

Boring B – 5 and piezometer N – 2 are in close proximity (20 ft. apart) from one another and the depth to groundwater at these locations is approximately 10 ft. and are in close agreement with one another. The depth to groundwater in N – 2 is only 0.4 ft. shallower than in B – 5, where N – 2 is closer to Parleys Fork (Table 3.4). Further south toward Red Butte Creek, piezometer P – 1 showed a slightly greater depth to groundwater of approximately 15 ft., with a 2.5 ft. difference in the depth to groundwater between P-1-1 and P-1-2 (Table 3.4). Lastly, the depth to groundwater in boring B – 2 was approximately 10 ft., but showed variation in depth being higher at 9.8 ft. in the late fall as opposed to 10.3 ft. in the summer because surface elevations are also 58 ft. higher at B – 5 and N – 2. The hydraulic gradient in the lower portion of the field site suggests flow towards Red Butte Creek.

Groundwater in B – 6, B – 7, B – 8

Groundwater was encountered in borings B – 6, B – 7, and B – 8 during drilling. Both B – 6 and B – 7 are also in close proximity to Parleys Fork and are on the valley floor. The depth to groundwater in B – 7 was 9 ft., whereas the depth to groundwater in B – 6 occurred at 15.8 ft. (Table 3.4). Lastly, groundwater was encountered in boring B – 8 at a depth of 11 ft.

Groundwater Levels and Slope Stability Models

The highest groundwater levels observed in the field were applied to all slope stability models and represent an unconfined aquifer. In addition, a high groundwater table scenario was modeled in slope stability models such that water levels were at the ground surface in order to represent an extreme rainfall or rapid snowmelt event as described in the Slope Stability Model Section.

Seismic Refraction Results

Seismic refraction survey data from Todd's Meadow (Table 3.5 and Figure 3.38) were processed and analyzed with the seismic refraction method (Sheehan et al., 2006: 65). The survey shows a distinct three layer system exists (Figure 3.39) with a distinct velocity contrast between the layers. Layer 1 shows a seismic P-wave velocity around 338 m/s and a varying thickness of 18.3 - 26.7 ft. Layer 2 shows a seismic P-wave velocity of 1347 m/s and layer thickness of 40.7 - 19.5 ft. Finally, Layer 3 shows a seismic P-wave velocity of 3588 m/s and an upward dip from north to south (Figures 3.38 - 3.39). The seismic refraction data seem to be high quality as indicated by the high

regression coefficients. The results are in good agreement with published seismic velocities for similar geologic materials and the measured groundwater depths in Todd's Meadow. The processed seismic data and sample calculations for determination of thicknesses are shown in Appendix D.

Geologic Cross-Sections

The depth to bedrock in Todd's Meadow increases from 46 ft. to 60 ft. from north to south over a 236 ft. length. The depth to bedrock throughout the study area has not been determined, but is assumed to be 45 ft. based on the minimum depth to bedrock found within Todd's Meadow as shown in cross-section A-A' (Figure 3.40).

Cross-section A-A' is distorted to a 0.35:1.0 horizontal to vertical ratio in order to fit on a standard 8.5 in. × 11 in. page. Dips have been accounted for true dip and apparent dip according to standard methods outlined by Marshak and Mitra (1998). Cross sections B-B', C-C', and D-D' were constructed perpendicular to cross section A-A' (Figures 3.41 – 3.43). Each of the cross-sections has unique features which are explained in Chapter 4.

Slope Stability Analysis

Slope stability models were constructed using Slope/W for Slope # 1, Slope # 2, and Slope # 3 (Figures 3.44 - 3.48). An infinite slope stability analysis was performed for the hill slope next to B – 8 (Figures 3.49 - 3.50). Figures 3.44 - 3.50 represent stability models for the drained condition and the undrained condition for $k_h = 0.0\ g$ and shallow groundwater conditions. These figures show the slope geometry, groundwater

table, soil types, and geotechnical properties. They also display the location of the minimum *F.S.* determined in Slope/W shown in red in addition to regions of other equivalent *F.S.* contour regions. Finally, the failure surfaces are shown as circular arcs.

Figure 3.49 and 3.50 show the infinite slope analysis case and shallow groundwater conditions. These figures also show the slope geometry, groundwater elevation, and geotechnical properties. The failure surface within an infinite slope analysis is typically represented as a shallow level failure that commonly occurs within the bedrock surface / upper soil surface interface (Abramson et al., 2002: 653).

Table 3.6 summarizes the slope stability for each of the three slope stability model types: 1) drained shear strength of soils for slopes under shallow groundwater elevations, 2) drained shear strength of soils under fully saturated slope conditions, and 3) undrained shear strength of soils under shallow groundwater conditions with and without horizontal seismic loads. Figures 3.51 and 3.52 summarize the factors of safety and horizontal seismic loads for the undrained condition. Note that $k_h = 0.10\ g$ is the assumed maximum horizontal seismic load for all slopes, but a range of seismic coefficients up to $k_h = 0.5\ g$ has been included in the graphs for illustrative purposes.

In short, it appears that all slopes have the highest factor of safety with the drained condition and lowest factor of safety with the drained condition and high groundwater table condition. The undrained conditions reveal that all slopes have a lower factor of safety under undrained conditions which decreases with an increasing seismic coefficient.

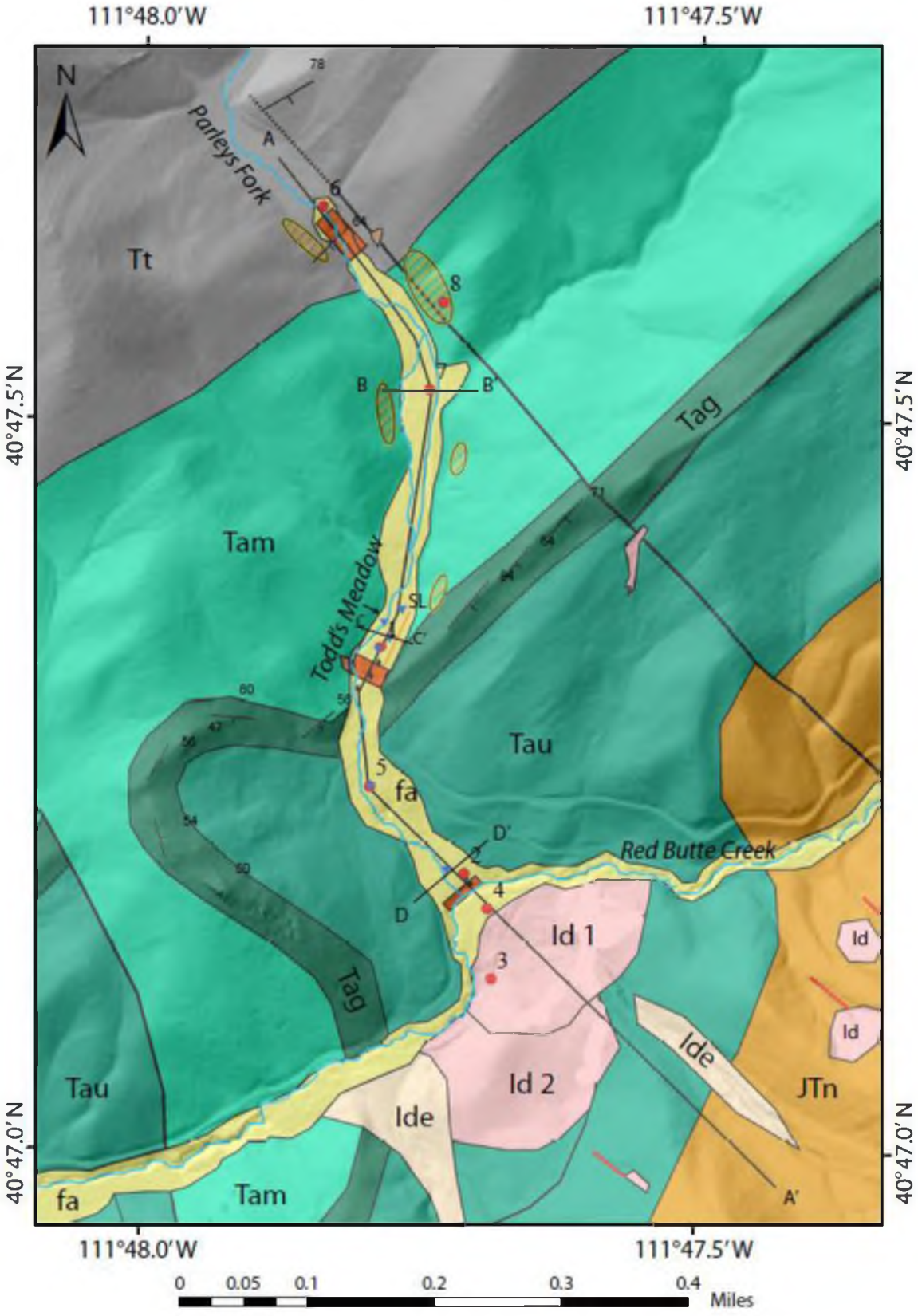

Figure 3.1, Geologic map of study area

Figure 3.2, Legend for geologic map of field site

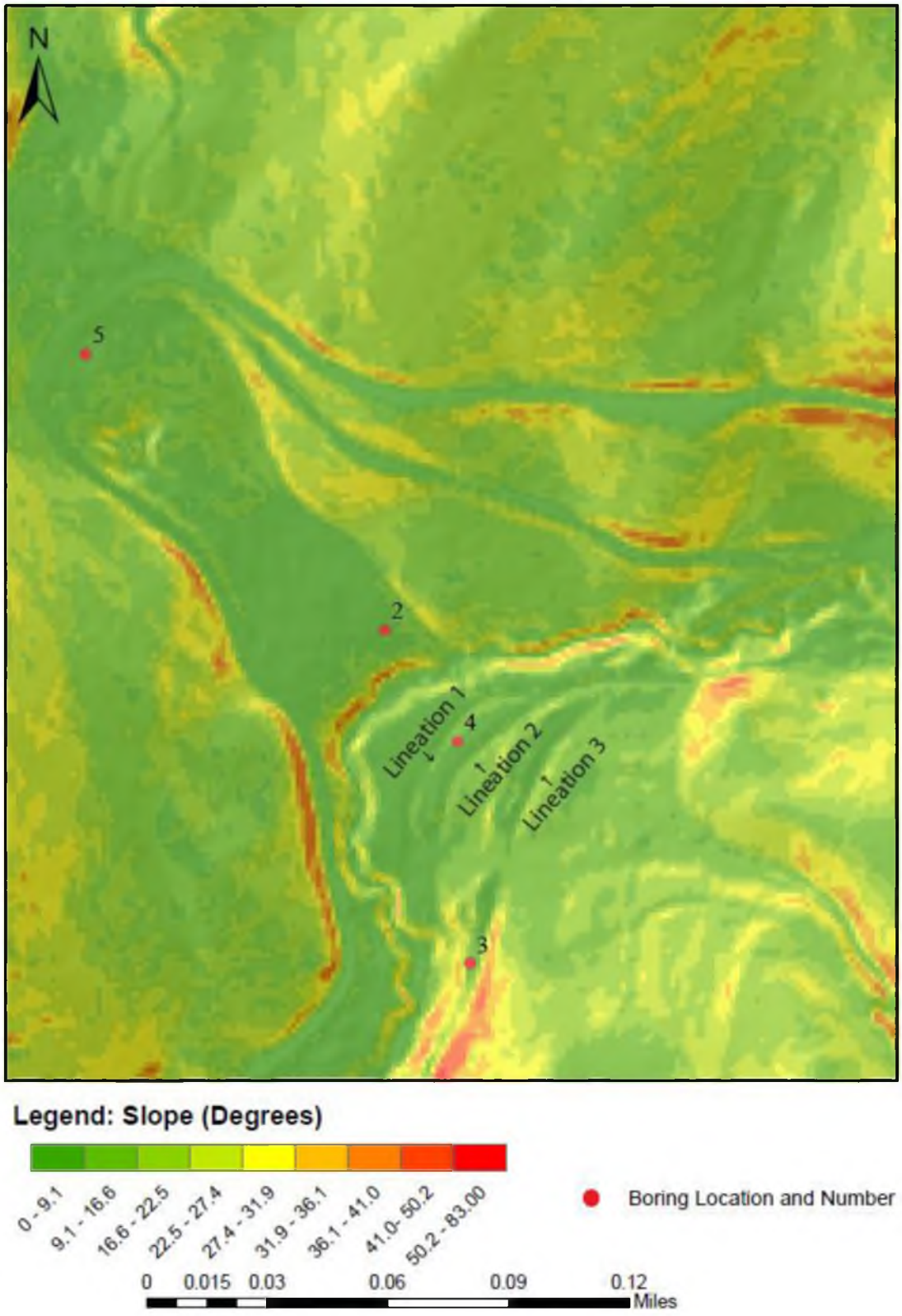

Figure 3.3, Slope map showing curvature of Red Butte Creek around the landslide feature and unusual lineations

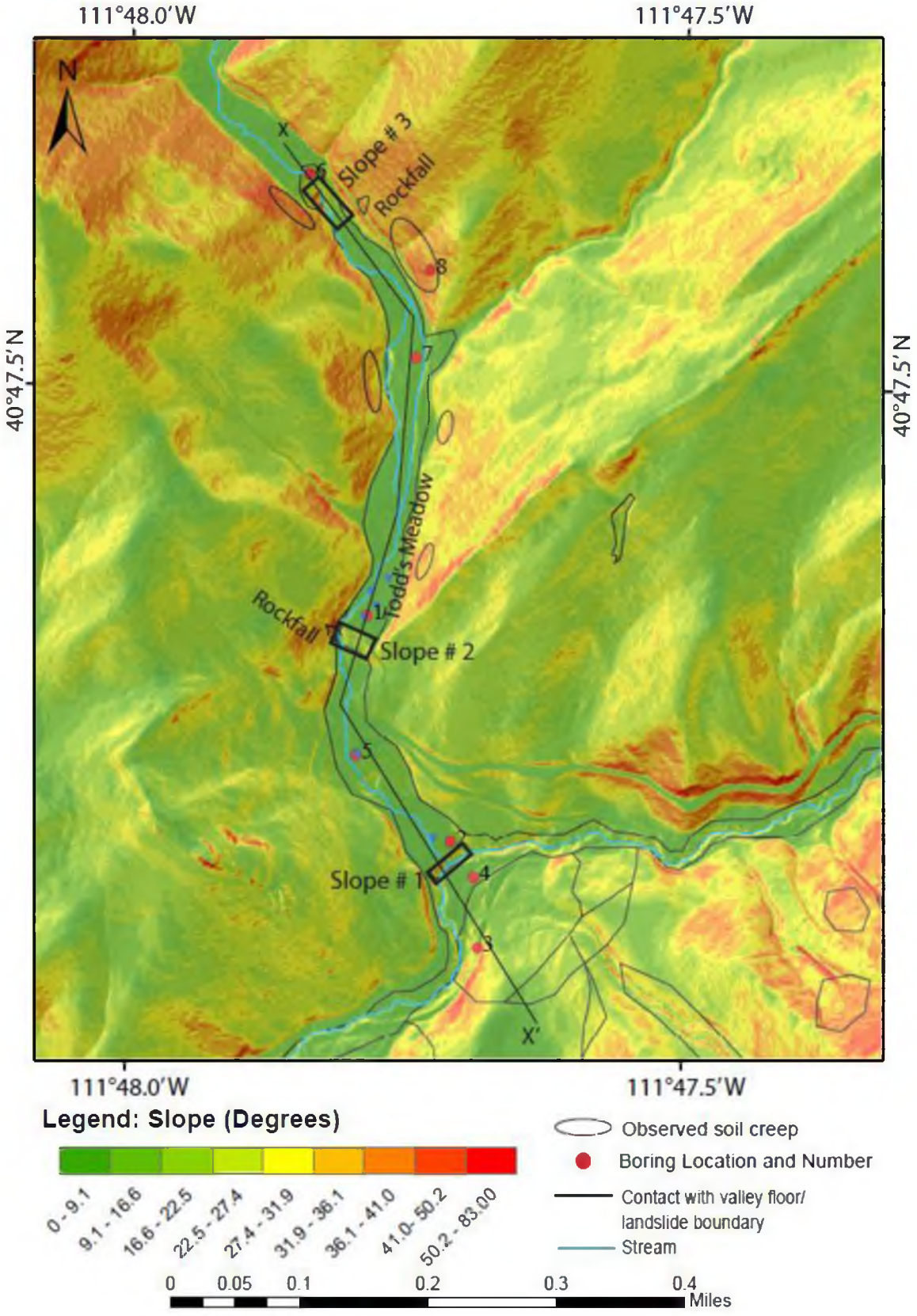

Figure 3.4, Slope map of study area

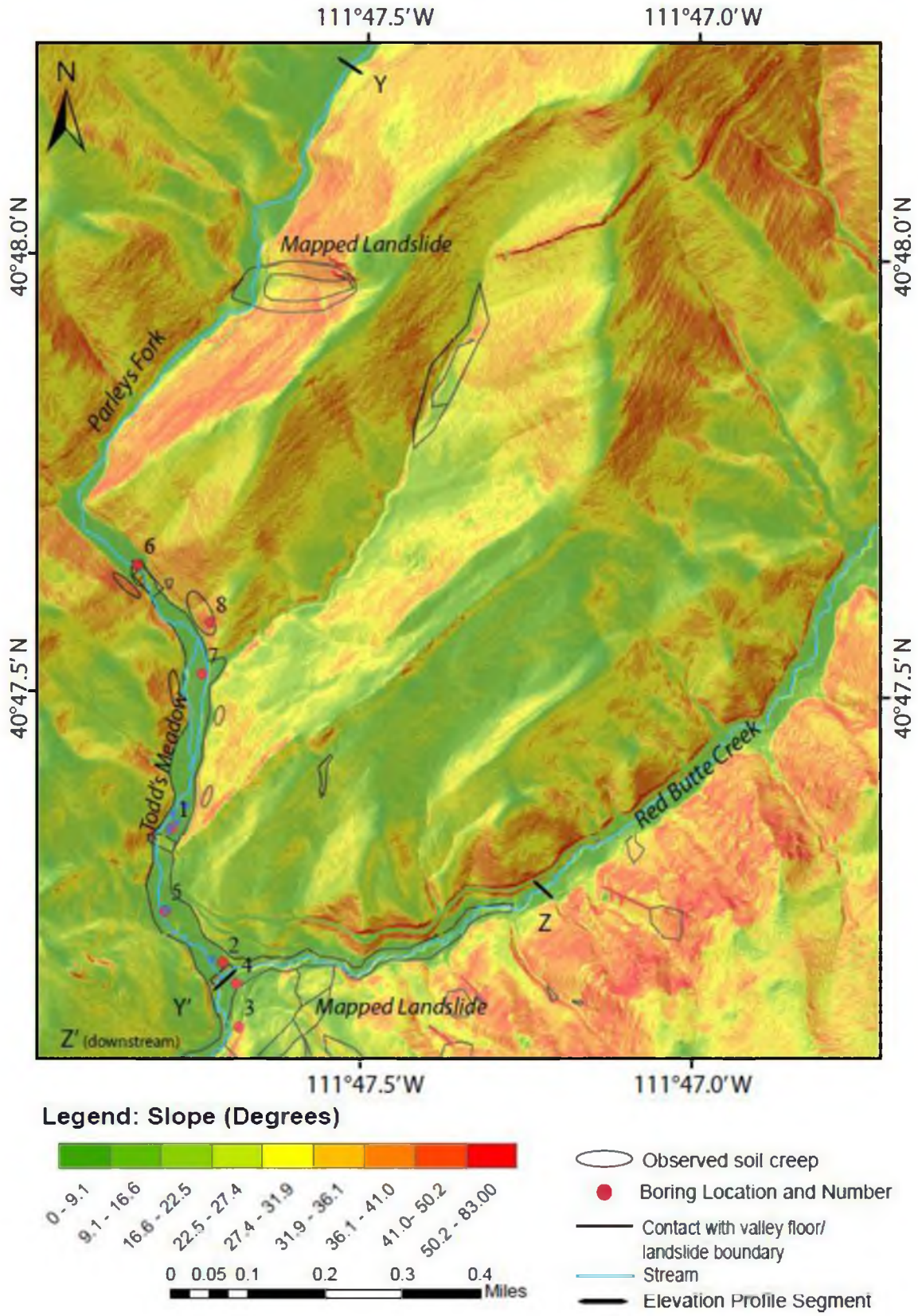

Figure 3.5, Slope map showing Red Butte Creek and Parleys Fork

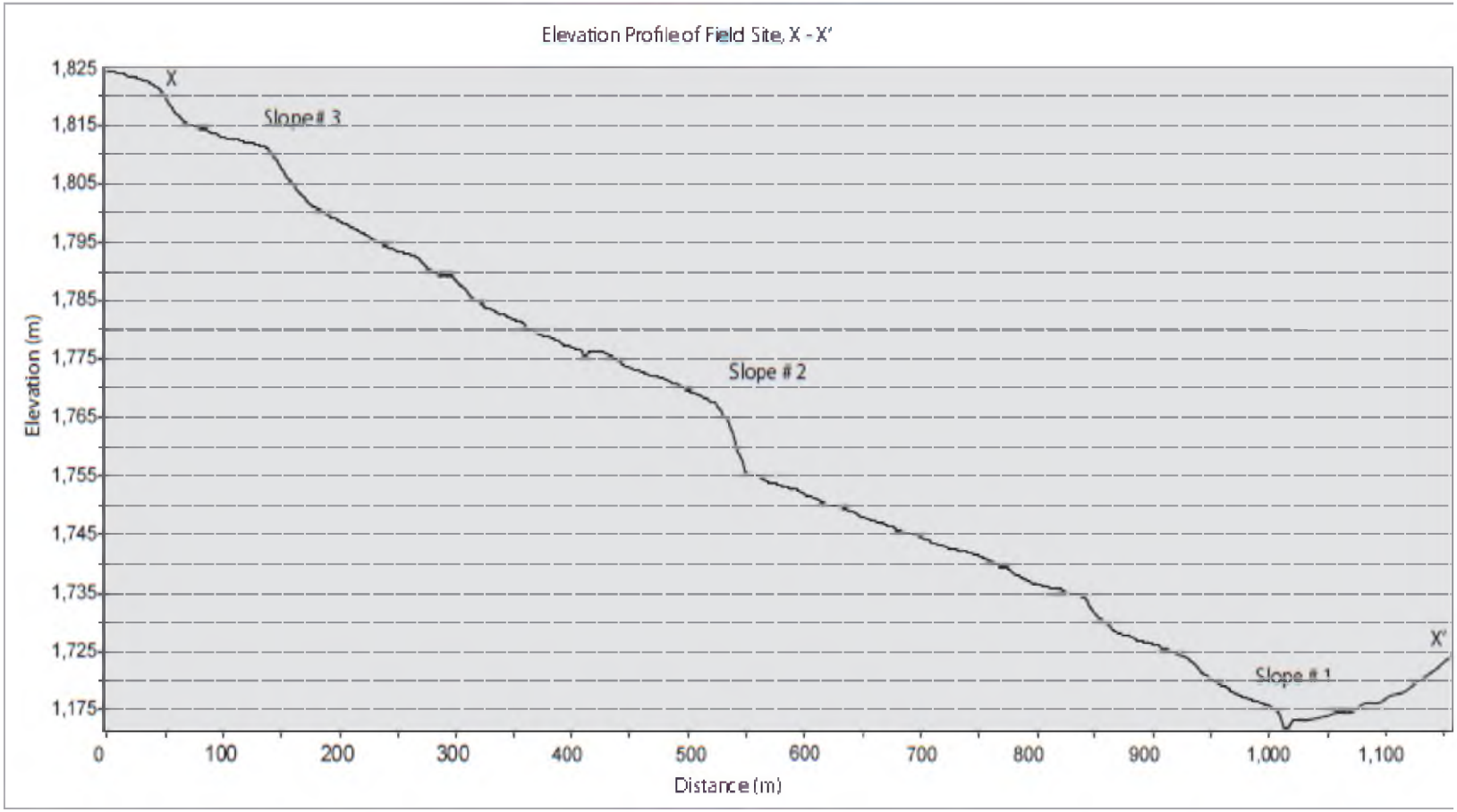

Figure 3.6, Elevation profile along line X-X' from slope map of field site map

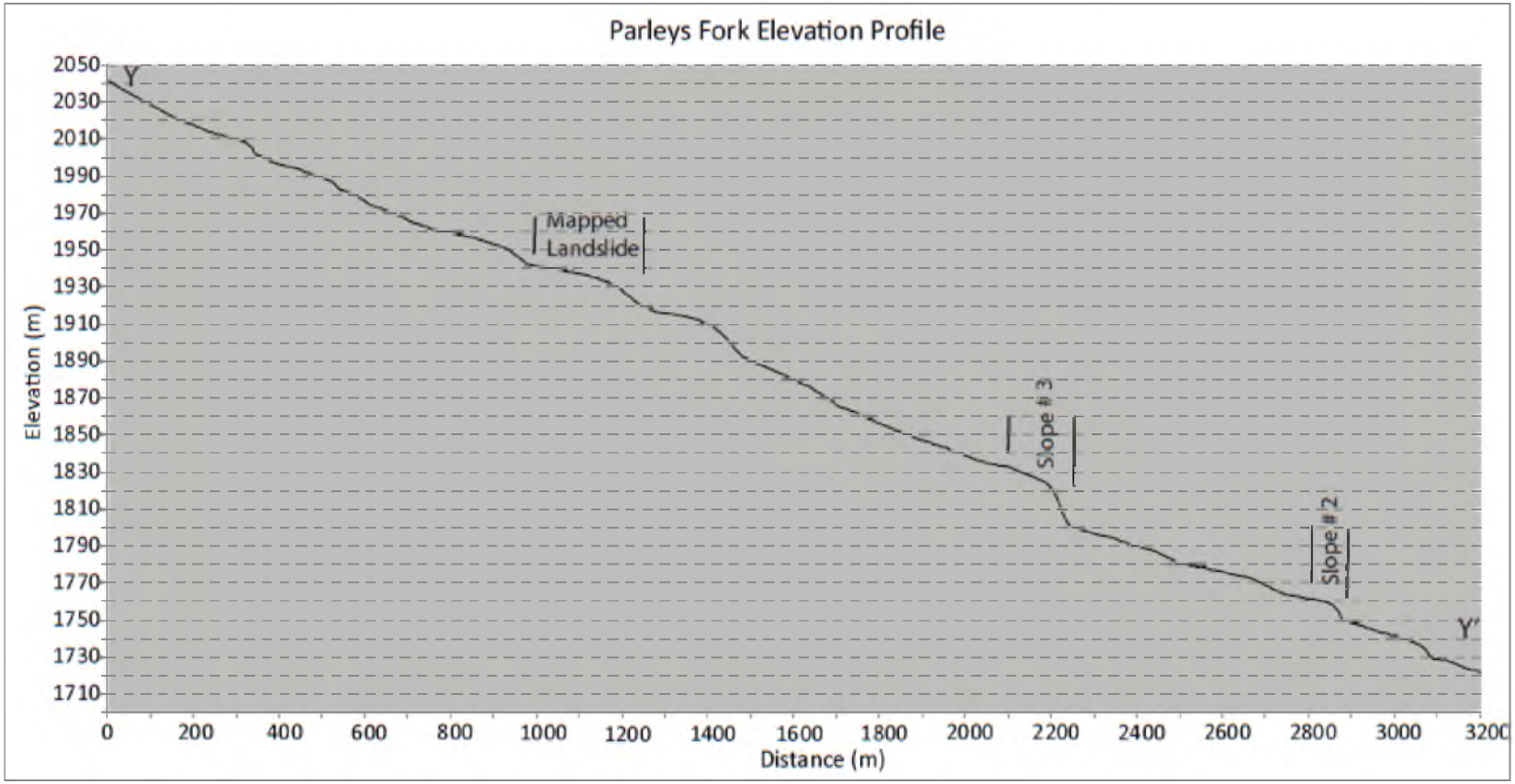

Figure 3.7, Stream elevation Y – Y' profile along Parleys Fork

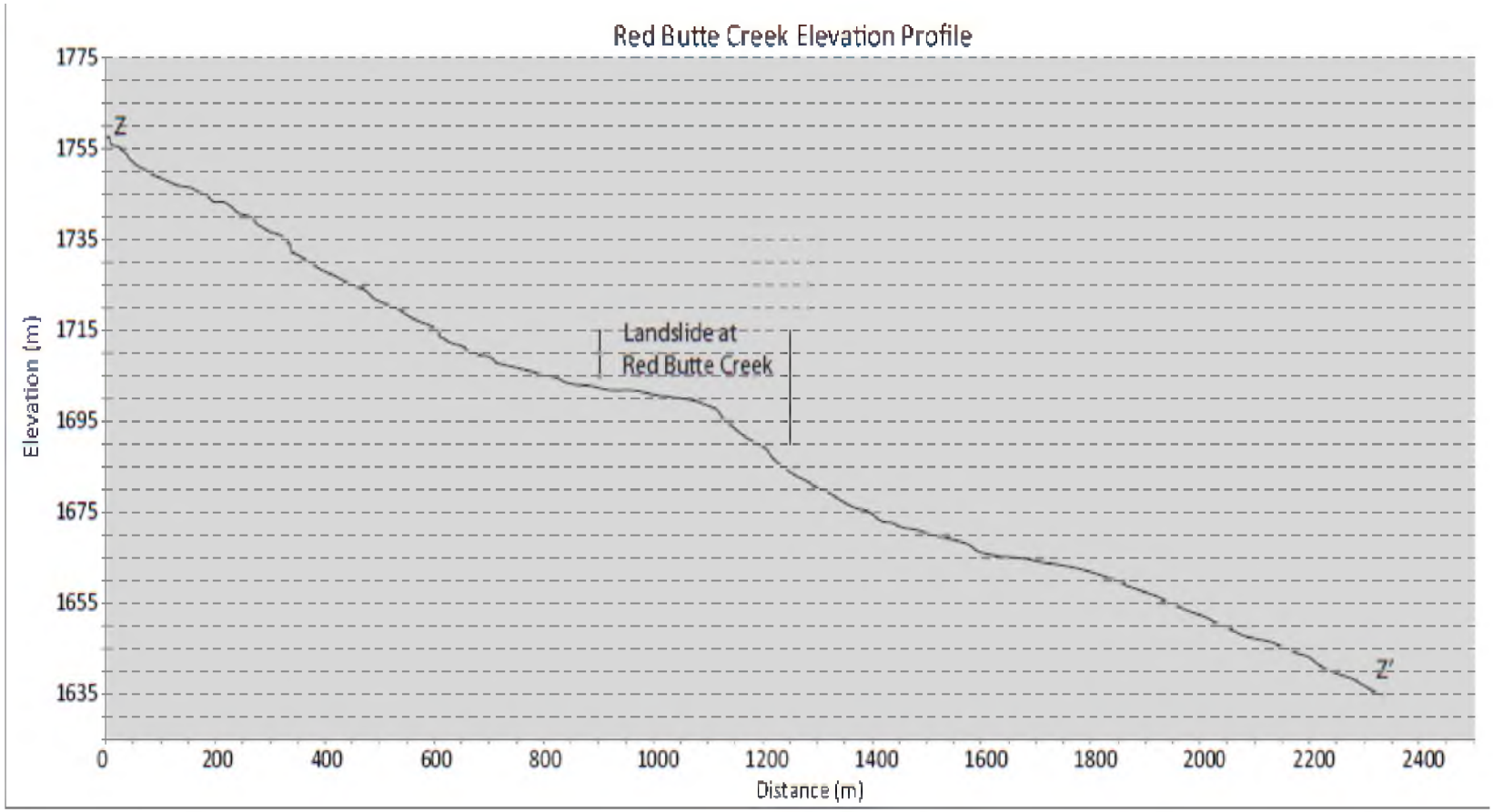

Figure 3.8, Stream elevation profile Z-Z' along Red Butte Creek

Figure 3.9, Rockfalls on hill slope northeast above Todd's Meadow, Tag member shown

Figure 3.10, Rockfall in Todd's Meadow from Tag

Figure 3.11. Rockfall adjacent to Slope # 2, pane on left shows angular boulders covered in soil and vegetation, pane of the right shows a more recent fall with a boulder in Parleys Fork (5/10/2012)

Figure 3.12. Rockfall near Slope # 3. Angular boulders from Thaynes Formation recently covered with leaves and branches (10/16/2011)

Figure 3.13. Pronounced soil creep next to Boring B – 8

Figure 3.14. Pronounced soil creep on west side of Todd's Meadow near boring B – 1

Figure 3.15, Stair-stepped Tufa deposit at Red Butte Creek and Parleys Fork

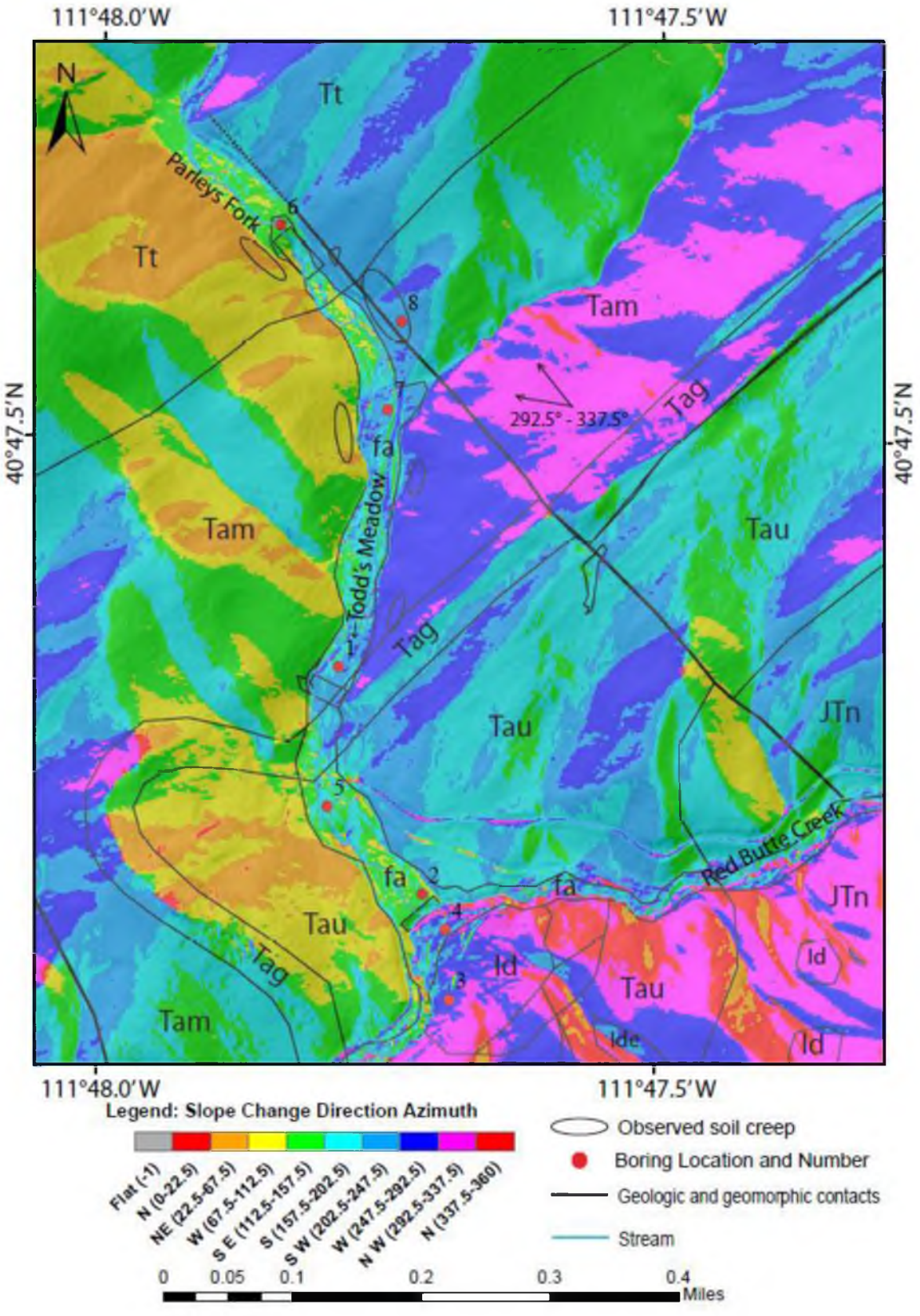

Figure 3.16, Aspect map of study area

B - 6 Dynamic Cone Pentrometer Data

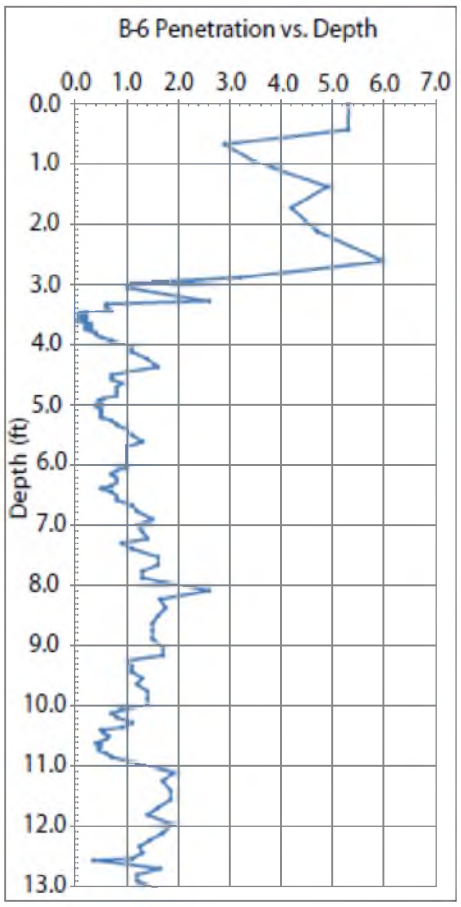

Boring: B - 6

Date Drilled: 11/15/2011 — Groundwater Depth / EL (ft): 15.8 / 5958.2

Elevation (ft): 5974 — Datum: MSL

Total Depth (ft): 19.5 — Logged By: Jimmy Schloss

Northing: 40.794083 — Easting: -111.797317

Depth (ft)	Graphic Log	Soil Desciption and Classifica (USCS System)	Moisture Content,%	Density, γ lb/ft^3	Atterberg Limits LL / IP(%
0.0–2.5		**CH Fat Clay with Sand** Clay, mostly black. Organic , plant roots. Medium sand to coarsegrained tufa and medium to coarse sand from Thaynes Fm.	26.6	108.8	60.9 / 35.9
3.0–4.5		**SC - Clayey Sand** Mostly fine-grained sand to gravel sized tufa. Interbedded brown clay. Interbedded angular to rounded medium grained sand to gravel from the Thaynes Fm.	19.6		
5.0–6.5			20.8		38.8 / 15.8
7.0–8.0		Many Thaynes Fm. grains are coated in tufa.	25.6		
8.5–9.5		Charcoal found intermittently at depth.	24.9		38.6 / 18.7
10.0–11.5		Mollusk shells found intermittently at depth.	23.9	108.8	
12.0–13.5		Encountered tufa layer @ 12.8 feet. Used split spoon sampler to penetrate through.	23.9		35.7 / 18.7
15.5–17.0			28.1		45.8 / 26.8
17.5–18.0			24.1	115	
18.5–20.0		Can't drill past 19.5 feet or obtain samples. Recovered large gravel fromThaynes Fm.	23.5		36.9 / 11.9

Figure 3.17, B – 6 boring log and DCP data

B - 7 Dynamic Cone Pentrometer Data

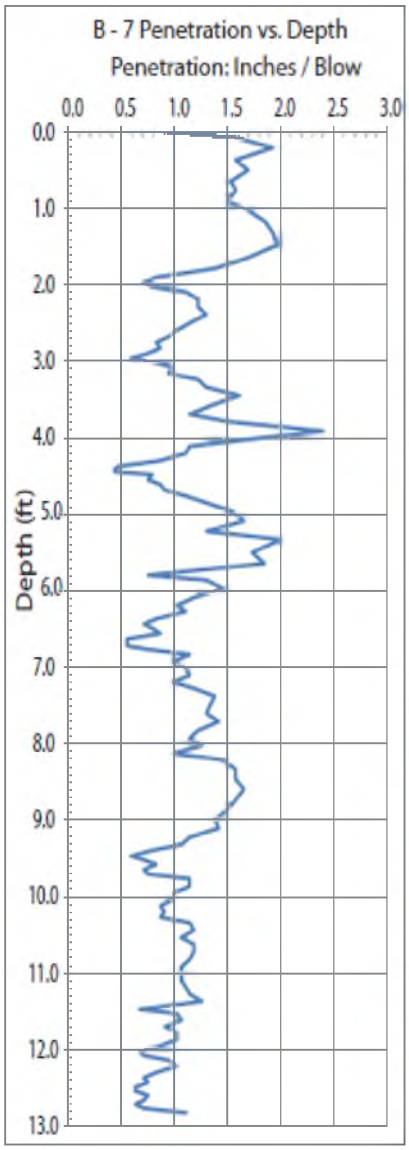

Boring: B - 7

Date Drilled: 11/15/2011

Groundwater Depth / EL (ft): 9.0 / 5844.0

Elevation (ft): 5852

Datum: MSL

Total Depth (ft): 14.5

Logged By: Jimmy Schloss

Northing: 40.791996

Easting: -111.795703

Depth (ft)	Graphic Log	Soil Description and Classification (USCS System)	Moisture Content (%)	Density, γ (lb/ft³)	Atterberg Limits LL / IP (%)
0.0		**CL - Sandy Lean Clay**			
0.5		Black, clayey, silty. Organic content, plant/tree roots. Some interbedded angular to subangular gravel from Ankareh & Thaynes Fm.	19.3	110	
1.0					
1.5			13.2		
2.0					
2.5		**CL - Sandy Lean Clay**			
3.0		Clay, dark brown to reddish. Interbedded sand and gravel. Angular to subangular gravel from Ankareh FM, Gartra Grit Member. Charcoal found intermittently at depth.			
3.5			11.9		
4.0					
4.5			15.1	110	34.0 / 17.0
5.0					
5.5			17.5		
6.0					
6.5					
7.0					
7.5					
8.0					
8.5			19.2		
9.0					
9.5			19.8		31.3 / 16.3
10.0		* Large gravel @ 9.5'. Some rounded gravel.			
10.5					
11.0					
11.5		Unable to retrieve samples from 10.5' - High water content. Muddy.		130	
12.0					
12.5					
13.0					
13.5		Mostly sandy & gravell. (Clay with sand and gravel matrix)			31.3 / 16.3
14.0					
14.5			20.0		

Figure 3.18, B – 7 boring log and DCP data

Boring: B - 8

Date Drilled: 11/15/2011, 7/18/12 — Groundwater Depth / EL (ft): 10.7 / 5937.6

Elevation (ft): 5948.3 — Datum: MSL

Total Depth (ft): 11.2 — Logged By: Jimmy Schloss

Northing: 40.793000 — Easting: -111.795500

Depth (ft)	Graphic Log	Soil Description and Classification (USCS System)	Moisture Content (%)	Density, γ (lb/ft³)	Atterberg Limits LL / IP (%)
0.0 - 0.2		**CL - ML Silty Sandy Clay** Clay, black. Plant leaves, organic detritus.			
0.2 - 0.5		**CL - ML Silty Sandy Clay** Clay, dark brown, reddish. Angular to subangular coarse-grained sand and gravel from Ankareh Fm. and Gartra Grit Member.			31.9 / 2.9
1.0					
1.5					
2.0			11.0		
2.5					
3.0				93.7	
3.5					
4.0					
4.5			14.8		
5.0					24.8 / 4.8
5.5		Clay, reddish/brown from 5.0 - 6.0'. Calcareous.	15.8		
6.0					
6.5					
7.0					
7.5				93.7	
8.0					
8.5		Clay, reddish brown. Some interbedded gravel from Anakerh, Mahongoany Member (Tam)			
9.0					
9.5					
10.0					
10.5					
11.0		Boulders from Ankareh Formation (Tam)			

Figure 3.19, B – 8 boring log

B - 1 Dynamic Cone Pentrometer Data

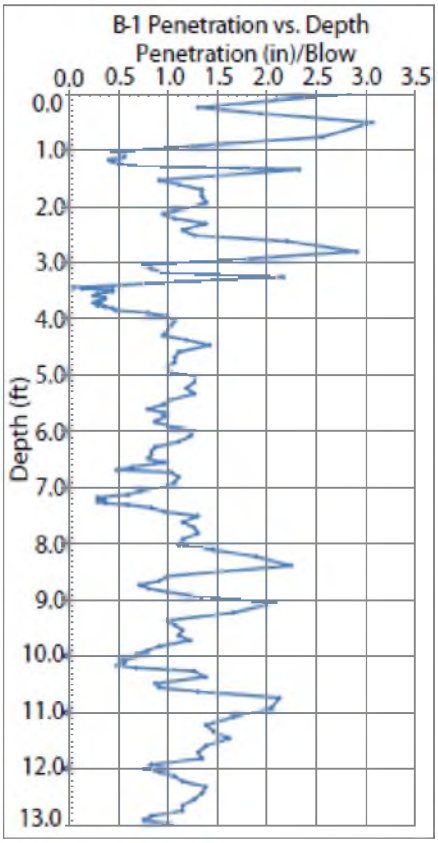

Boring: B - 1

Date Drilled: 10/18/2011 — Groundwater Depth / EL (ft): 16.0 / 5756.0

Elevation (ft): 5772 — Datum: MSL

Total Depth (ft): 22.0 — Logged By: Jimmy Schloss

Northing: 40.789067 — Easting: -111.796400

Depth (ft)	Graphic Log	Soil Description and Classification (USCS System)	Moisture Content (%)	Density, γ (lb/ft³)	Atterberg Limits LL / IP (%)
0.0–0.5		**CL - Sandy Lean Clay** Black. Plant leaves, detritus.	17.5	99.4	53.8 / 13.8
0.5–17.0		**CL - Sandy Lean Clay** Clay, gray and brown. Interbedded sub-angular to sub-rounded coarsegrained sand to gravel-from Ankareh Fm. Both mollusk and mussell shells found at intermittent depths. Charcoal found at intermittent depths. Fine sand to gravel-sized tufa throughout section.	11.8 13.9 17.7 13.9 19.1 18.0 16.8 27.7 22.2 23.3 29.9 29.0 33.5 28.5	99.4 99.4	49.0 / 19.0 41.8 / 13.8 39.4 / 14.4
17.0–22.0		**SC - Clayey Sand** Mostly fine sand to gravel-sized tufa withinterbedded clay. Slight increase in grainsize by weight. Both mollusk and mussell shells. Charcoal found intermittently at depth.	31.2 30.5	115	40.2 / 20.2

Figure 3.20, B – 1 boring log and DCP data

B - 5 Dynamic Cone Penetrometer Data

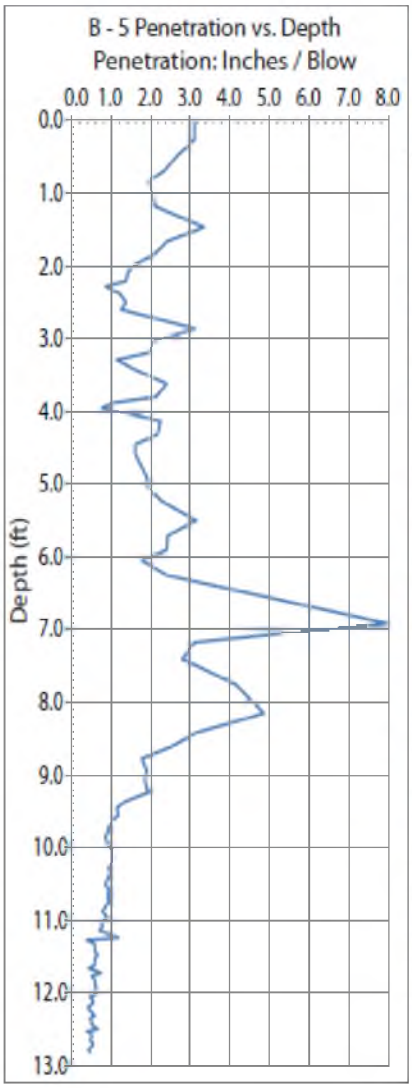

Boring: B - 5

Date Drilled: 10/30/2011

Groundwater Depth / EL (ft): 8.0 / 5692.3

Elevation (ft): 5700.3

Datum: MSL

Total Depth (ft): 16.0

Logged By: Jimmy Schloss

Northing: 40.787483

Easting: -111.787483

Depth (ft)	Graphic Log	Soil Description and Classification USCS System	Moisture Content (%)	Density, γ (lb/ft^3)	Atterberg Limits LL / IP (%)
0.0 – 1.5		**CL - Sandy Lean Clay** Clay with plant detritus.Interbedded coarse to fine grained sands from Ankareh Fm and Gartra Grit Member	22.0	110	45.6 / 15.6
2.0 – 9.0		**CL - Sandy Lean Clay** Clay with interbedded subangular coarse to fine grained sands from Ankareh Fm and Gartra Grit Member Also has interbedded fine to gravel-sized tufa grains. Mollusk shells. Charcoal found interminttently.	21.1		38.0 / 13.2
					29.6 / 11.6
			22.0	110	
			23.1		40.4 / 25.4
			26.0		37.0 / 17.0
9.5 – 15.5	B-C	**CL - Lean Clay with Sand** Mostly clay, finer grains. * Decrease in grain size by weight. Some angular to subangular coarse-grained sand to gravel from Ankareh Fm Upper member and Gartra Grit Member. Little to no tufa. Mollusk and mussell shells found intermittently. Charcoal found intermittently. Charcoal dated at 4370 Years B.P.	21.5		
			24.3	130	
			26.0		30.0 / 10.0
			22.0		

Figure 3.21, B – 5 boring log and DCP data

B - 2 Dynamic Cone Penetrometer Data

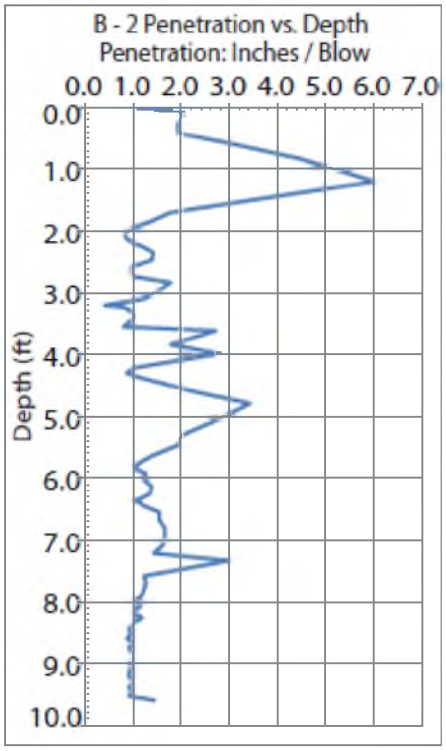

Boring: B - 2

Date Drilled: 10/18/2011 — Groundwater Depth / EL (ft): 10.0 / 5632.0

Elevation (ft): 5642 — Datum: MSL

Total Depth (ft): 16.0 — Logged By: Jimmy Schloss

Northing: 40.786500 — Easting: -111.795120

Depth (ft)	Graphic Log	Soil Description and Classification (USCS System)	Moisture Content(%)	Density, γ (lb/ft³)	Atterberg Limits LL / IP(%)
0.0–1.5		CH - Sandy Fat Clay Clay with interbedded coarse to fine grained sand from Ankareh		99.4	55.4 / 15.4
1.5–7.5		**CL - Sandy Lean Clay** Clay with interbedded subangular coarse to fine grained sands from Ankareh Fm. Also has interbedded fine to gravel-sized tufagrains. Mollusk shells. Charcoal found interminttently.	20.8 16.5 19.0 18.0 21.4 23.8 27.0	99.4	38.4 / 18.4
7.5–15.5		**CH - Sandy Fat Clay** Clay with interbedded subangular coarse to fine grained sands from Ankareh Fm. Possibly weathered Nugget Fm * Decrease in grain size by weight. Also has interbedded fine to gravel-sized tufa grains. Mollusk shells. Charcoal found interminttently. Charcoal dated at 4370 Years	26.0 28.4 26.4 36.2 31.3 40.2 38.6	99.4 110	58.2 / 30.2 65.5 / 39.4
15.5–19.5		**Landslide Material** Angular to sub-angular coarse sand to gravel from Nugget Sandstone Fm. Boulder-sized Nugget Fm. sandstone recovered with split spoon sampler. Splintered wood and charcoal.		120	

Figure 3.22, B – 2 boring log and DCP data

Boring: B - 4

Date Drilled: 10/18/2011 Groundwater Depth / EL (ft): NA

Elevation (ft): 5642 Datum: MSL

Total Depth (ft): 4.5 Logged By: Jimmy Schloss

Northing: 40.786100 Easting: -111.794767

Depth (ft)	Graphic Log	Soil Desciption and Classification (USCS System)	Moisture Content (%)	Density, γ (lb/ft^3)	Atterberg Limits LL / PL (%)
0.0		**CL - Sandy Lean Clay** Clay with organic detritus, plant roots. Coarse grained sand to gravel-sized Ankareh Fm. and Nugget SS Fm.	16.1	110	
0.5					
1.0			16.8		
1.5					
2.0		**CL - Sandy Lean Clay** Clay with coarse grained sand sized Ankareh Fm. and Nugget SS Fm. Gravel-sized tufa.	14.1	110	
2.5					
3.0					
3.5		**SC - Clayey Sand** Mostly coarse-grained sand to gravel-sized tufa with interbedded clay. Mollusk shells, charcoal.	15.6	130	
4.0			18.0		
4.5		**Tufa Layer** Assumed tufa layer. Could not drill thorugh layer or penetrate with split spoon sampler.			
5.0?					
5.5?	?	**Unknown - Sandy Clay or Landslide** Assumed to be sandy clay or landslide deposit based on observations from creek bed and topography.			
6.0?					
6.5?					

Figure 3.23, B – 4 boring log

Boring: B - 3

Date Drilled: 10/30/2011 Groundwater Depth / EL (ft): NA

Elevation (ft): 5631 Datum: MSL

Total Depth (ft): 3.5 Logged By: Jimmy Schloss

Northing: 40.785300 Easting: -111.794700

Depth (ft)	Graphic Log	Soil Desciption and Classification (USCS System)	Moisture Content (%)	Density, γ (lb/ft^3)	Atterberg Limits
					LL / PL (%)
0.0		**CL - Lean Clay with Sand**			
0.5		Clay with organic detritus, plant roots.			
1.0		**Landslide Material**			
1.5		Poorly sorted materials including angular boulders from the Nugget SS Fm. Reddish clay matrix derived from the Ankareh Fm., highly plastic clay. Some plant roots.			
2.0					
2.5		* Impossible to drill thorugh due to boulders. Needed to trench a section to 3.5 feet.			
3.0					
3.5					

Figure 3.24, B – 3 boring log

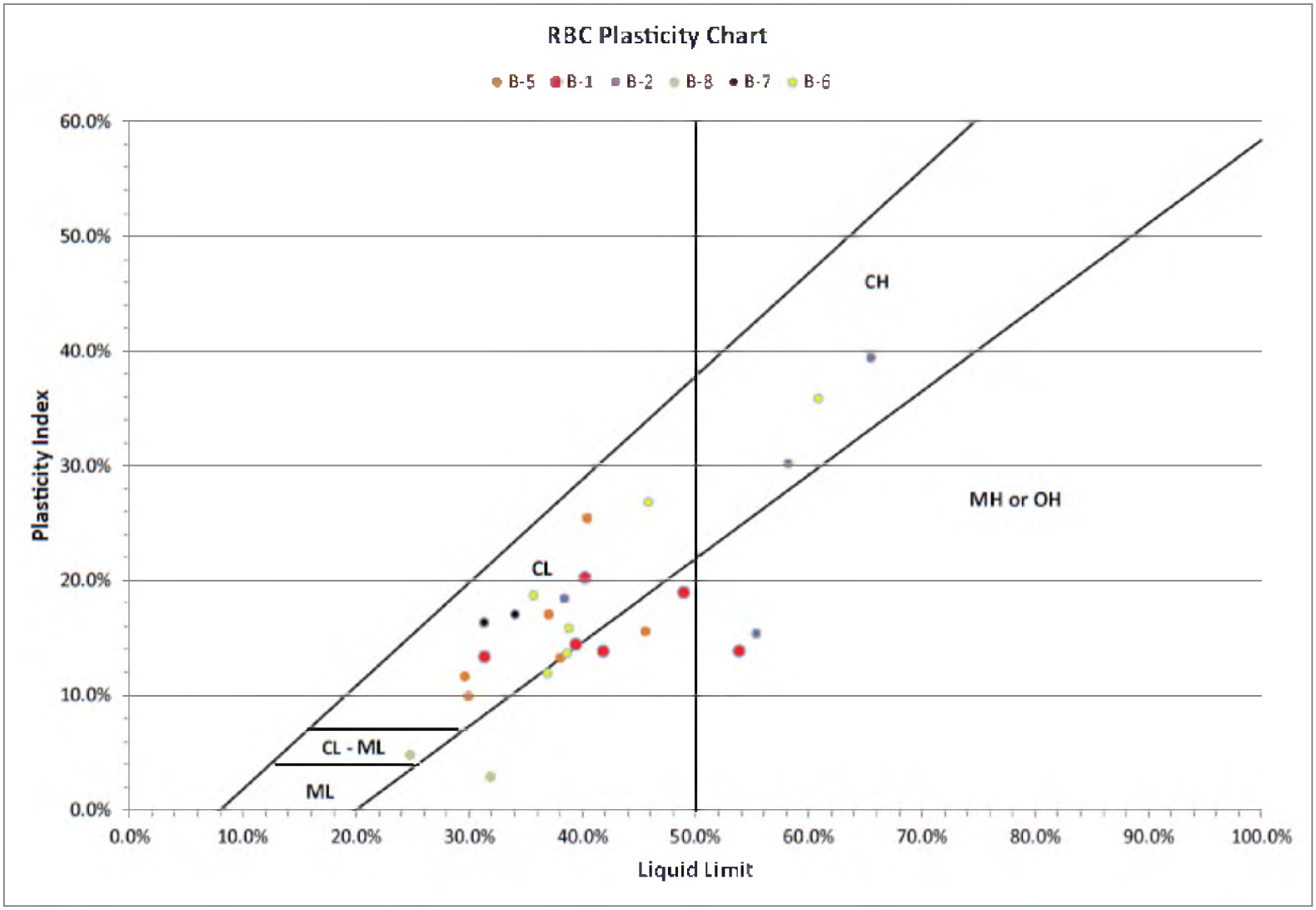

Figure 3.25, Plasticity chart

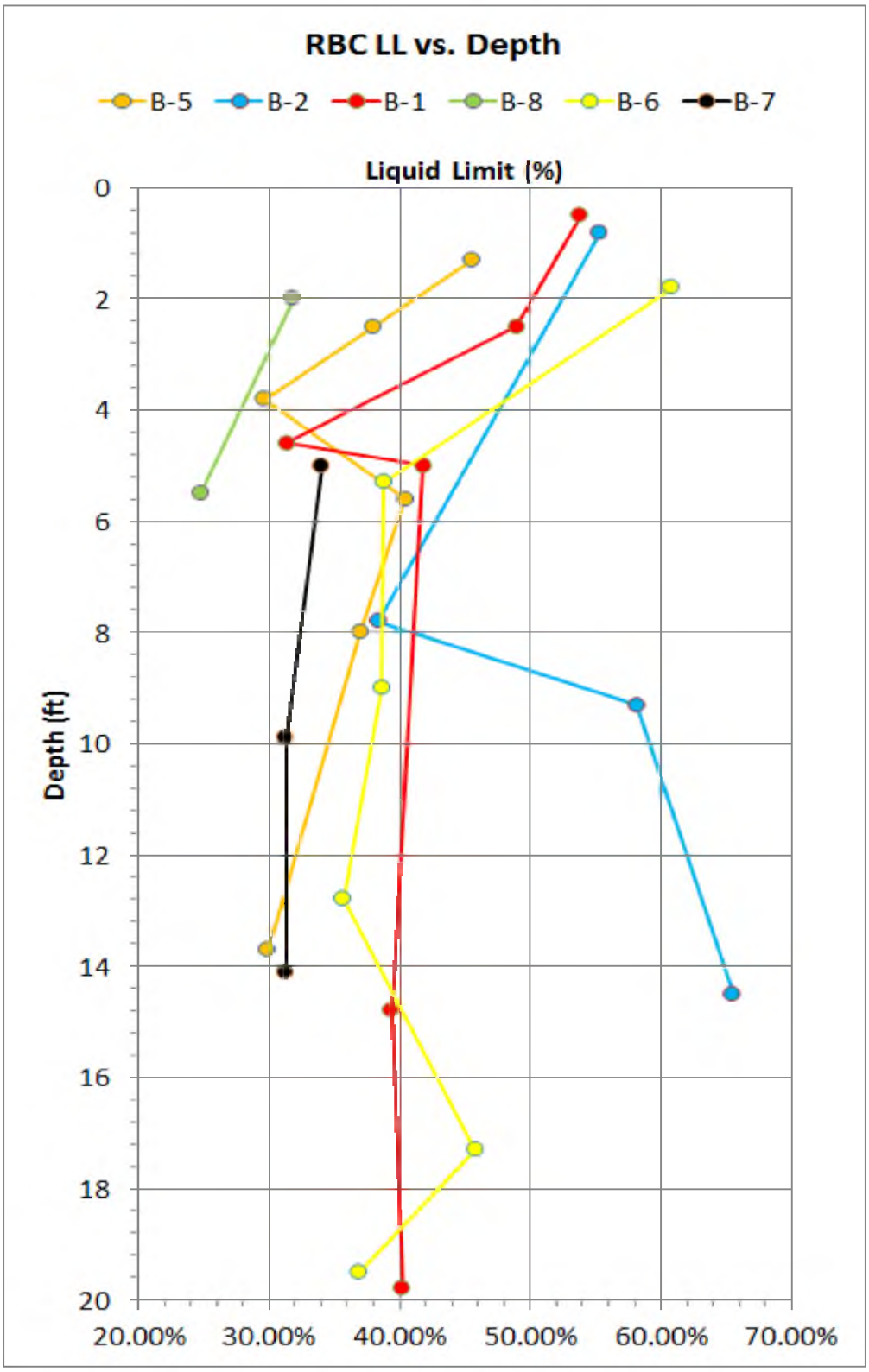

Figure 3.26, Liquid limit vs. depth

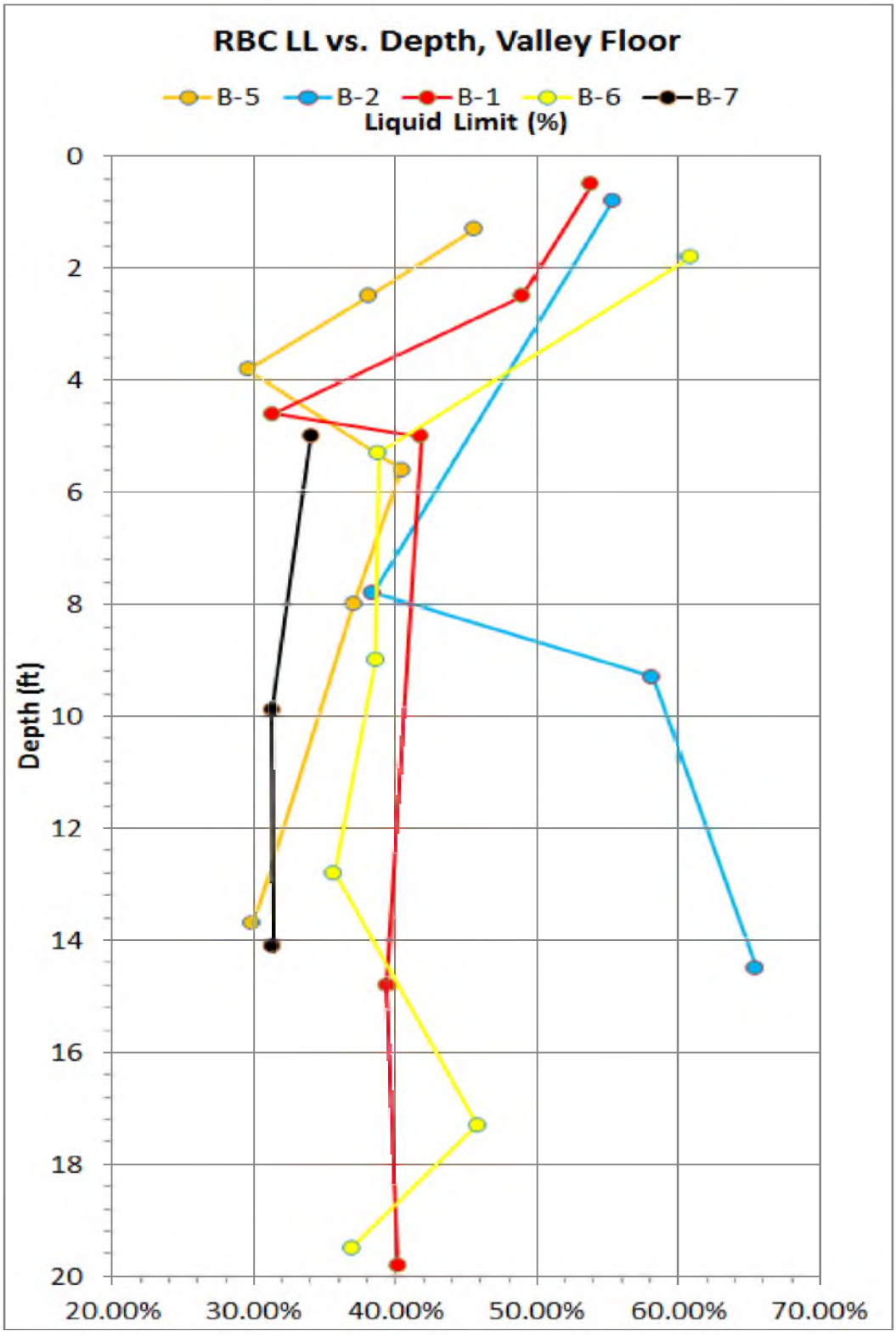

Figure 3.27, Specific gravity vs. depth

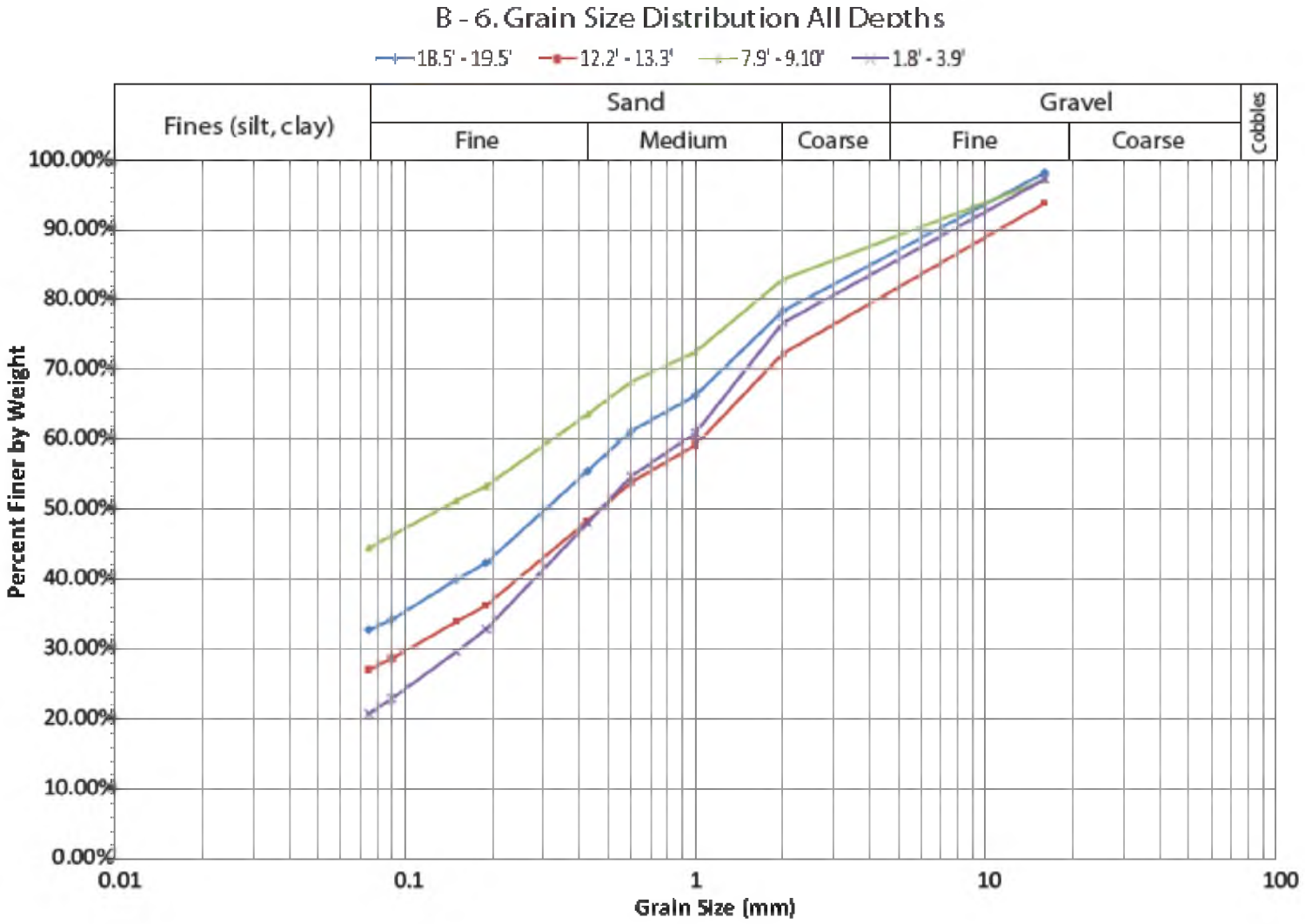

Figure 3.28, B – 6 Grain size distribution curves

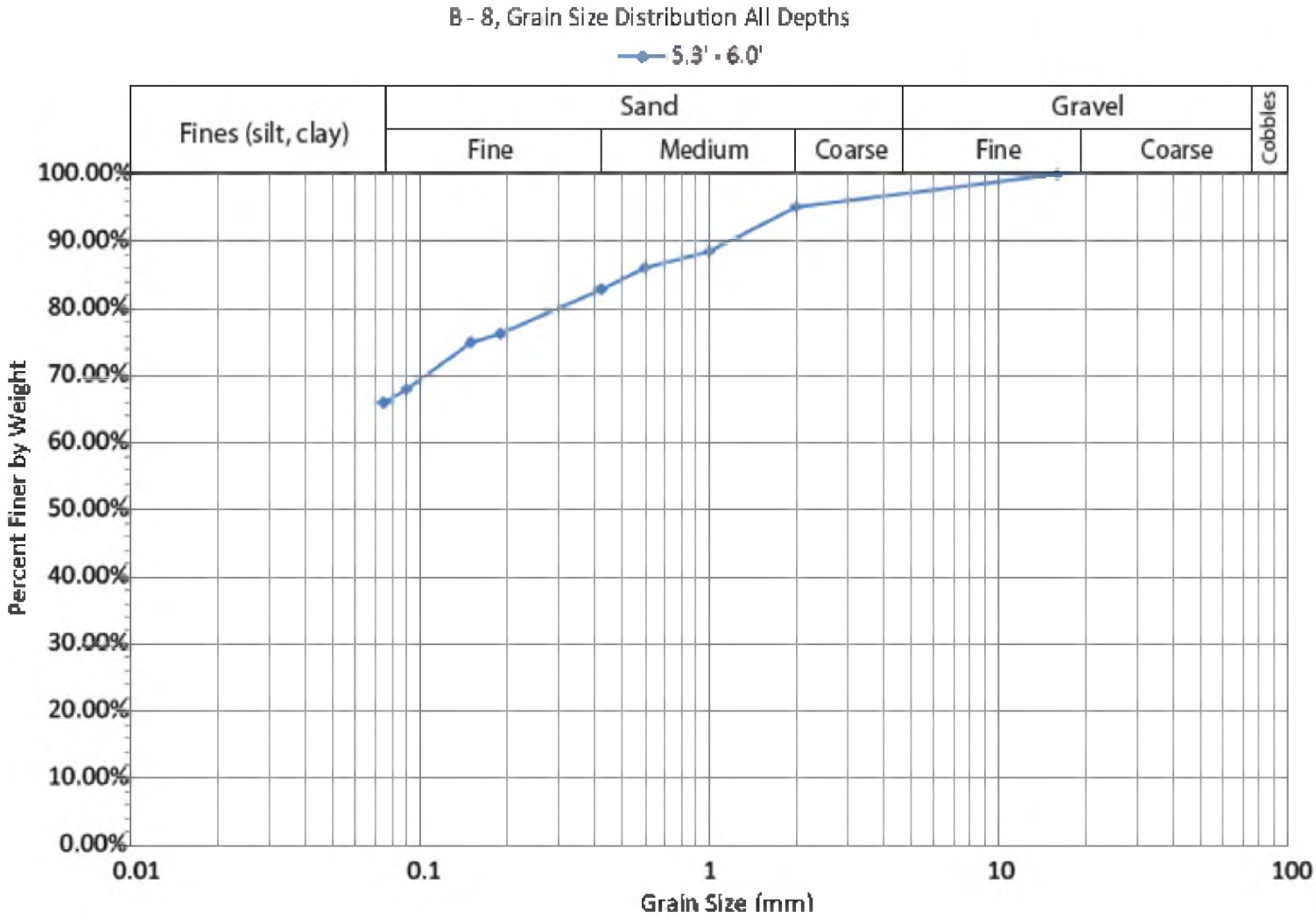

Figure 3.29, B – 8 Grain size distribution curves

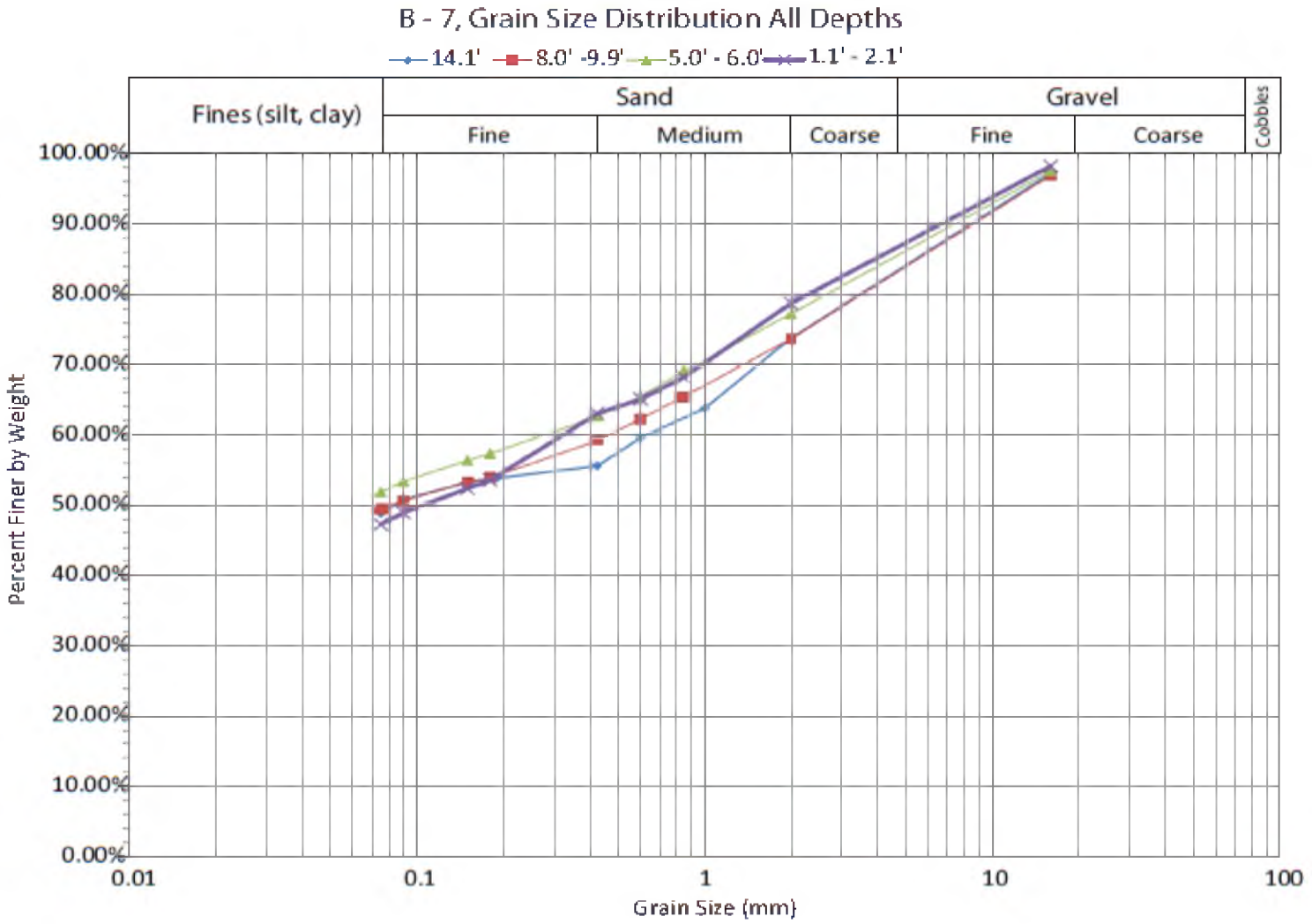

Figure 3.30, B – 7 Grain size distribution curves

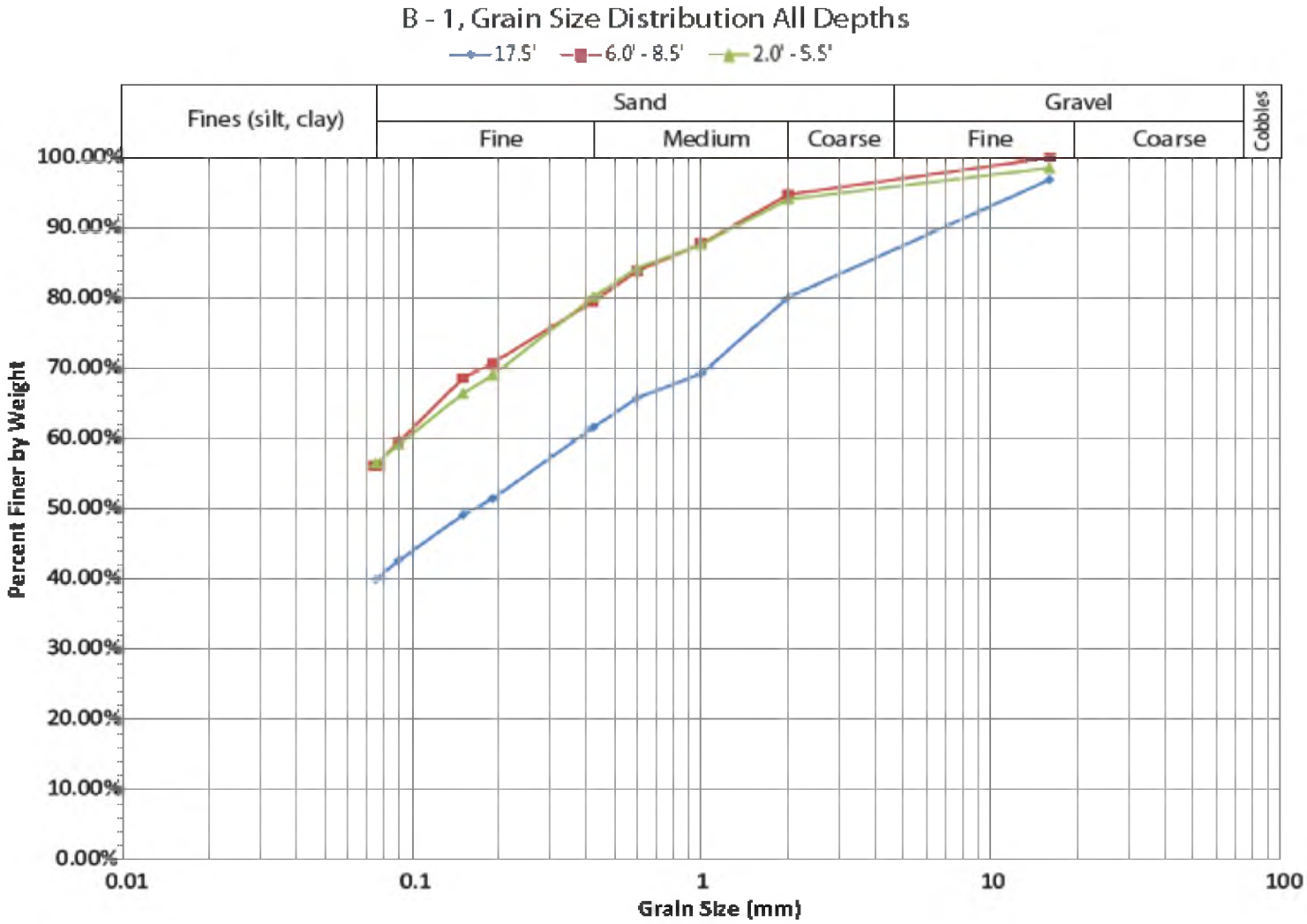

Figure 3.31, B – 1 Grain size distribution curves

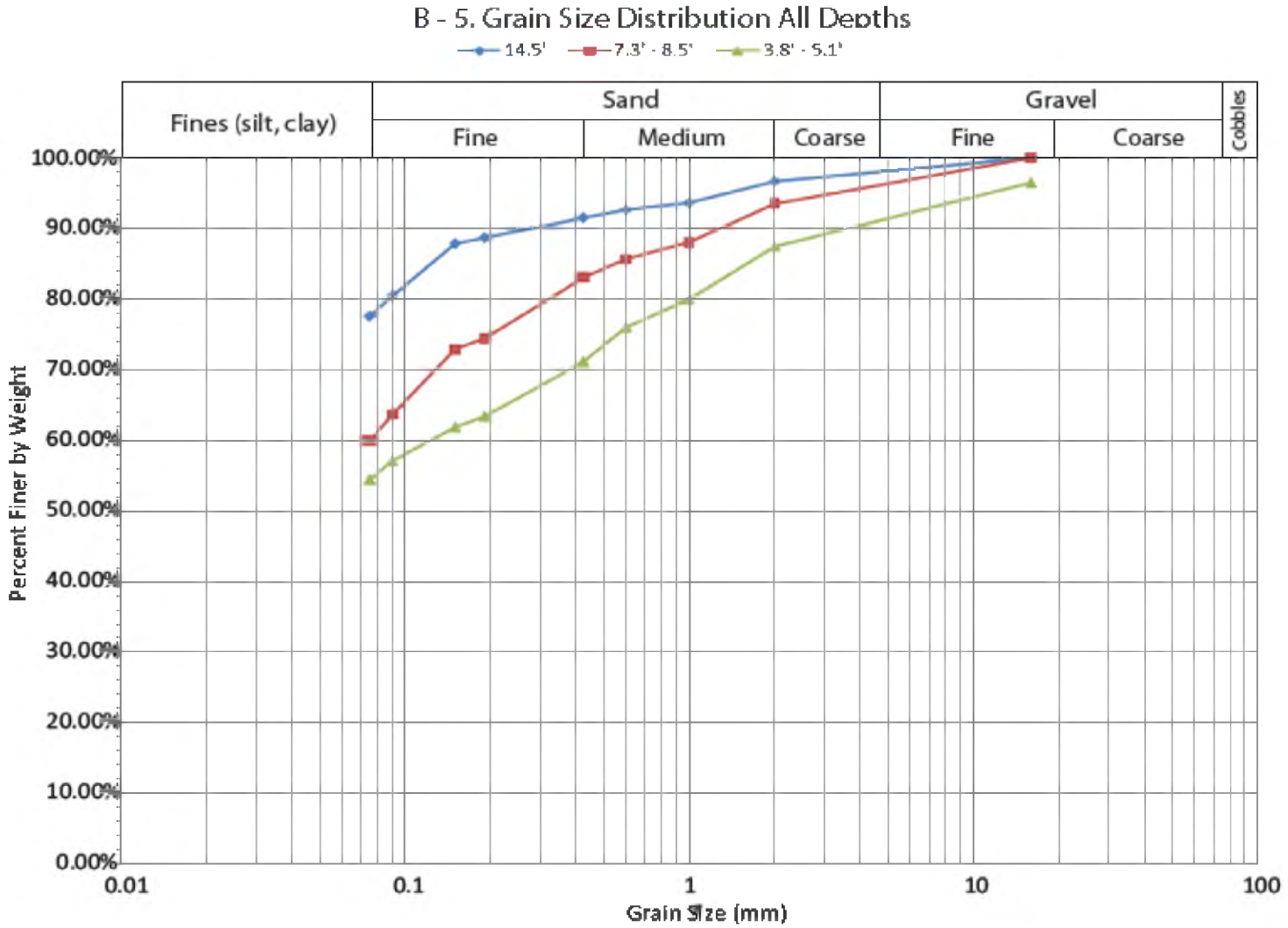

Figure 3.32, B – 5 Grain size distribution curves

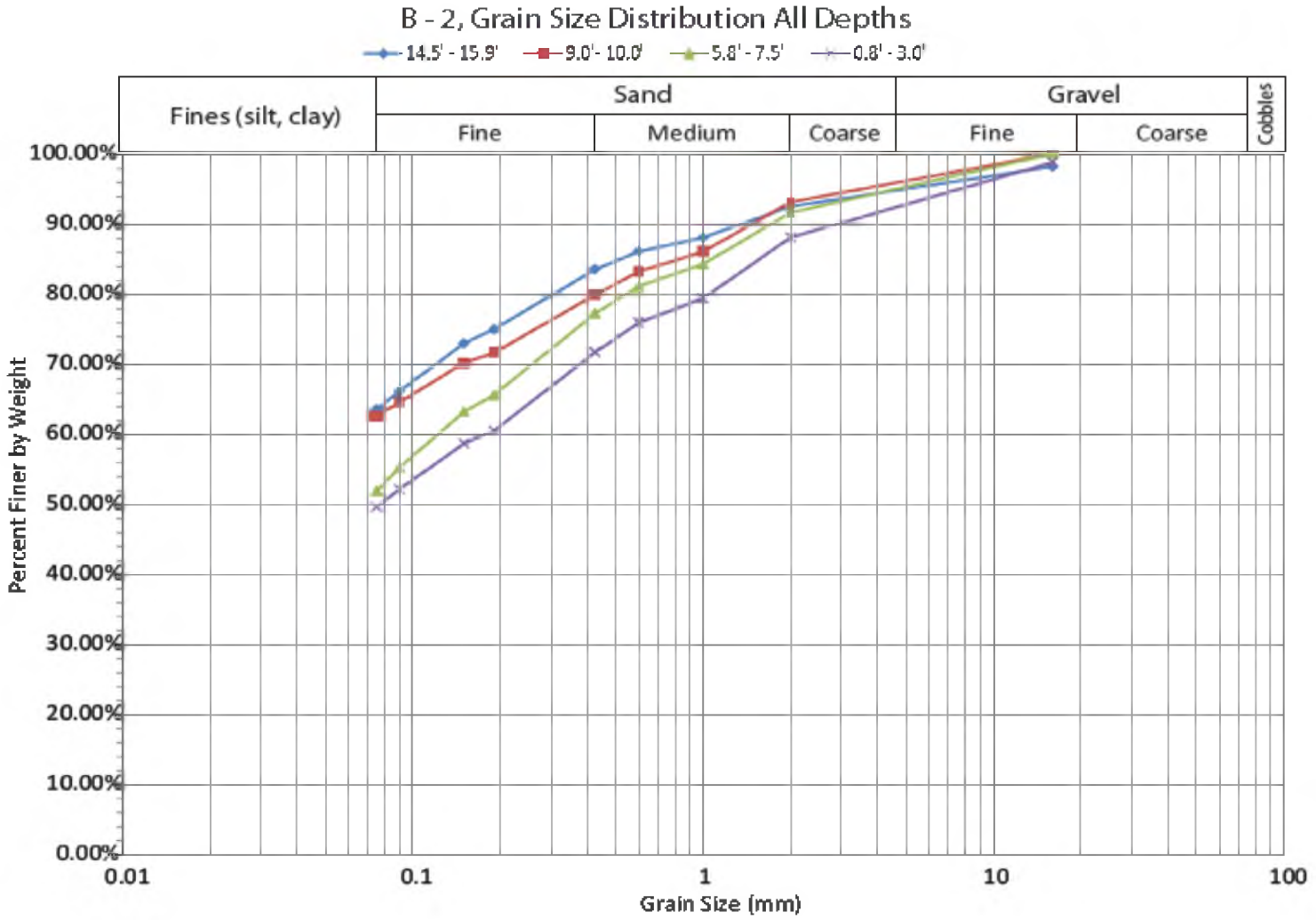

Figure 3.33, B – 2 Grain size distribution curves

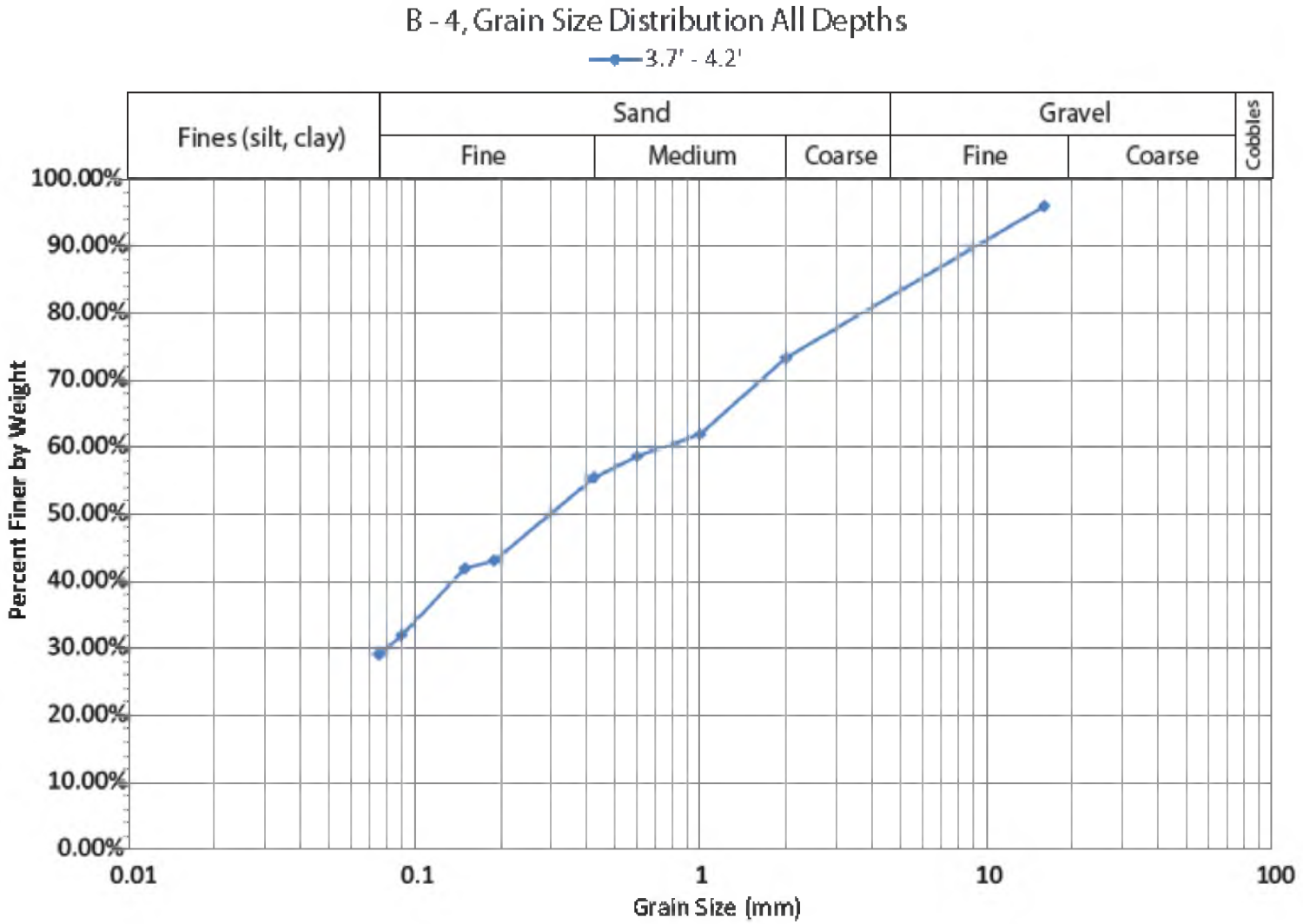

Figure 3.34, B – 4 Grain size distribution curves

Table 3.1, Unit weight of soils

Boring #	USCS Soil Type	γ (lb/ft^3)	γ_{sat} (lb/ft^3)	Determination
B - 1	CL	99.4	115	**Laboratory, Knight Pièsold**
B - 2	CL	80 - 110	75 - 130	Coudto, 1999
B - 2	CH	80 - 100	70 - 125	Coudto, 1999
B - 3	-	-	-	-
B - 4	CL	80 - 110	75 - 130	Coudto, 1999
B - 5	CL	80 - 110	75 - 130	Coudto, 1999
B - 6	SC	108.8	115	**Laboratory, Knight Pièsold**
B - 7	CL	80 - 110	75 - 130	Coudto, 1999
B - 8	CL - ML	93.7	112.6	**Laboratory, Knight Pièsold**

Table 3.2, Drained shear strength parameters

Stability Model	Boring #	Layer #	γ (lb/ft^3)	USCS Soil Type	Stress Cohesion, a, (lb/ft^2)	Friction angle, ψ	Stress Cohesion, c', (lb/ft^2)	Stress Friction angle, ϕ'
Slope # 2	B-1	1	99.4	-	-	-	-	-
Slope # 1	B-2	1	99.4	CL	132.0	35.0	184.9	44.4
Slope # 3	B-6	1	108.8	SC	0.0	35.0	0.0	42.4
Infinite Slope	B-8	1	93.7	CL - ML	0.0	32.0	0.0	38.7

Table 3.3, Undrained shear strength parameters

Slope Stability Model	Boring #	Layer #	γ (lb/ft^3)	USCS Soil Type	Total Stress Cohesion, c_u, (lb/ft2)	Total Stress Friction angle, ϕ_u
Slope # 2	B-1	1	99.4	CL	0	37.6
Slope # 1	B-2	1	99.4	CL	25	33
	B-2	2	110	CH	150	25
	B-2	3	120	GW-GC	0	40
Slope # 3	B-6	1	108.8	SC	0	33
Infinite Slope	B-8	1	93.7	CL - ML	0	33

Figure 3.35, Freshwater mollusk (snail shells), left pane shows what is believed to be a *Gyraulus* and right pane shows what is believed to be a *Pyrgulopsis*

Figure 3.36, B – 2, 13.0 ft. Sedimentary structures, left pane shows graded bedding, right pane shows cross-bedding with snail shells, sand, and tufa

Figure 3.37, B – 7, 7.5 ft. Cross-bedded gravel and sand interbedded within clay.

Table 3.4, Groundwater data

				Casing	Casing	10/18/2011		10/30/2011		11/15/2011		11/21/2011		7/18/2012	
Boring / Piezometer	Elevation (ft)	Northing	Easting	Height Above Surface (ft)	Depth Below Surface (ft)	Measured Depth (ft)	Water Elevation (ft)	Measured Depth (ft)	Water Elevation (ft)	Measured Depth (ft)	Water Elevation (ft)	Measured Depth (ft)	Water Elevation (ft)	Measured Depth (ft)	Water Elevation (ft)
B - 2	5642.8	40.787	-111.795	-	-	-	-	10.00	5632.80	-	-	9.80	5633.00	10.30	5632.50
P - 1 - 1	5643.3	40.787	-111.795	1.67	28.23	-	-	-	-	-	-	16.50	5628.47	17.10	5627.87
P - 1 - 2	5643.8	40.787	-111.795	2.13	19.28	-	-	-	-	-	-	14.25	5631.68	14.80	5631.13
P - 1 - 3	5644.3	40.787	-111.795	2.58	11.92	-	-	-	-	-	-	-	-	-	-
P - 2 - 1	5700.6	40.787	-111.797	2.00	19.25	-	-	-	-	-	-	10.27	5692.37	10.70	5691.94
P - 2 - 2	5700.6	40.787	-111.797	2.46	12.79	-	-	-	-	-	-	-		-	-
B - 5	5700.6	40.787	-111.797	-	-	-	-	8.00	5692.64	-	-	7.90	5692.74	8.30	5692.34
N5-10	5771.0	40.789	-111.796	0.60	26.3	-	-	-	-	-	-	15.00	5756.60	15.20	5756.40
N5-14	5771.0	40.789	-111.796	1.00	50.40	-	-	-	-	-	-	25.15	5746.85	26.20	5745.80
N5-15	5771.0	40.789	-111.796	0.40	51.10	-	-	-	-	-	-	24.35	5747.05	25.10	5746.30
B - 1	5771.2	40.789	-111.796	-	-	16.00	5755.20	-	-	-	-	16.00	5755.20	16.00	5755.20
N5-10	5771.6	40.789	-111.796	0.70	30										
N5-14	5771.6	40.789	-111.796	1.00	48.2										
N5-15	5771.6	40.789	-111.796	0.35	51.4	-	-	-	-	-	-	-	-	-	-
S3-12	5771.3	40.789	-111.796	0.40	48.10	-	-	-	-	-	-	-	-	23.50	5748.20
S2-8	5775.9	40.789	-111.796	0.40	25.70	-	-	-	-	-	-	-	-	24.40	5755.9
S2-13	5775.9	40.789	-111.796	0.50	41.50	-	-	-	-	-	-	-	-	27.20	5753.2
B - 7	5852.0	40.792	-111.796	-	-	-	-	-	-	9	5843.0	-	-	-	-
B - 6	5974.0	40.794	-111.797	-	-	-	-	-	-	15.8	5958.2	-	-	-	-

Table 3.5, Seismic refraction data and calculations

FORWARD TRAVERSE		
Geophone	Distance (m)	Time (s)
1	0	0.006111
2	3	0.010556
3	6	0.02
4	9	0.027222
5	12	0.036944
6	15	0.0425
7	18	0.051944
8	21	0.055833
9	24	0.056528
10	27	0.06
11	30	0.060556
12	33	0.060694
13	36	0.061111
14	39	0.061667
15	42	0.061806
16	45	0.062222
17	48	0.065278
18	51	0.065556
19	54	0.066111
20	57	0.066667
21	60	0.067222
22	63	0.07
23	66	0.070556
24	69	0.071111

REVERSE TRAVERSE		
Geophone	Distance (m)	Time (s)
24	69	0.000833
23	66	0.007222
22	63	0.016389
21	60	0.025556
20	57	0.036111
19	54	0.041944
18	51	0.045556
17	48	0.046667
16	45	0.05
15	42	0.051667
14	39	0.055556
13	36	0.056389
12	33	0.056944
11	30	0.060556
10	27	0.061389
9	24	0.061944
8	21	0.0625
7	18	0.065
6	15	0.065667
5	12	0.066111
4	9	0.066389
3	6	0.066667
2	3	0.066944
1	0	0.07

FORWARD TRAVERSE		
	Slope = 1/v	1/Slope = v (m/s)
Line 1	0.002556	391.3043
Line 2	0.000713	1402.597
Line 3	0.00031	3230.238
tif1 (s)	0.0422	
tif2 (s)	0.0482	
v 1 (m/s)	391.3	
v 2 (m/s)	1402.6	
v 3 (m/s)	3230.2	
h 1(m)	8.6	
h 1 (ft)	28.2	
h 2(m)	3.6	
h 2 (ft)	11.7	
BR (ft)	46.2	

REVERSE TRAVERSE		
	Slope = 1/v	1/Slope = v (m/s)
Line 1	-0.00296	337.5
Line 2	-0.00074	1347.193
Line 3	-0.00028	3588.401
tir1 (s)	0.032	
tir2 (s)	0.05	
v 1 (m/s)	337.5	
v 2 (m/s)	1347.2	
v 3 (m/s)	3588.4	
h 1(m)	5.6	
h 1 (ft)	18.3	
h 2(m)	12.4	
h 2 (ft)	40.7	
BR (ft)	59.0	

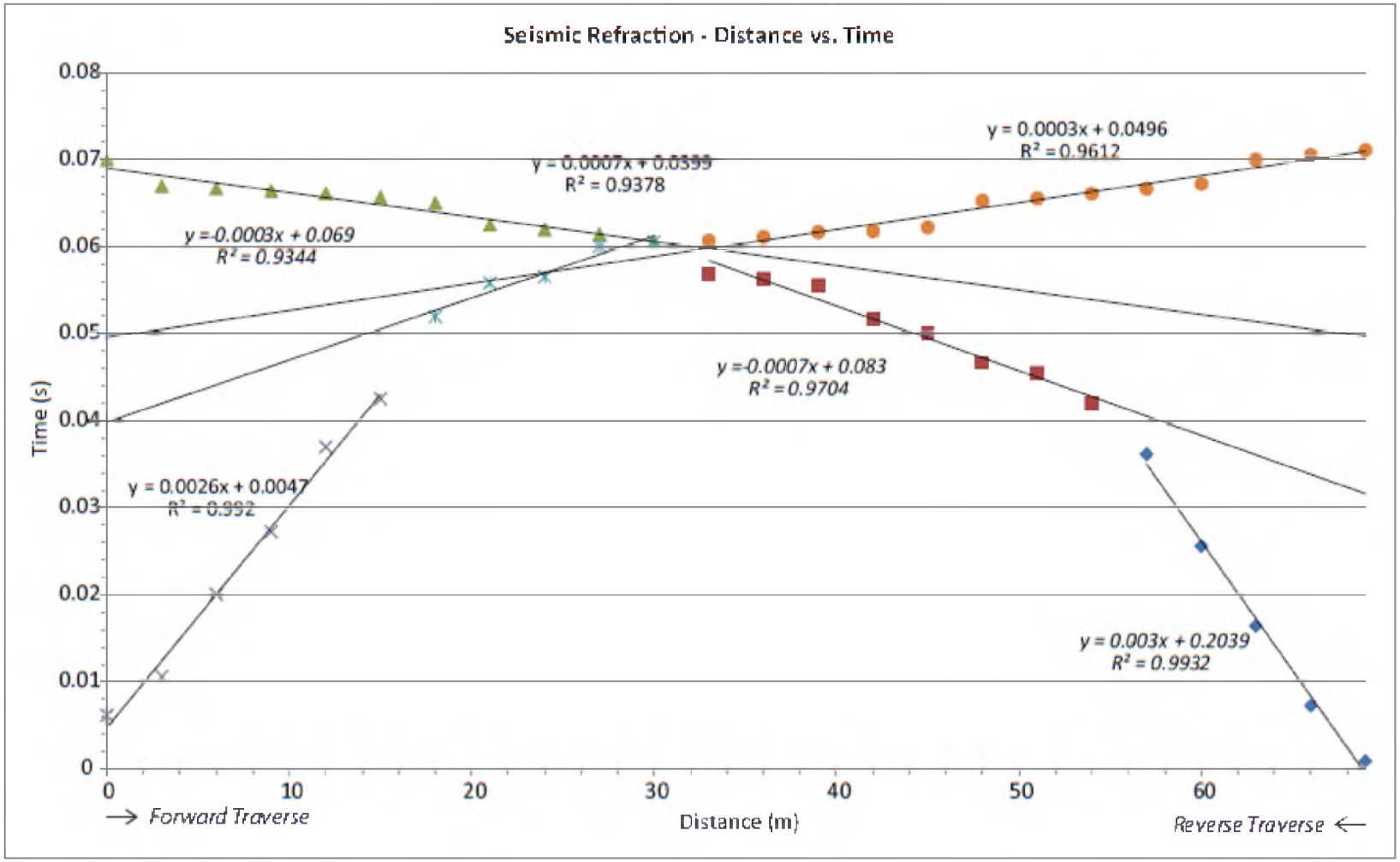

Figure 3.38, Plot of seismic refraction data

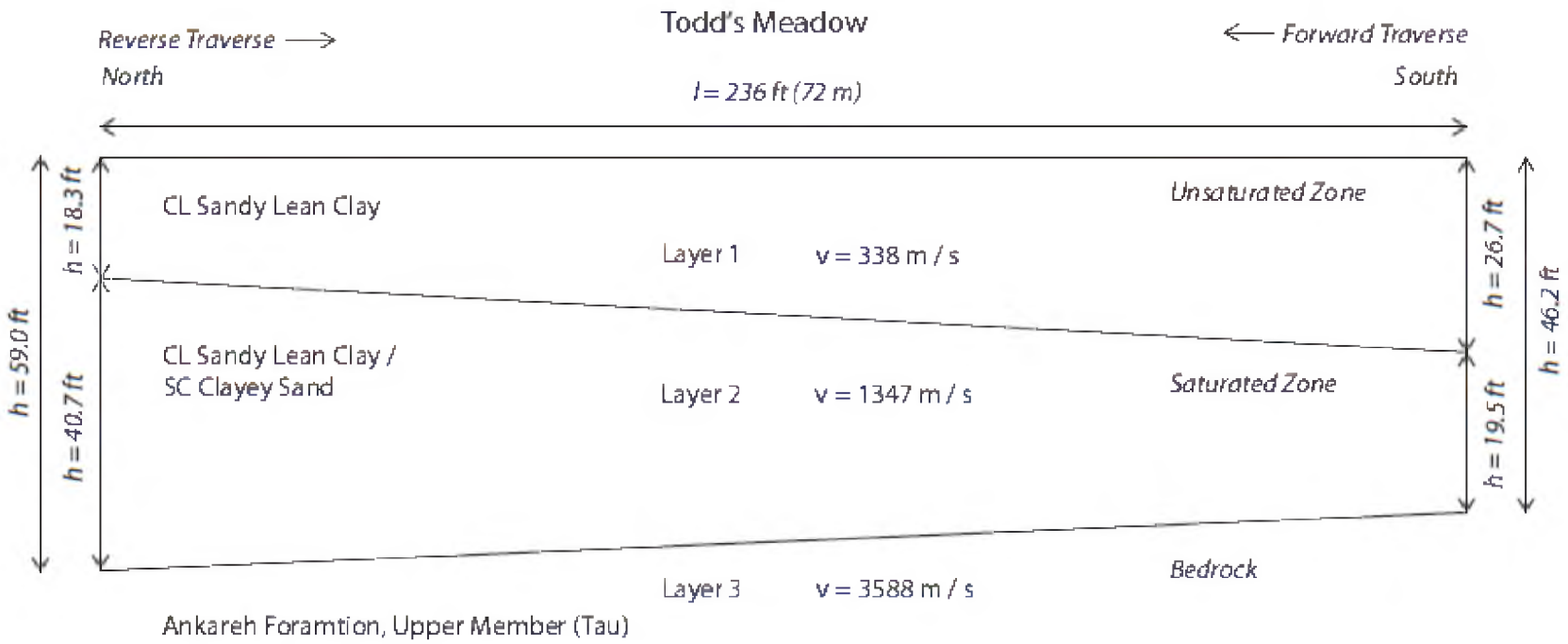

Figure 3.39, Subsurface model based on seismic refraction data, Todd's Meadow

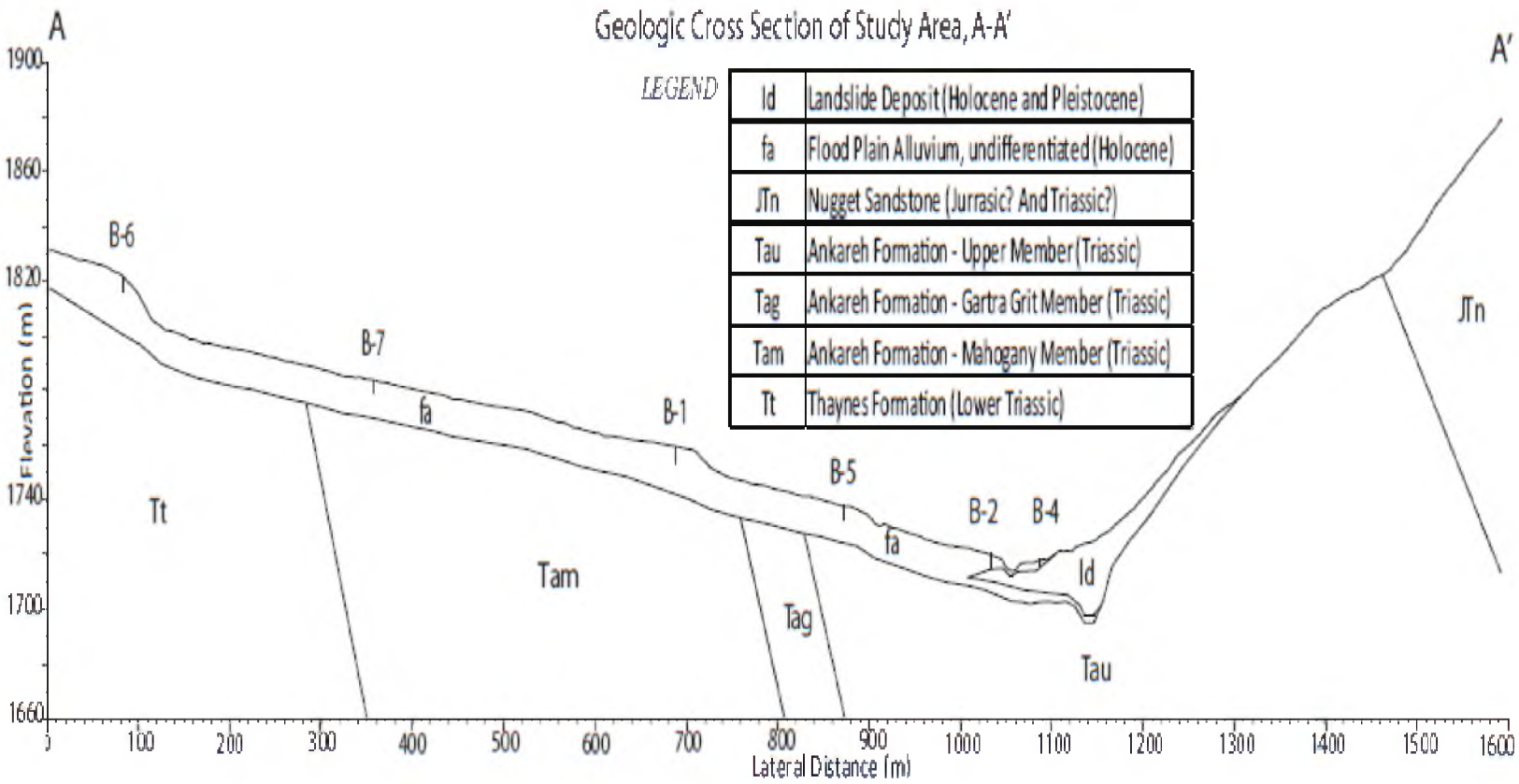

Figure 3.40, Cross section of study area A-A'

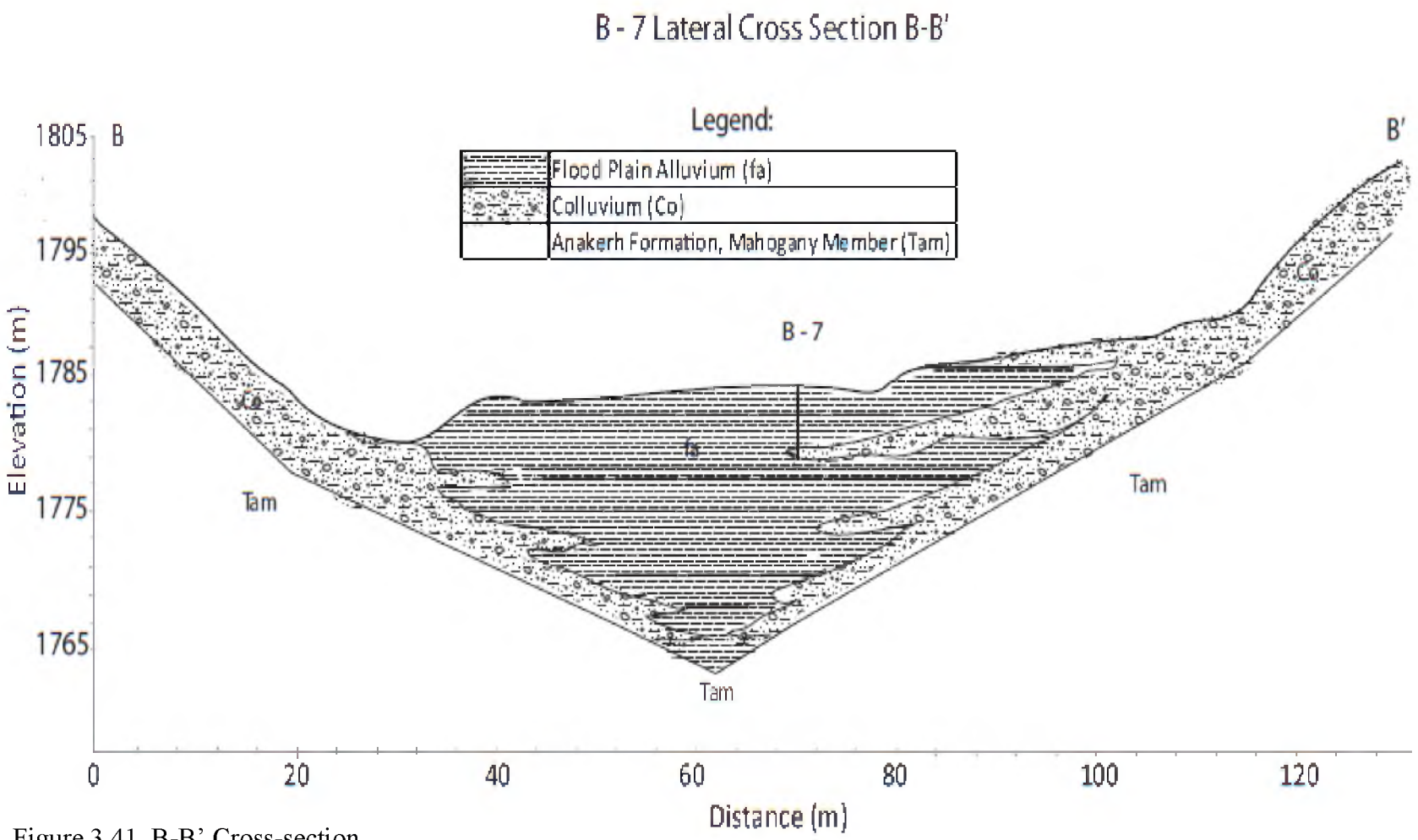

Figure 3.41, B-B' Cross-section

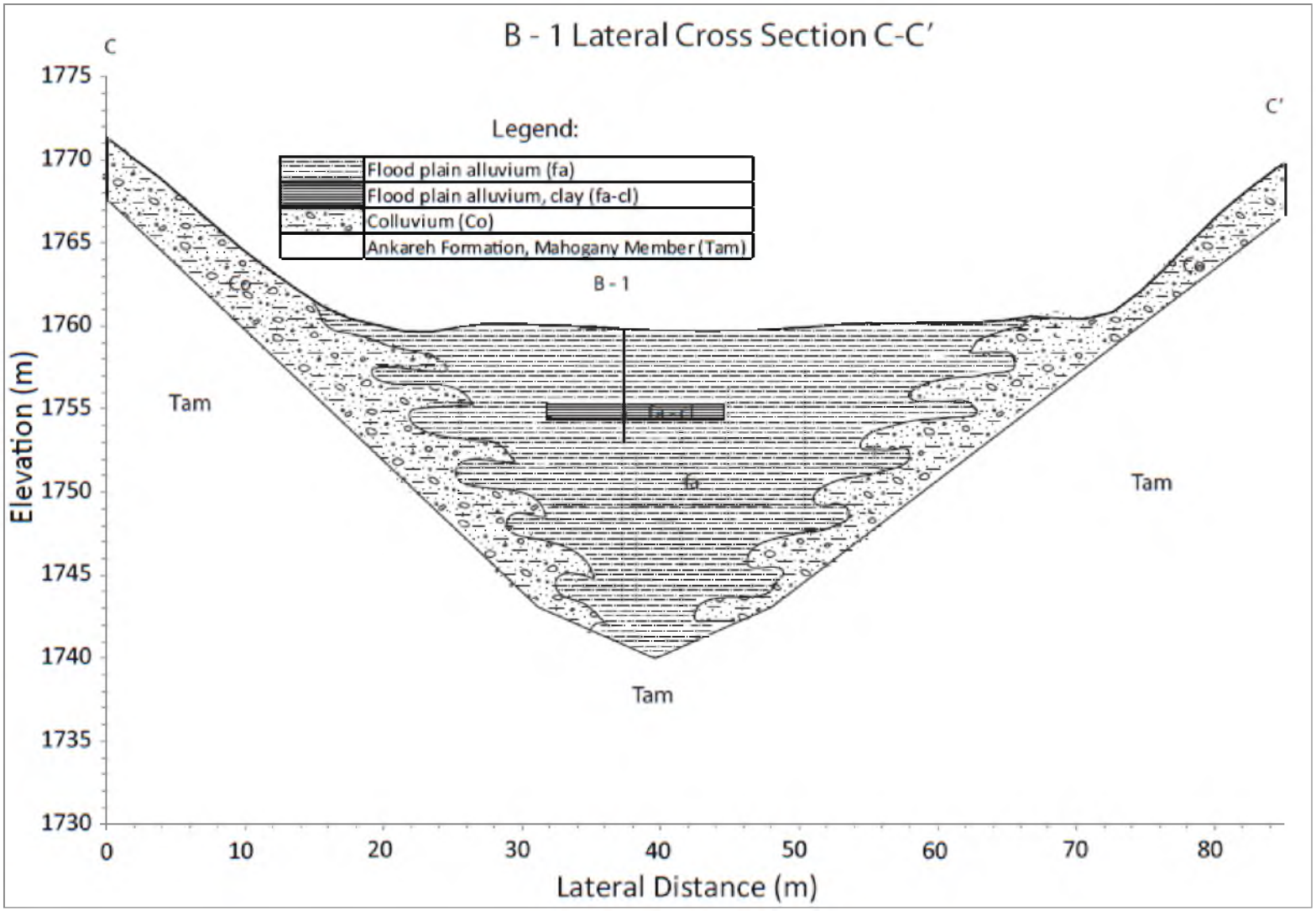

Figure 3.42, B – 1 Lateral cross-section C-C'

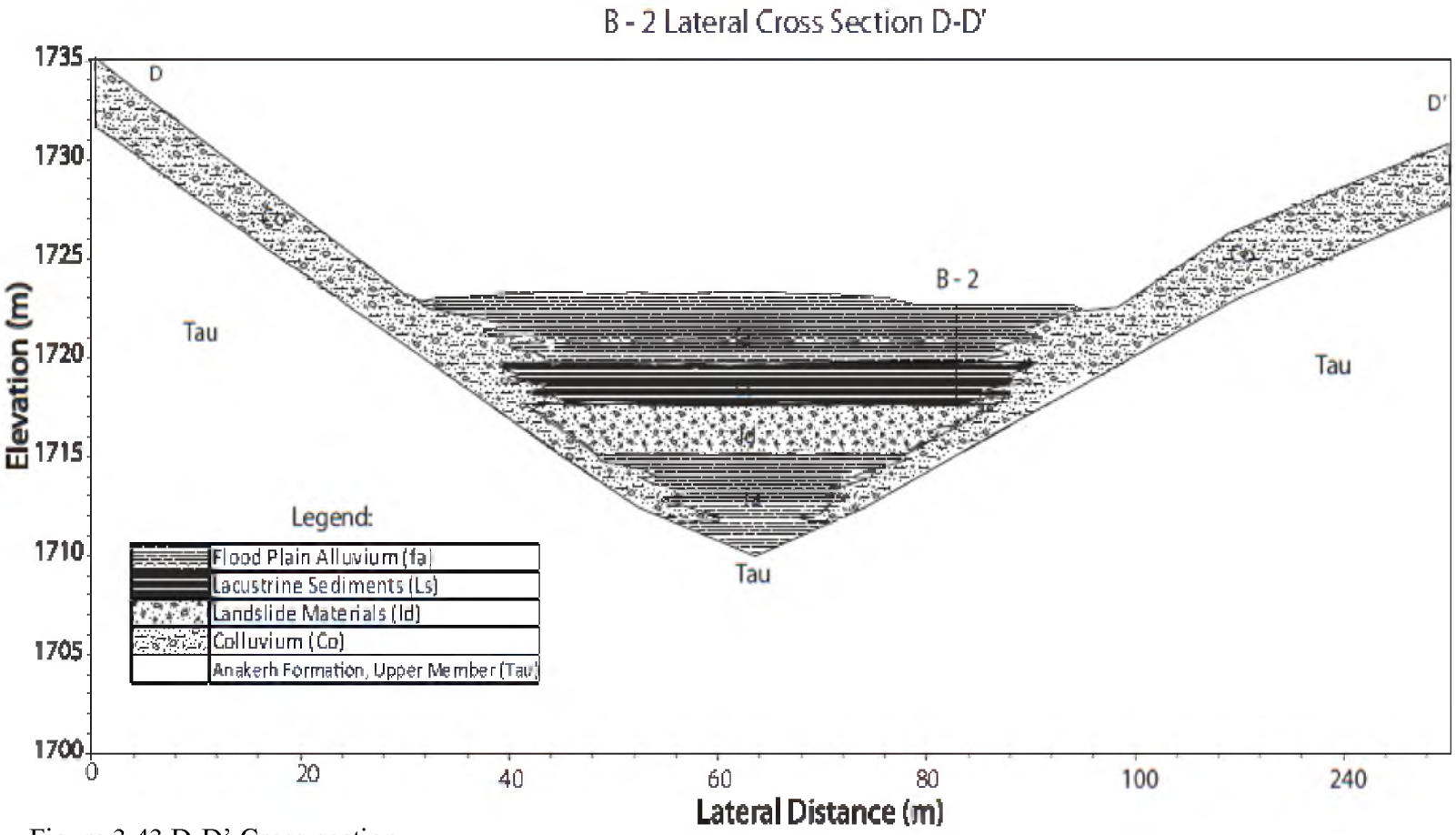

Figure 3.43 D-D' Cross-section

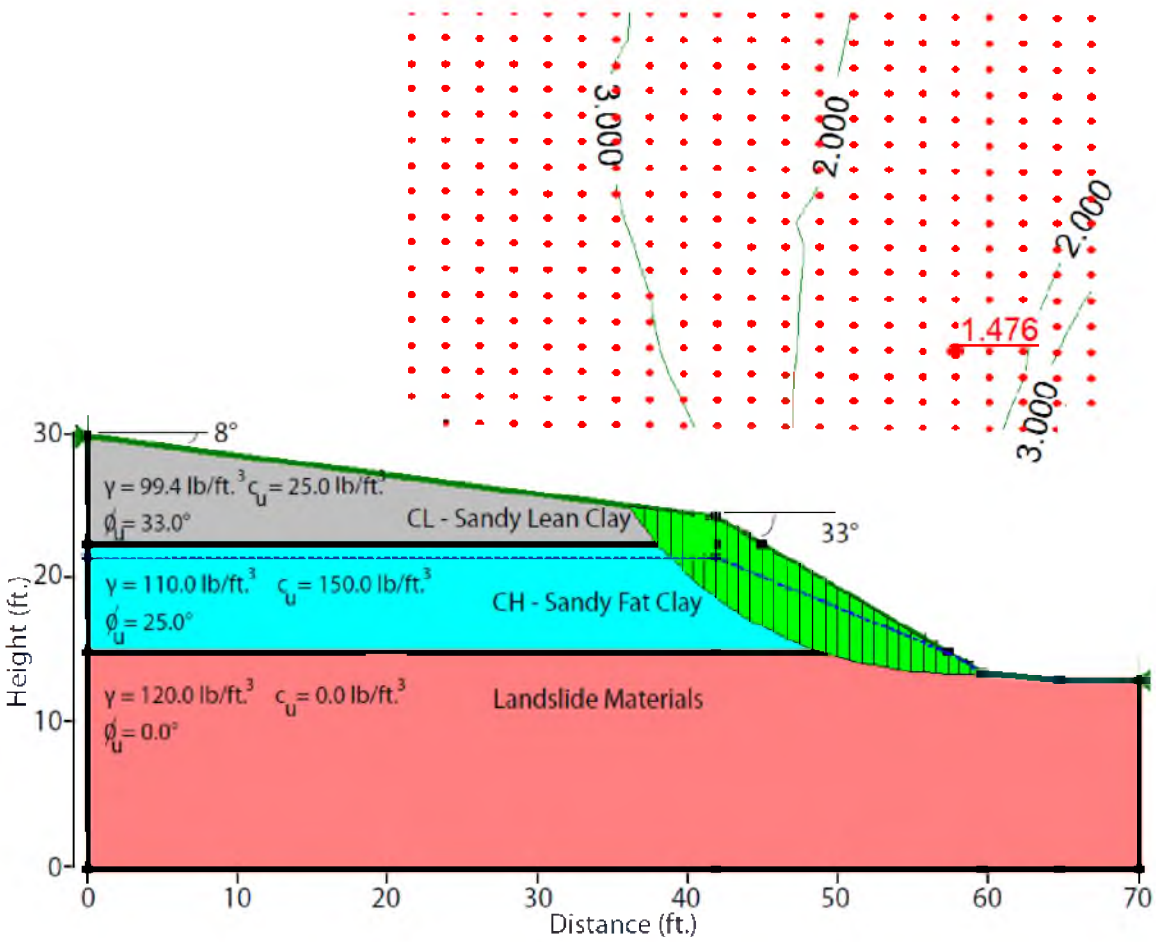

Figure 3.44, Slope # 1 undrained condition Slope/W model

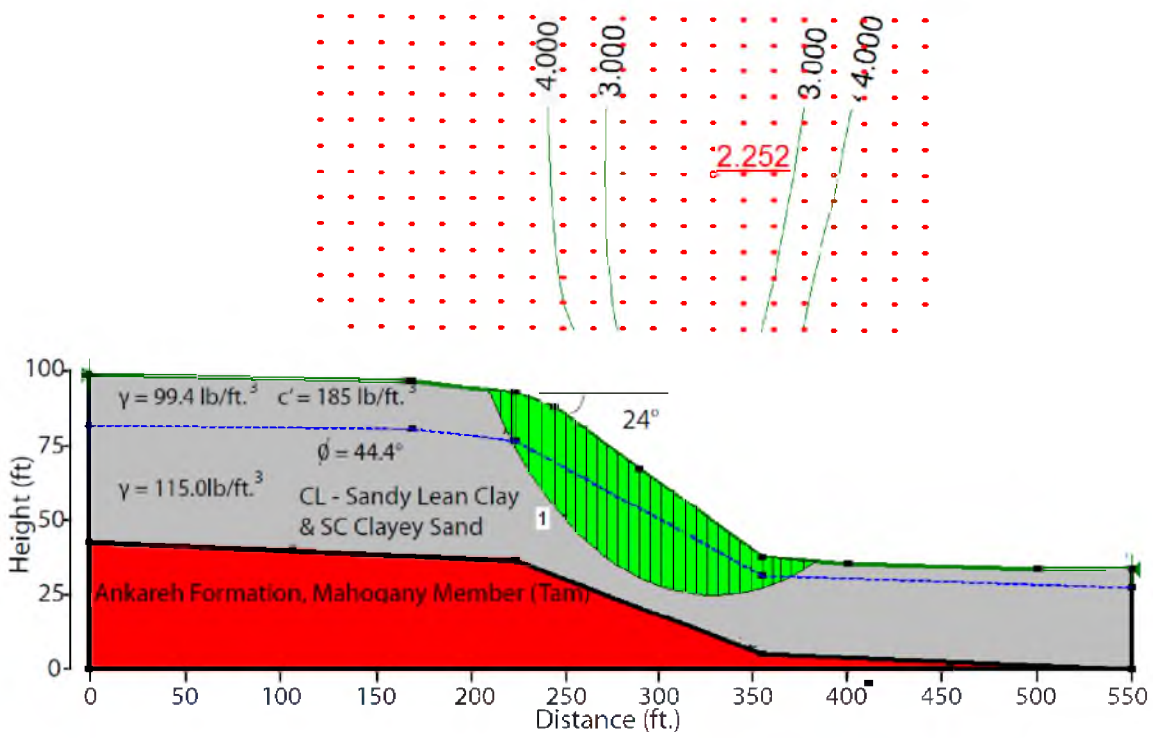

Figure 3.45, Slope # 1 Drained condition Slope/W model

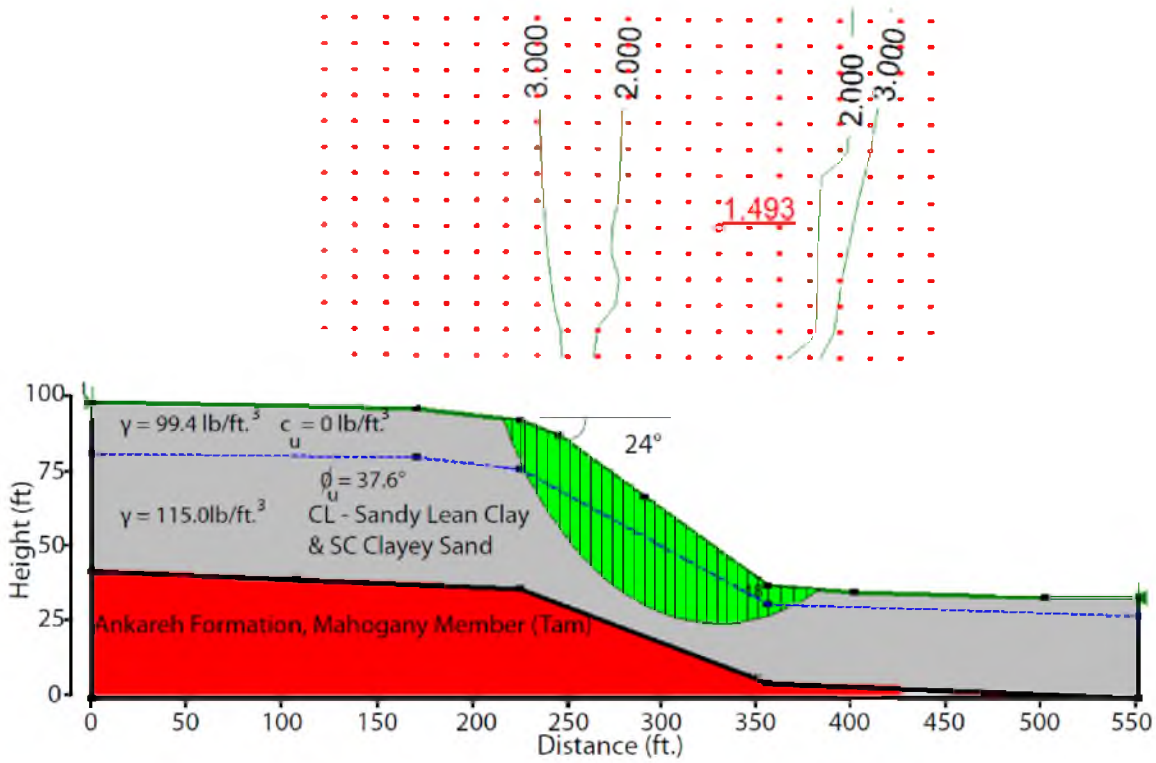

Figure 3.46, Slope # 2 Undrained condition Slope/W model

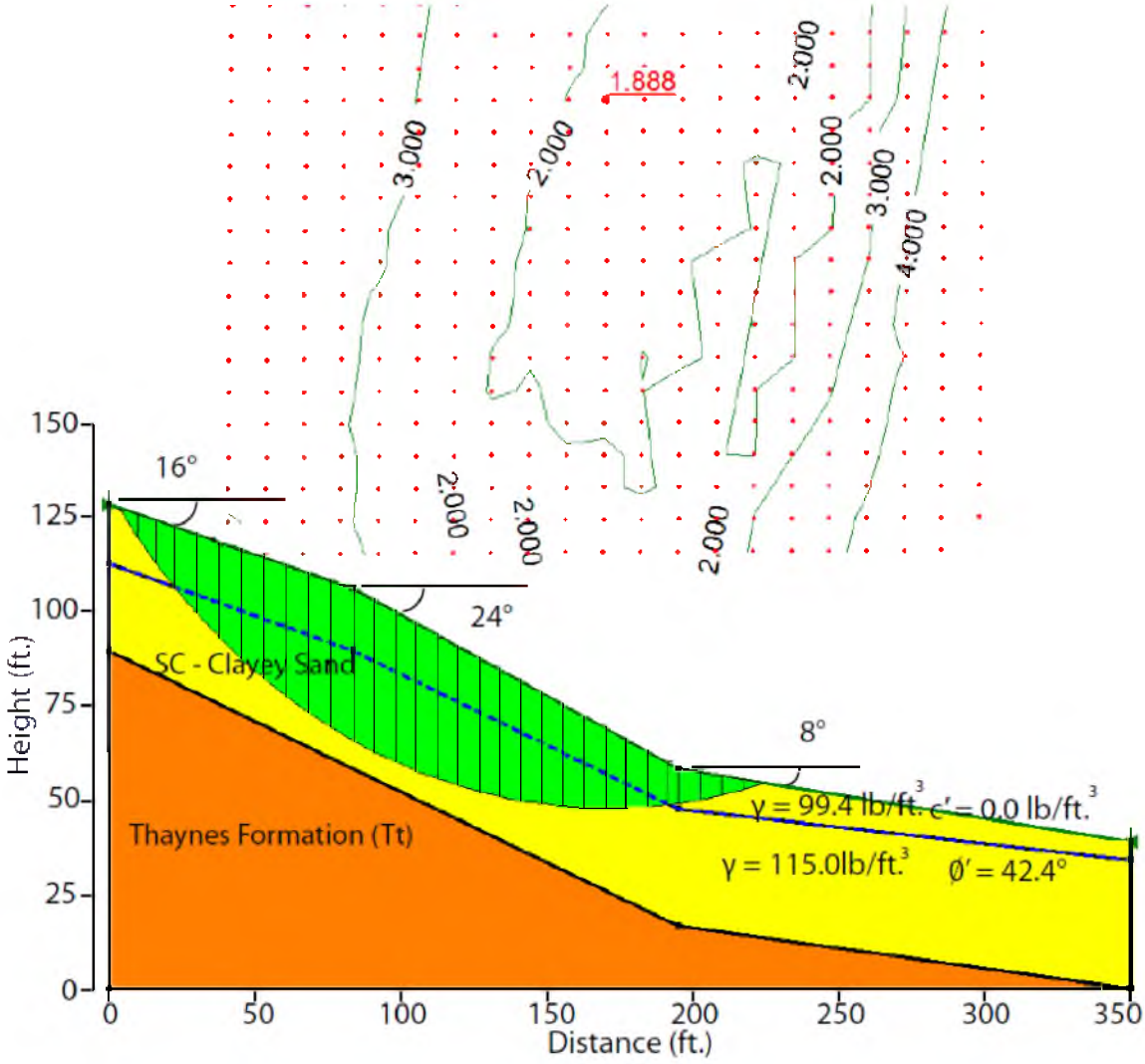

Figure 3.47, Slope # 3 Drained condition Slope/W model

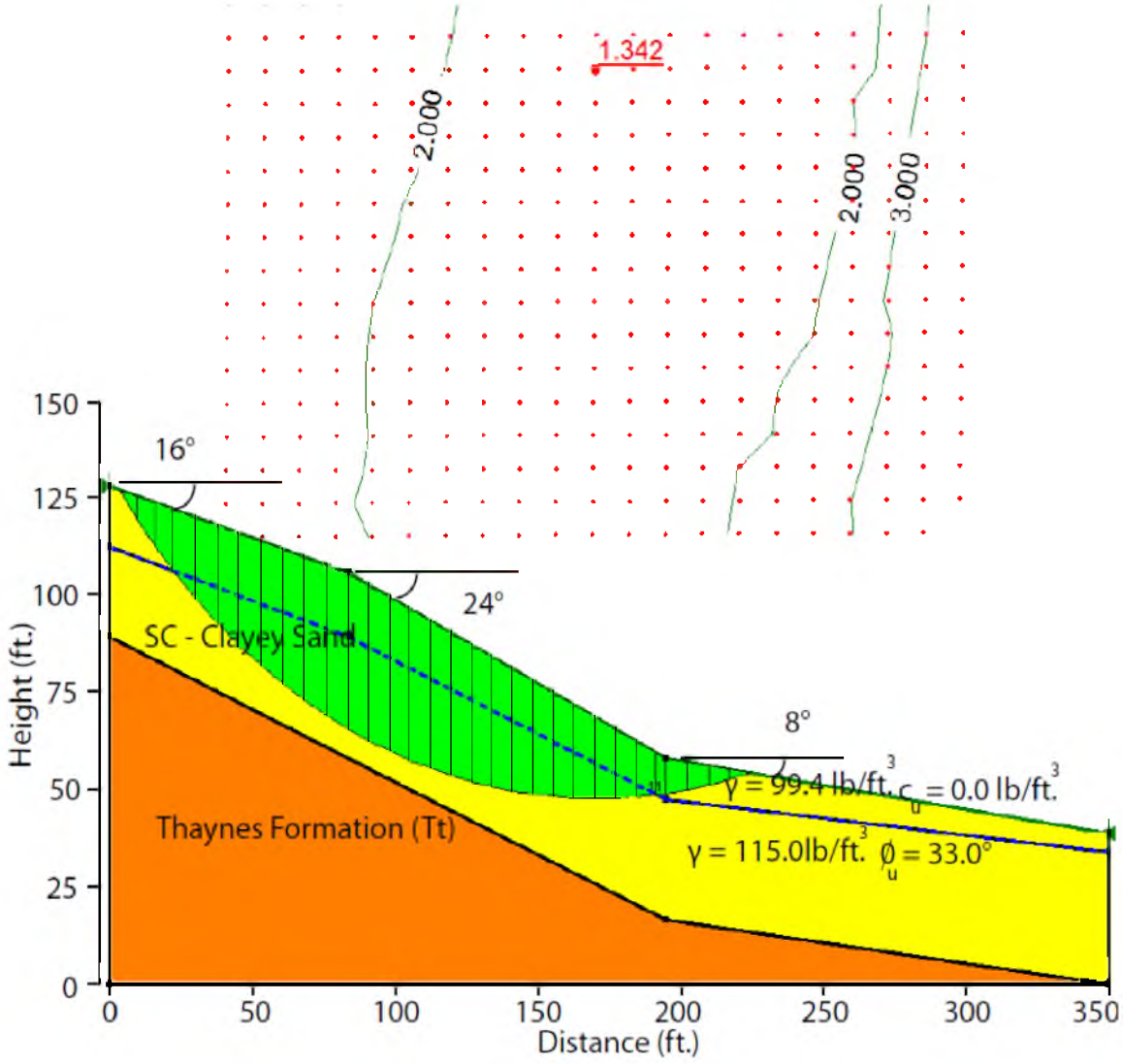

Figure 3.48, Slope # 3 Undrained condition Slope/W model

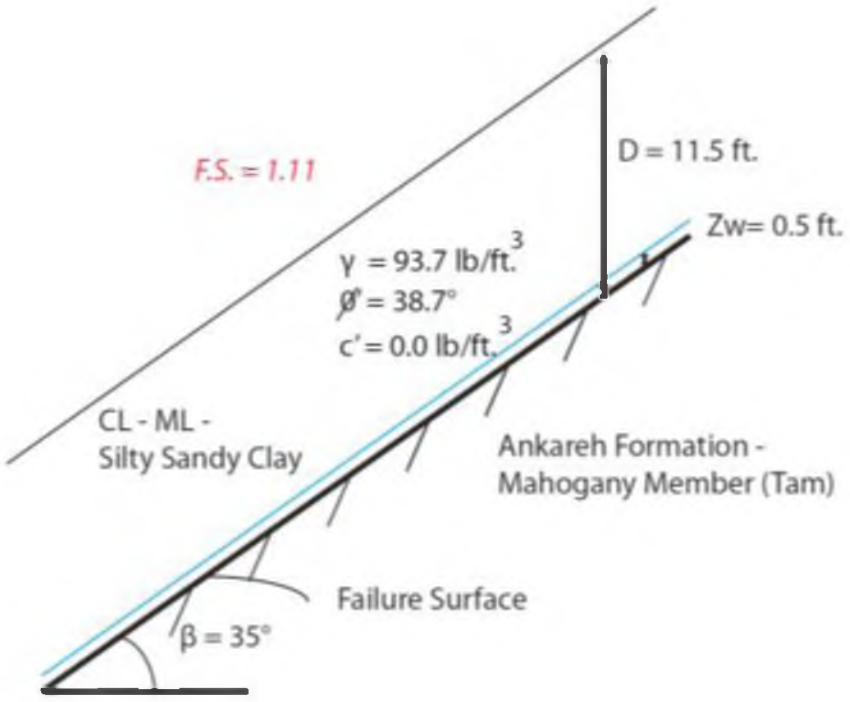

Figure 3.49, Infinite slope drained condition stability model near B – 8

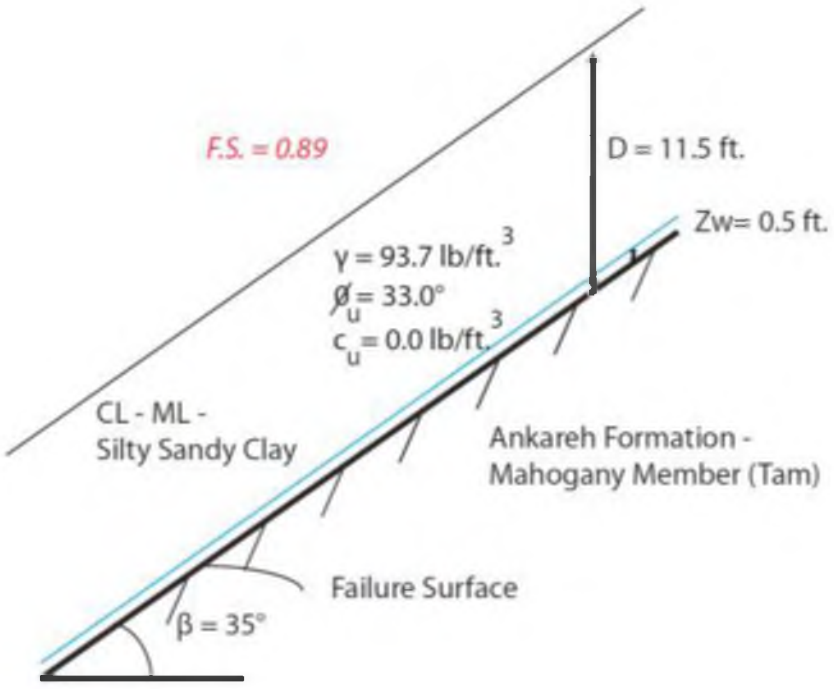

Figure 3.50, Infinite slope undrained condition stability model near B – 8

Table 3.6, Summary of slope stability models factors of safety

Drained Conditions

	Model Type # 1	Model Type # 2
	Low Water Table	*High Water Table*
Slope	**F.S.**	**F.S.**
Slope # 1	-	-
Slope # 2	2.252	0.726
Slope # 3	1.877	0.726
Infinite Slope	1.11	0.5

Undrained Conditions

	Model Type # 3	
Slope	k_h	**F.S.**
Slope # 1	0.00	1.476
	0.05	1.336
	0.10	1.215
	0.15	1.111
	0.20	1.019
	0.25	0.938
	0.30	0.866
	0.35	0.797
	0.40	0.737
	0.45	0.685
	0.50	0.638
Slope # 2	0.00	1.493
	0.05	1.299
	0.10	1.145
	0.15	1.019
	0.20	0.914
	0.25	0.826
	0.30	0.75
	0.35	0.686
	0.40	0.63
	0.45	0.581
	0.50	0.537
Slope # 3	0.00	1.342
	0.05	1.161
	0.10	1.04
	0.15	0.911
	0.20	0.818
	0.25	0.74
	0.30	0.674
	0.35	0.616
	0.40	0.567
	0.45	0.523
	0.50	0.484
Infinite Slope	0.00	0.89
	0.05	0.83
	0.10	0.78
	0.15	0.73
	0.20	0.69
	0.25	0.65
	0.30	0.62
	0.35	0.59
	0.40	0.56
	0.45	0.54
	0.50	0.52

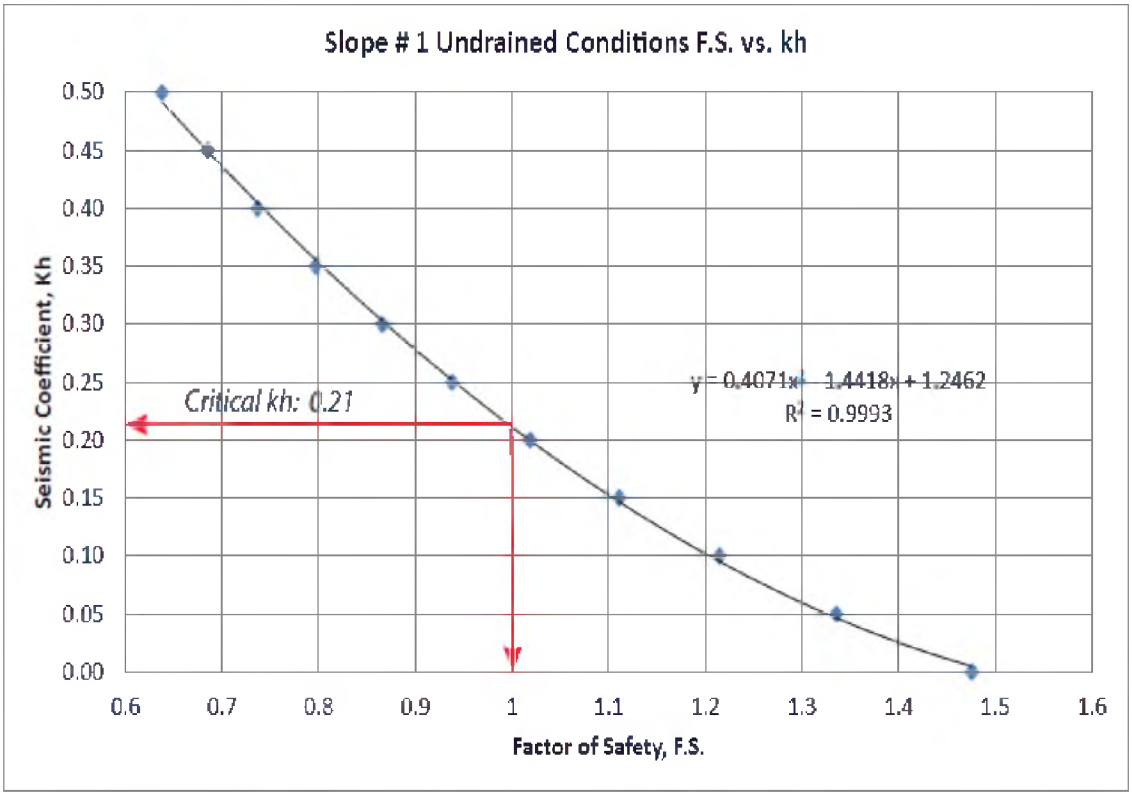

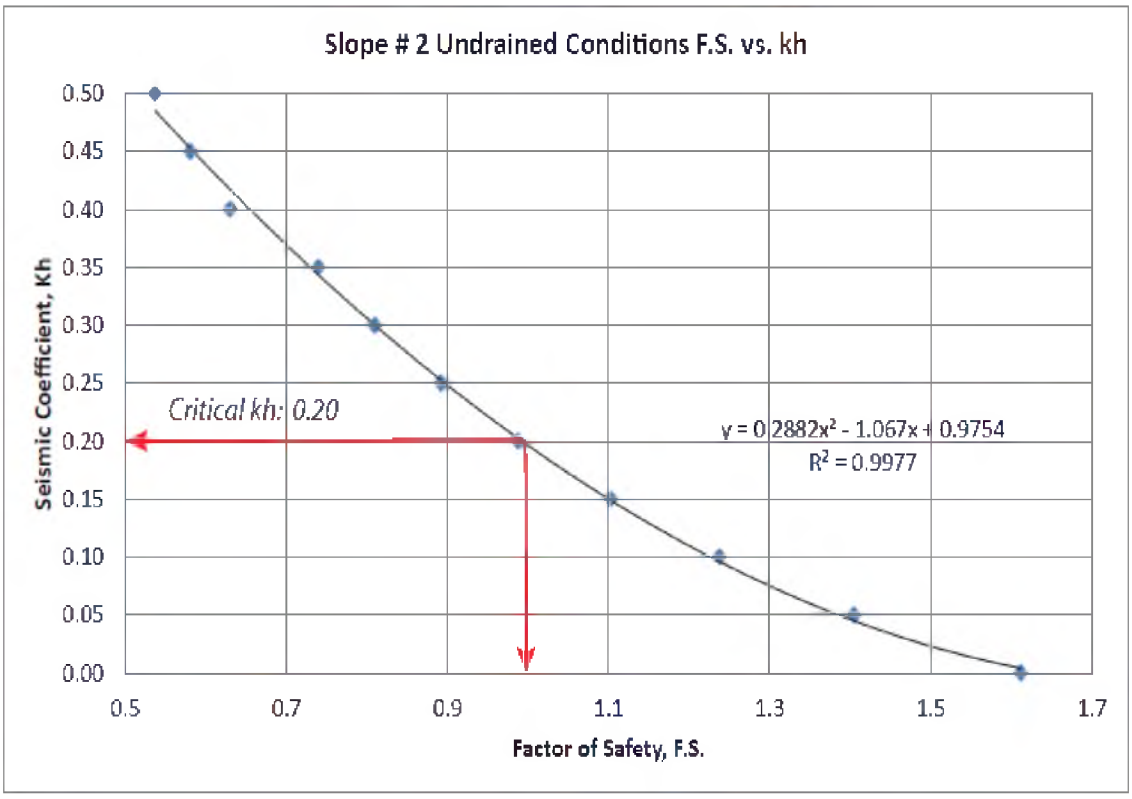

Figure 3.51, Slope # 1 and Slope # 2 undrained condition and critical k_h

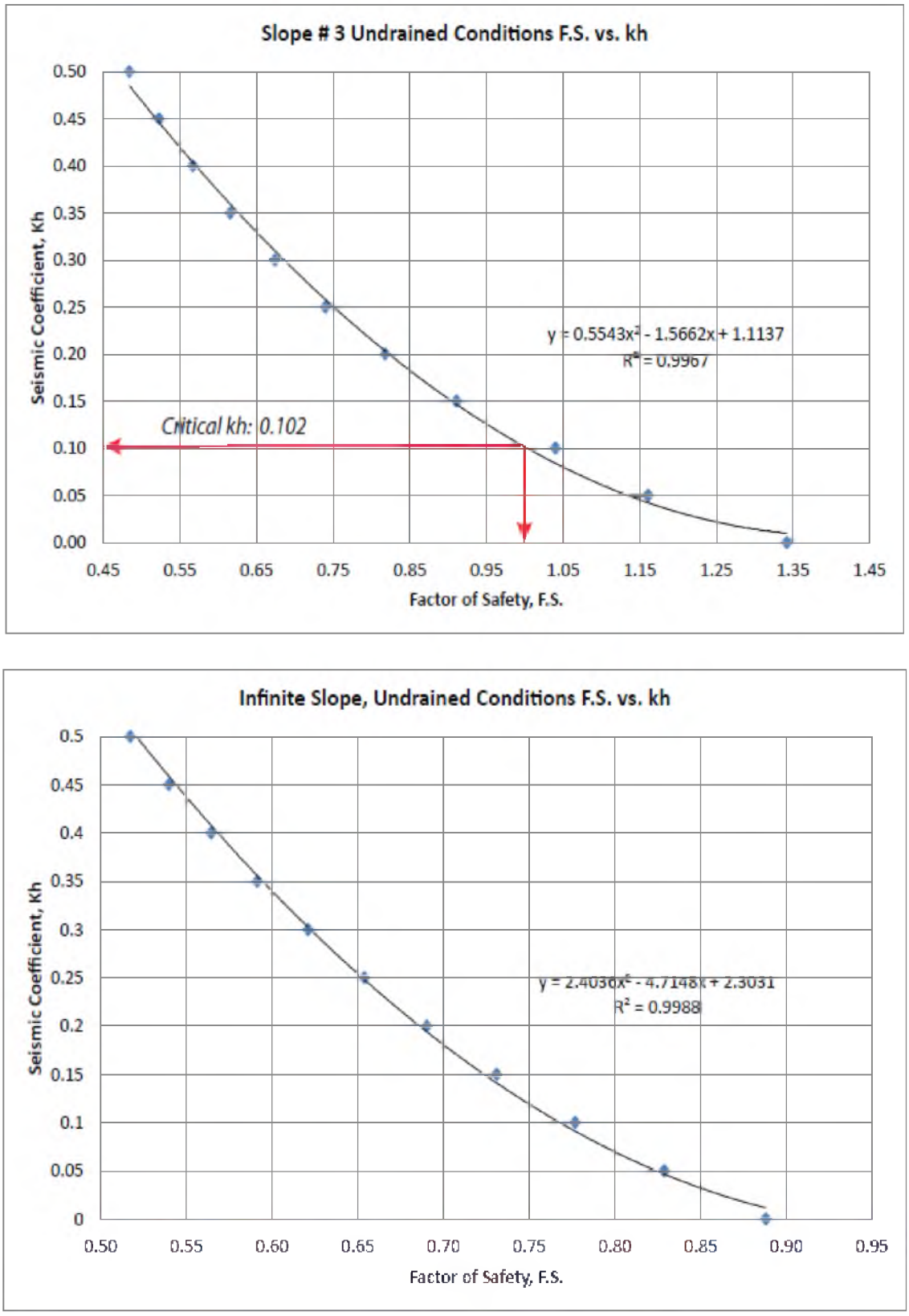

Figure 3.52, Slope # 3 and infinite slope undrained condition and critical k_h

CHAPTER 4

DISCUSSION AND CONCLUSIONS

Surficial Geology and Geomorphology

Geomorphic Features in the Landslide at Red Butte Creek

The first observation concerning features of the landslide at Red Butte Creek is that Red Butte Creek distinctly bends around the mapped landslide feature (Figure 3.3). Red Butte Creek generally has a narrow linear behavior that sharply turns to the north upstream of the landslide. Similar behavior is noted by Anderson (2010) with examples of a debris flow that diverted a stream channel around the debris flow.

Three lineations within the landslide are peculiar (Figure 3.3). These could be older stream beds from Red Butte Creek that formed sometime after the landslide when Red Butte Creek was at a higher elevation than today before the stream bed incised downward over time.

Another possibility is that these lineations represent hummocky surfaces commonly associated with landslides. If so, the high elevations of these features relative to modern Red Butte Creek would suggest they are some sort of landslide toe surface.

Abrupt Changes in Slope in Stream Channels

Elevation profiles for Red Butte Creek clearly show an abrupt change in elevation around a mapped landslide feature (Figure 3.8). Similar observations have been made of other abrupt changes in stream elevation intersecting landslides in the Grand Canyon within a subcanyon called Fishtail Canyon. Fishtail Canyon shows a sudden decrease in slope and sharp increase in slope within the stream elevation profile of Fishtail Creek (Figure 4.1 and Figure 4.2) (Watkins et al., 2004). Watkins et al. (2004) demonstrated that the landslide created a landslide dam, a behavior that seems to mirror the features in Red Butte Creek.

The same pattern of an abrupt change in slope near a landslide is also shown in the elevation profile of Parleys Fork. Slope # 2 and Slope # 3 drastically change slope extremely close to other mapped landslides (Figure 3.7). Parleys Fork crosses another mapped landslide (Figure 3.5). The behavior of the elevation profile of Parleys Fork also matches the observations by Watkins et al. (2004).

Soil Creep

The soil creep observed in the study area is evidence that the hill slopes are unstable and gradually moving downhill under the influence of gravity. Soil creep has been known to be a precursor for failure. These slopes could be more susceptible to failure because they already have strong evidence for soil creep and is discussed more with the infinite slope stability model discussion. For instance, Abramson et al. (2002) mentions how soils displaying creep are of concern: "Slope movements before total failures range from barely perceptible movements of creep to the more discernible

movements of several in.es per week" (Abramson et al., 2002: 654).

Subsurface Geology

Geotechnical Properties

Moisture content was highest between 0.0 and 4.0 ft. a pattern commonly caused by rainfall events and infiltration (Lewis and Veissman., 2002: 181). The moisture content data is most likely the result of infiltration from winter snowmelt and late spring storms.

For most geotechnical analysis, clays are assumed to have a specific gravity of 2.65 and sands a specific gravity of 2.70 (Coduto, 1999: 34). Specific gravity values in this report significantly outside this range are believed to be due to analytic error, particularly values near 2.2. This error is most likely due to testing a mass of soil unrepresentative of the correct volume such as those with high gravel or organic content. Gravels and organic material have specific gravities significantly less than clay minerals resulting in large errors if these constituents make up a significant fraction of the representative samples.

Two unusual patterns are seen in the liquid limit characteristics of the soil. First, the organic soil horizon has high plasticity while the rest of the subsurface soils have low plasticity. This pattern could be explained by the interaction of organic content with clay mineralogy and clay chemistry (Coduto, 1999: 37).

The second anomaly is the liquid limits in B – 2 from 10.0 ft. to 15.0 ft. (58.2% - 65.5%), which are also unlike any of the liquid limits in the majority of the clays in the subsurface soils. One possible explanation for this behavior is different clay mineralogy

at this location. Another possibility is that these clays have a high organic content as stated above.

Environment of Deposition

The abundance of the *Gyraulus* and the *Pyrgulopsis* freshwater mollusk shells suggests the environment of deposition. The *Pyrgulopsis* is generally associated with a variety of aquatic environments from cobble-bottom streams to reservoir bottom samples (Lysne, 2009: 16). The *Gyraulus* is common throughout North America in rivers and lakes; residing on various substrates from fine silt to large cobbles. It is believed that these mollusks do not exist in springs (Lysne, 2009: 17). Therefore both species of snail reside in either alluvial environments within streams or rivers or lake environments.

All borings except for B – 8 and B – 3 were drilled in flood plain alluvium and are in agreement with boundaries previously mapped by Crittenden and Van Horn (1987). Grain size distribution tests showed a wide range of sediment size by weight, implying rather poorly sorted materials. Poorly sorted materials ranging from clays to gravels are often indicative of alluvial systems as are cross-bedding and graded bedding (Boggs, 2006). Subangular to subrounded coarse grained sand to gravel was found in all borings and is believed to have originated from hill slopes near the borings (Figure 3.16). For instance, gravel derived from the Thaynes Formation was commonly found within boring B – 6 (Figure 3.17). The aspect map (Figure 3.16) shows that B – 6 is entirely surrounded by the Thaynes Formation and it is thus logical that any coarse grained materials in this boring could only come from surrounding hill slopes or from upstream.

B – 7 showed the greatest amount of sand and gravel interbedded in the clay

(Figure 3.18). Gravel and sand from the Ankareh Formation - Mahogany Member, Gartra Grit Member, and Thaynes Formation were found in this boring. The aspect map (Figure 3.16) shows flow paths extending from the Gartra Grit and surrounding Ankareh Formation. B – 7 is located close to the Thaynes Formation/Anakreh Formation contact and although no flow direction vectors intercept B - 7, it is downstream from the Thaynes Formation. Finally B – 7 is much closer to the hill slopes than all of the other boring, which could explain why significantly more gravel was found in this boring than all others.

The aspect map (Figure 3.16) shows that the only flow direction at B – 2 is from the Ankareh Formation, upper member. However, the Nugget Sandstone is south of B – 2 (Figure 3.1). Gravel and what is believed to be a boulder derived from the Nugget Sandstone were identified at a depth of 15.7 ft. and is assumed to be landslide material. The aspect map also shows a potential flow direction vector from the Nugget Sandstone toward B – 2.

The gravels found intermixed in the hill slopes as well as gravels found within the flood plain alluvium represent colluvium deposits. Colluvium is a chaotic mixture of coarse grained and fine grained materials (Carlson, 2003: 390). There is clearly an interaction from the colluvium on the hill slopes with the flood plain alluvium on the as is demonstrated in B – 7.

The first significant finding from the grain size distribution curves was the composition and behavior of B – 7 (Figure 3.30) compared to other borings within the flood plain alluvium. B – 7 shows nearly identical weight compositions for grains ranging from gravels to clays at all depths. However, the finer percentage by weight is

essentially the same at all depths, which is not seen in any other boring. The most critical feature is that B – 7 contains virtually no tufa and the vast majority of the weight percentage is coarse sand and gravel from the Ankareh Formation, upper member. For all other borings, tufa composed the majority of coarse grain weight percentage.

The second noteworthy trend is the grain size distribution of the lower sediments in B – 5 (Figure 3.32) and B – 2 (Figure 3.33) where grain size decreases from 55% to 80% finer by weight from 7.5 ft. - 14.5 ft. depth. B – 2 increases from 50% to 65% finer by weight from 5.8 ft. to 15.9 ft.

Landslide Dams and Lacustrine Deposits

The subsurface investigation produced several observations of the landslide at Red Butte Creek, including what is believed to be landslide material at 15.7 ft. in B – 2. Additionally, the grain size distribution characteristics, clam shells, and radiocarbon dating of charcoal in the lower portions of B – 2 and B – 5 suggest that a landslide dammed Red Butte Creek and created a lake. The sharp decrease in grain size in the lower sections of both B – 5 and B – 2, with mostly clay and silt-sized grains is indicative of a lacustrine environment since deeper parts of a lake are characterized particularly by the presence of fine silt and clay (Boggs, 2006: 268).

Lastly, clam shells found in the lower depths of both B – 5 and B – 2 also suggest a lacustrine environment. Clams live in a variety of environments and can be found in rivers, streams, lakes or reservoirs in depositional habitats with fine sediments (Lysne, 2009: 15). In addition, clams and snails (bivalves and gastropods) are some of the principal types of invertebrate remains found in lacustrine sediments (Boggs, 2006: 269).

Clam shells found in B – 2 also suggest a landslide dam and lake formed at this location at the base of Todd's Meadow.

Radiocarbon Dating and Sedimentation Rate

Canton (2009) evaluated the age of a laminated tufa from Parleys Fork using a combination of stable isotope analysis and radiocarbon dating. Her collection site is approximately 100 ft. due north of B – 5. Canton collected a laminated tufa specimen from Parleys Fork that extended to 25 cm (0.82 ft.) below the surface and dated several sections of tufa by depth in order to gain a sense of environmental conditions (Canton, 2009). Her analysis yielded a radiocarbon age of 1,450 years before present at a depth of 25 cm (0.82 ft.).

A few basic assumptions allow correlation of the ages of the charcoal of this investigation to the ages of the laminated tufa of Canton (2009). Boring B – 5 and Canton's tufa collection site are in close proximity therefore the age of the sediments at these two localities should share the same ages at the same depths. A second assumption is that the age of the tufa at depth is approximately the same age as surrounding sediments within the flood plain. A basic sedimentation rate can be derived from these assumptions. 4,370 years at 15.5 ft. (4.72 m) yields a sedimentation rate of 1.1 mm/year. Canton's data of 1,450 years at 0.82 ft. (0.25m), yields a sedimentation rate of 0.17 mm/year

Another explanation for the variance in the decrease in sedimentation rates could be attributed to accommodation space the space available at any point in time in which sediments can accumulate (Boggs, 2006: 274). The decrease in sedimentation rate is the

result of accumulation of sediments over time within Parleys Fork and Red Butte Creek has filled the available accommodation space.

Additional Radiocarbon Data Correlation

DuRoss et al. (2012) studied the paleoseismology of the Salt Lake City segment of the Wasatch Fault in detail through C-14 dating of sediments in test pits and trenches of fault scarps. Figure 4.3 captivates one noteworthy finding is from a trench on the East Bench Fault, located on Penrose Drive within one mile of the field site where earthquakes were dated from sediments at 4,000 ± 500 calendar years (DuRoss et al., 2012). The age of this earthquake is very close to the age of the charcoal in this report at 4,370 ± 30 years.

Ancient Lake Elevations

A pattern of geomorphic and geological features suggest an ancient lake formed in response to a landslide triggered by an earthquake 4,000 ± 500 years ago. The combination of geomorphic features such as parallel lineations adjacent to the landslide zone south of Red Butte Creek, grain size characteristics of alluvial sediments overlying what could be lacustrine sediments within both B – 2 and B - 5, and identical radiocarbon ages for charcoal in B – 2 and B – 5 at the same subsurface elevations support this interpretation.

Figure 4.4 and Figure 4.5 summarize the characteristics of a possible ancient lake. Notice the three lineations and also what appears to be a fourth lineation labeled Lineation # 4 at 1740 m (5742 ft.). Each of the lineations may represent a paleo-channel

from Red Butte Creek or an ancient lake level. If lineation # 3 at 1722 m (5683 ft.) is an ancient lake level it would have submerged the surface at B – 2. However, since radiocarbon dating results from both B – 2 and B – 5 yielded the same age at the same subsurface elevation, the lake level must have been higher to match the elevations and same deposited surface between B – 2 and B – 5. Lineation # 1, # 2, and # 3 would therefore represent lower lake stage levels. Figure 4.5 summarizes the cross-sectional geometry and extent of the proposed ancient lake and the possible subsurface location for the lake bottom.

Groundwater Monitoring and Aquifers

Although the historical data record is limited to Todd's Meadow, there appears to be seasonal changes in groundwater levels that match the known hydrologic behavior for Red Butte Canyon. For instance, data from Todd's Meadow indicate the greatest depths to groundwater occur in the late fall months and shallowest depths to groundwater occur in the early spring months (Table 3.4). These groundwater observations coincide with the hydrologic behavior of Red Butte Canyon because the majority of precipitation is in the form of snow in the winter and early spring months (Ehleringer, 1992).

The presence of groundwater in B – 8 suggests the presence of groundwater in the hill slopes surrounding Parleys Fork. Groundwater likely exists within many, if not all, of the hill slopes within the field site and likely flows into Parleys Fork. Surface water clearly flows into Parleys Fork and groundwater likely also flows into Parleys Fork from both the eastward and westward slopes of the valley from recharge due to snow pack and

precipitation. However, the extent to which groundwater occurs in hill slopes remains unknown due to the limitations of this investigation.

The overall hydrogeological profile from each of the boring logs within the alluvium shows an unsaturated zone and a saturated zone, typical of an unconfined aquifer. All borings except for B – 3, B – 4, and B – 8 were drilled in alluvium adjacent to Parleys Fork and encountered groundwater at various depths. An unconfined aquifer likely exists within the valley because of the consistent presence of groundwater in saturated portion of the alluvial sediments.

Perched aquifers may also exist within the study area, particularly at the southern portion of Todd's Meadow. The depth to groundwater in piezometer N5-10 is approximately 15 ft., nearly 10 ft. higher than the depth to groundwater in neighboring piezometers N5-14 and N5-15 while the screened interval of N5-10 is seated 25 ft. below the surface, whereas the screened intervals of both piezometers N5-14 and N5-15 are seated nearly 50 ft. below the surface (Table 3.4). In addition, the depth to groundwater in boring B – 1occurs nearly at the same depth as N5-10 at 16 ft. and was drilled to a total depth of 16 ft. (Table 3.4). The shallower depth to groundwater observed in both N5-10 and B – 1 in addition to the presence of groundwater at greater depths in the same area may suggest the presence of a perched aquifer.

The groundwater observations in this investigation confirm previous research. The groundwater table apparently decreases in elevation from north to south as observed in each of the borings in the alluvium adjacent to Parleys Fork. Data from the lower field site also showed a decrease in water table elevations from north to south, suggesting

discharge into Red Butte Creek. Hill (2006) also demonstrated that groundwater ultimately discharges to Red Butte Creek.

Seismic Refraction

The three layer system represents the unsaturated sandy clays in the upper layer, saturated sandy clays in the second layer, and bedrock which is the Ankareh Formation, upper member. The findings are more or less consistent with the geology observed in boring B – 2 in Todd's Meadow in addition to the other borings drilled within flood plain alluvium.

The seismic P-wave velocities for all layers are in close agreement to published seismic P-wave velocities of similar geologic materials (Table 4.1). Layer 2 represents the saturated zone. The depth to layer 2 on the north side of Todd's Meadow was 18.7 ft. while the depth to groundwater near piezometer S – 2 near this location was 17 ft. No piezometers or borings are located near the southern end of the seismic line so this groundwater depth cannot be verified.

The orientation of bedrock depths determined from the seismic survey is counterintuitive since seismic refraction data indicate the bedrock is deeper to the north than the south. However, the seismic data is actually believed to be related to the subsurface geometry. Eastern hill slopes in Todd's Meadow are close to the base of the meadow toward the south and are further from the base of the meadow toward the north. The subsurface geology for the Ankareh Formation, upper member in Todd's Meadow is assumed to have a v-shaped cross-section typical of fluvial systems and paleochannels (Figure 3.43). With these considerations, the deeper depth to the Ankareh Formation

toward the north could be explained as representing the subsurface closer to the medial portion and deepest part of a paleochannel. The shallower depth to the Ankareh Formation toward the south of the seismic line could be explained as being closer to the edges and shallowest portions of a paleochannel. Figure 4.6 summarizes the interpreted geometry and subsurface geology for the above considerations. This figure shows two intersecting planes in three-dimensions, one representing the plane of the top of Ankareh Formation, mahogany member (Tam) extending below the subsurface. The second plane represents the flat plane of Todd's Meadow.

There is some variability of data points in the seismic refraction data, especially along the layer 3 (bedrock) slopes. Both the forward traverse and reverse traverse data points display a stair-stepped pattern in relation to the best fit curves. A possible explanation for this is human error from selecting traces on the raw seismic data. Another possibility is that the data represent interface diffractions (Sheehan et al., 2006). The bedrock itself could actually be stair-stepped and have abrupt changes in elevation. When this happens, seismic P-waves reflect off the bedrock at earlier times on top of a stepped feature and reflect at later times at the bottom of the stepped feature in the bedrock. One possible explanation for the stair-stepped Ankareh Formation bedrock is that the interface diffractions actually represent an irregular surface of rockfall piles from paleo-landslides now buried from the east and west hill slopes adjacent to Todd's Meadow.

Slope Stability Discussion

Drained Condition Slope Stability Models

Drained condition models with a low groundwater table (Model Type # 1) yielded the highest factors of safety for all model types and represent models with the greatest stabilities. Slope # 2 had a *F.S.* of 2.252, Slope # 3 had a *F.S.* of 1.877, and the infinite Slope had a *F.S.* of 1.11. No drained condition model was constructed for Slope # 1 due to a lack of geotechnical data for drained soil conditions; however, its stability is also likely highest under these conditions. The drained conditions with a shallow groundwater table (Model Type # 1) represent the typical loading and climatic conditions within Red Butte Canyon and the field site. For instance, the drained shear strength represents the typical stresses a soil is exposed to, and in terms of Red Butte Canyon's climate, loads such as the accumulation of snowpack in winter are gradual over time.

Each of the drained condition models with a high groundwater table (Model Type # 2) yielded the lowest factors of safety for all the model types and thus represented the lowest stability condition. Slope # 2 had a *F.S.* of 0.726, Slope # 3 had a *F.S.* of 0.726, and the infinite Slope had a *F.S.* of 0.50. A high groundwater table condition would be expected due to the fact that groundwater increases pore water pressure and reduces the shear strength of soils. High groundwater tables can be generated by powerful thunderstorms as well as rapid snowmelt events; the correlation between major thunderstorms and the occurrence of landslides has been documented worldwide (Brand, 1982). Because the majority of precipitation within Red Butte Canyon comes from snowfall, one would expect a rapid snowmelt event to cause slope instabilities and landslides. In fact, in Utah, during an unusually warm ten day period from late May to

early June 1983, a heavy winter snowpack along the Wasatch Front began to melt rapidly and triggered approximately 150 debris flows and other types of landslides (Pack, 1984).

Undrained Condition Slope Stability Models

The undrained condition slope stability models with shallow groundwater tables (Model Type # 3) display lower factors of safety than drained condition models, especially when seismic loads are applied to the models. For $k_h = 0.0\ g$, Slope # 1 *F.S.* = 1.476, Slope # 2 *F.S.* = 1.493, Slope # 3 *F.S.* = 1.342, and the infinite slope model *F.S.* = 0.89. Each of these slope's factors of safety reduces even further under the influence of seismic loads and for $k_h = 0.10\ g$, Slope # 1 *F.S.* = 1.215, Slope # 2 *F.S.* = 1.145, Slope # 3 *F.S.* = 1.04, and the infinite slope model *F.S.* = 0.78. Figures 3.44 to 3.45 indicate that a factor of safety less than 1.0 would occur in Slope # 1 if $k_h = 0.21\ g$, Slope # 2 if $k_h = 0.20\ g$, and Slope # 3 if $k_h = 0.102\ g$, an increase of only 0.002 *g*. The slopes are less stable during an earthquake and although Slope # 1 and Slope # 2 have factors of safety above 10, Slope # 3 is near failure whereas the infinite slope is unstable under any undrained condition. Clearly, all of the slopes show the potential to have slope stability decreased by seismic loads from earthquakes.

Slope Geometry and Geotechnical Properties

Each of the slope models has a different geometry, geotechnical properties, and groundwater elevations which ultimately influences the slope stability. The average slopes (Figures 3.38 to 3.43) are: Slope # 1 = 33°, Slope # 2 = 24°, Slope # 3 = 24° Slope # 4 = 35°. The geotechnical properties and groundwater elevations are different for each

slope which influences the cohesive strength of the soils and the internal angle of friction which plays a pivotal role in the slope stability calculations as a consequence of the Mohr-Coulomb strength criterion. No one single factor alone can ultimately dictate the slope stability due to the many variables involved in slope stability analysis.

Infinite Slope Stability Model

The infinite Slope near B – 8 shows by far the lowest factors of safety and lowest The drained condition *F.S.* is 1.11 and with a high groundwater condition *F.S.* is 0.50. The undrained condition *F.S.* is 0.89 when $k_h = 0.0\ g$, indicating a slope failure in any undrained condition. The geologic data from boring log B – 8 indicate that there is only 0.5 ft. of groundwater above the base of Ankareh Formation/ colluvium. Even a slight increase in water levels of 0.5 ft. to 2.1 ft. causes *F.S.* to be 1.0.

Key indicators of slope instability already exist on the hill slopes surrounding B – 8. Soil creep was previously noted to exist near B – 8 in Chapter 3 and is an indication of the gradual downhill movement of soil regolith under the influence of gravity (Anderson, 2010). Low factors of safety even in the drained low groundwater table condition indicate the slope is potentially unstable. Further evidence comes from the geological materials found within boring B – 7 as discussed above in regards to the grain size distribution curves for B – 7. The presence of gravels from both the Thaynes Formation and the Ankareh Formation within B - 7 could indicate a sequence of landslide or debris flows in this vicinity. Cross-Section B – B' supports this observation (Figure 3.34).

Recurrence Intervals of Storms and Earthquakes

Slope stability and slope failure is a function of groundwater levels, precipitation and infiltration, rapid snow melt, freezing and thawing as well as earthquakes (Abramson et al., 2002: 31). Hydrological-related failures are the most common modes of failure because of the recurrence interval of such events (Abramson et al.). For instance, changes in groundwater levels are an annual occurrence, but may vary significantly over the course of tens of years. Earthquakes on the other hand have much lower recurrence intervals. The recurrence interval for a magnitude 7.0 earthquake along the Salt Lake City Segment of the Wasatch Fault is approximately 1,200 years (Utah Geological Survey, 1996: 6). The combination higher groundwater tables from storms coupled with the occurrence of earthquakes could be evaluated from a conditional probability standpoint in possible future studies.

Determining changes in groundwater levels and changes in the unit weight of soils due to precipitation and infiltration is technically challenging (Abramson et al., 2005). Although it is possible to determine these changes as a result of precipitation events from runoff and infiltration analysis for Slope # 1, Slope # 2, Slope #, and B – 8, these methods are challenging and beyond the scope of this investigation. Future investigations in Red Butte could determine these fluctuations as well as the changes in slope stability from these changes. Such models could be constructed using the Rational Method for runoff and using Horton infiltration models or Green-Ampt infiltration models to determine changes in ground water levels (Lewis & Viessman, 2003: 192).

Conclusions – Surficial Geology and Geomorphology

The surficial geology within the study area reveal key geological and geomorphic features, including the known landslide at Red Butte Creek, enigmatic lineations adjacent to the landslide area, unusual changes in slope within both Red Butte Creek and Parleys Fork, evidence of modern rockfalls, and tufa deposits within both Red Butte Creek and Parleys Fork. Some conclusions can be drawn from these observations.

The landslide at Red Butte Creek suggests that the creek has responded to the landslide. It is possible that Red Butte Creek was dammed behind the landslide feature and that the lineations within the landslide boundary represent a point in time when Red Butte Creek overtopped the landslide dam and incised the features.

Conclusions – Subsurface Geology

The environment of deposition was confirmed to be that of an alluvial system with a localized lake. However, there also appears to be some interaction with the colluvium in the soils. Van Horn and Crittenden (1987) had previously classified the valley floor as flood plain alluvium. The subsurface investigation has confirmed these results with the nature of the grain size characteristics and abundance of freshwater mollusk shells that are only known to live in alluvial and other aquatic environments. However, colluvium seems to play a role in the alluvial sediments as shown by the presence of coarse-grained materials derived from the surrounding geologic formations on the hill slopes. Colluvium deposits are more prevalent closer to the hill slopes, as would typically be expected.

An unconfined aquifer appears to exist throughout the subsurface within the field site in addition to the possibility of a perched aquifer in Todd's Meadow. Groundwater from the borings, piezometers, and seismic refraction data indicate the presence of groundwater throughout the site. Parleys Fork surely influences the unconfined aquifer.

The results of the seismic refraction survey indicate that bedrock exists approximately 45 ft. to 60 ft. below the subsurface within Todd's Meadow. A more detailed investigation will need to be performed to find the depth to bedrock across the study area.

Lastly, the known landslide at Red Butte Creek could have created a landslide dam triggered by a large earthquake. Data from DuRoss et al. (2012) suggest a correlation of the age of the sediments at 4,370 ± 30 years found in this study correlate closely to the age of a known earthquake at 4,000 ± 500 years ago. Grain size data, biological data, and radiocarbon dating from B – 2 and B – 5 provide compelling evidence to support the observation that a landslide dam and lake formed within Red Butte Creek in response to the earthquake.

Conclusions – Slope Stability Modeling

Several slopes observed in the study area appear to be stable under the groundwater elevations and loading conditions observed during the field investigation. Slope # 1, Slope # 2, Slope # 3 and the infinite slope have stable slopes under drained conditions, but not for a high groundwater table. Slope # 1, Slope # 2, and Slope # 3 also have stable slopes under undrained conditions even when $k_h = 0.10\ g$. The infinite slope on the other hand is near failure under drained conditions and fails with a high

groundwater table as well as under all undrained conditions. The presence of soil creep and low factors of safety indicate an unstable slope.

Lastly, although slope stability analysis was not performed on the precise location of the landslide at Red Butte Creek, there is compelling evidence to suggest that the subsurface geology in this area was influenced by a large magnitude earthquake. All of the slopes in this study failed under horizontal accelerations far below 0.6 *g* (Figure 4.44 and Figure 4.45). It is only logical to assume that since all slopes within the study area highly susceptible earthquakes, all slopes within Red Butte Canyon would be susceptible to a 0.6 *g* ground acceleration from a significant earthquake. The combination of evidence provided from the geomorphology within the study area, depositional environment, geochronology, and slope stability modeling strongly suggest that geomorphic features in Red Butte Canyon are influenced by earthquakes.

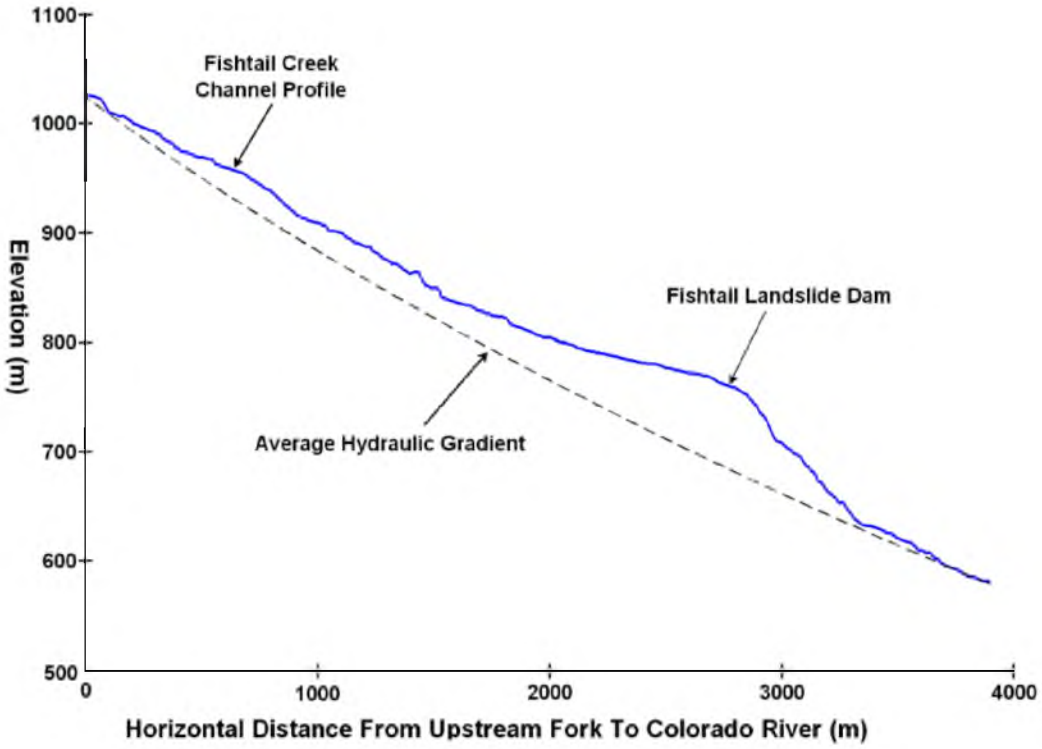

Figure 4.1, Fishtail Creek elevation profile, adapted from Watkins et al. (2004)

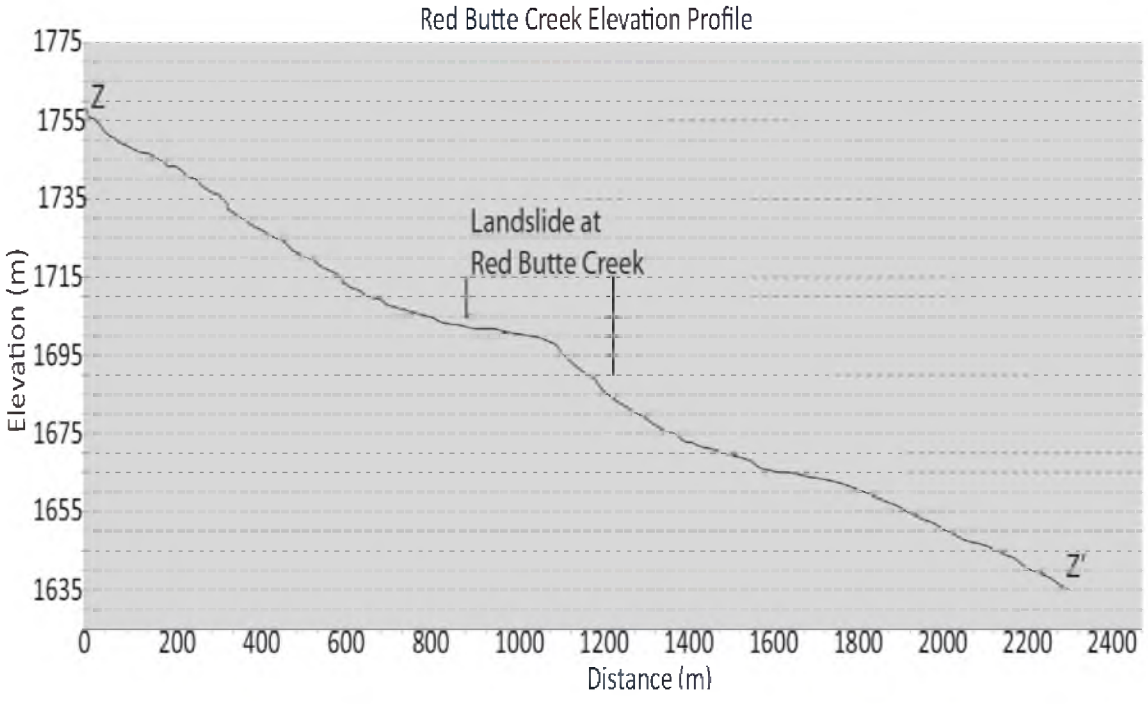

Figure 4.2, Stream elevation profile Z-Z' along Red Butte Creek

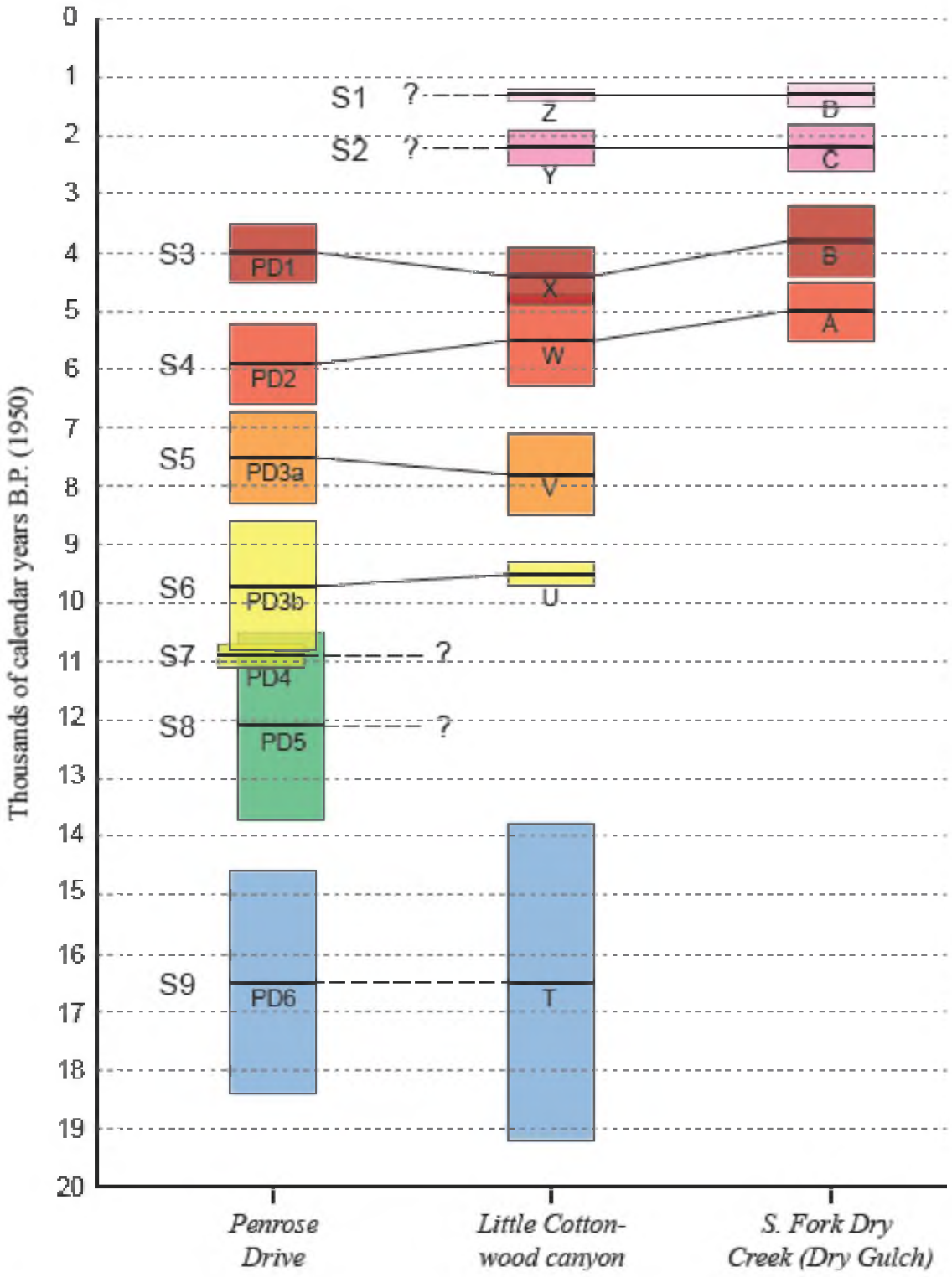

Figure 4.3, Radiocarbon dating results. DuRoss, C.B. and Hylland, M.D., 2012, Paleoseismic investigation to compare surface faulting chronologies of the West Valley fault zone and Salt Lake City segment of the Wasatch Fault zone, Salt Lake County, Utah: Final technical report to the U.S. Geological Survey, National Earthquake-Hazards Reduction Program, award no. G10AP00068, 61 p., 2 plates.

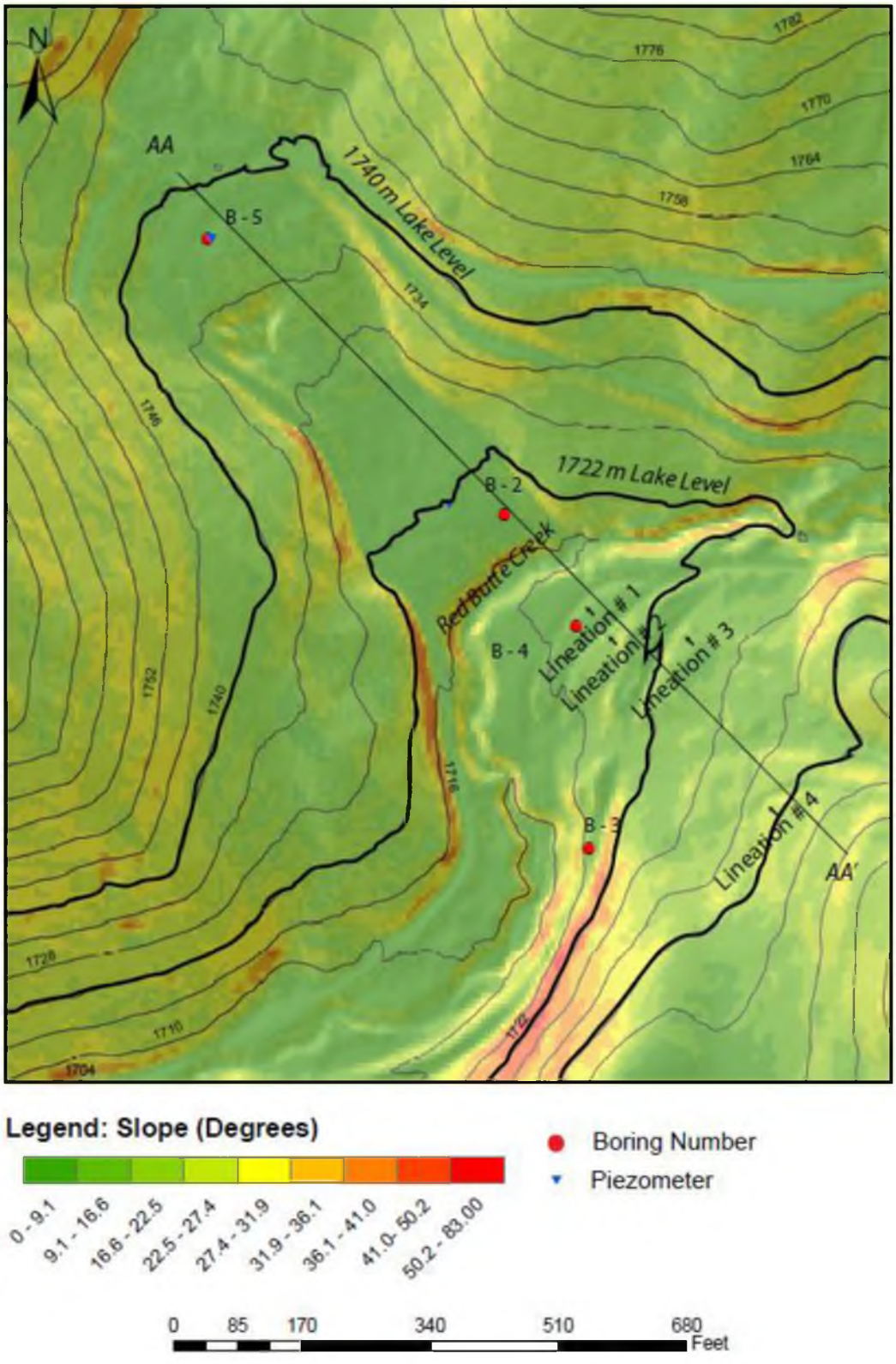

Figure 4.4, Plan view location of ancient lake levels with contour elevation overlay

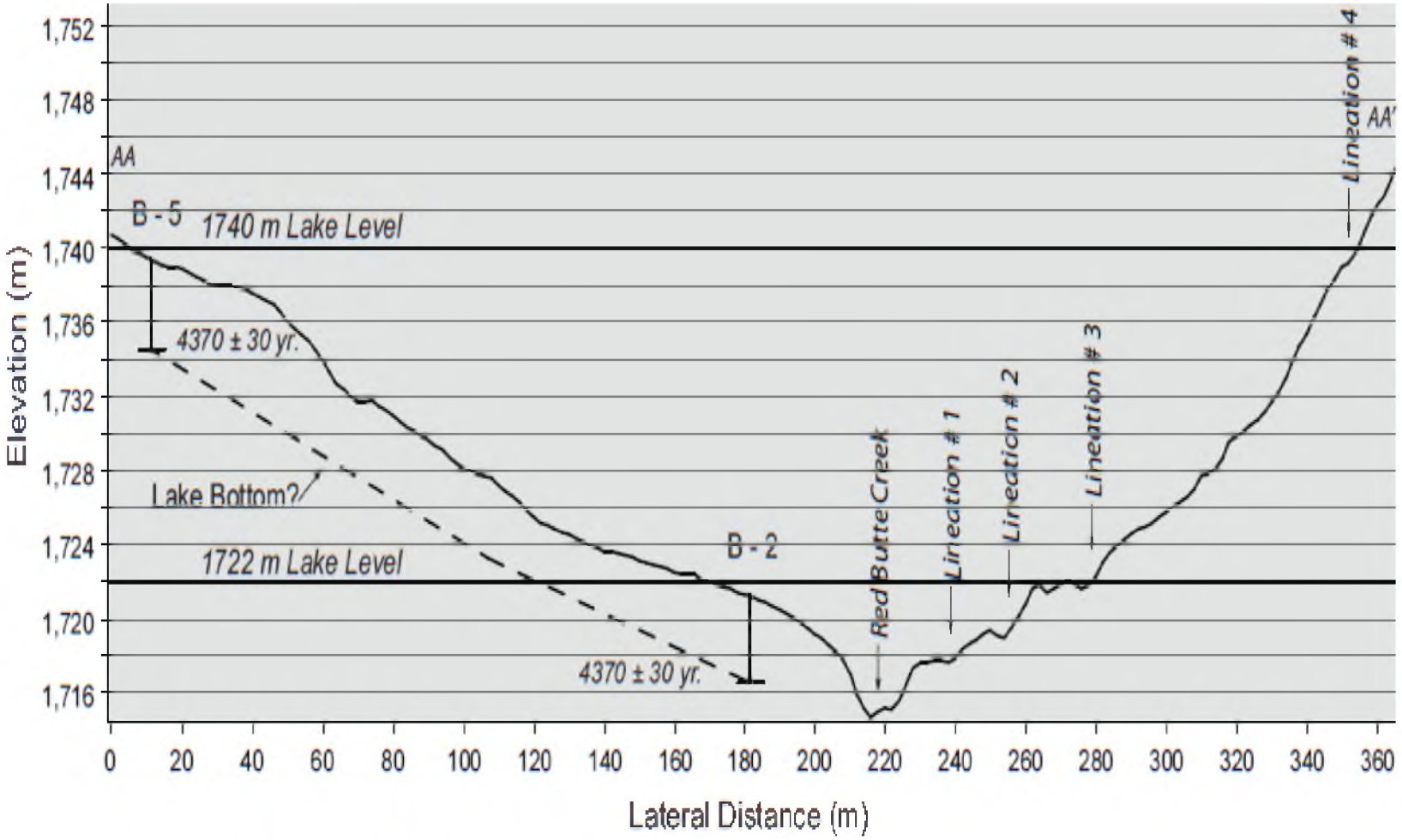

Figure 4.5, Cross-section of surface elevation of ancient lake

Table 4.1, Comparison of field/published seismic p-wave velocities (Adapted from Sheehan et al., 2006)

Seismic Refraction Results		*Unconsolidated Materials*		*Consolidated Materials*	
Layer #	Velocity (m/s)	Material	Velocity (m/s)	Material	Velocity (m/s)
Layer 1	**338**	Weathered Layer	300 - 900	Granite	5000 - 6000
Layer 2	**1347**	**Soil**	**250 - 600**	Basalt	5400 - 6400
Layer 3	**3588**	Alluvium	500 - 2000	Metamorphic Rocks	3500 - 7000
		Clay	**1100 - 2500**	Sandstone and shale	2000 - 4500
		Sand (unsaturated)	**200 - 1000**	Limestone	2000 - 6000
		Sand (saturated)	800 - 2200	*Other*	
		Glacial till (unsaturated)	400 - 1000	Material	Velocity (m/s)
		Glacial till (saturated)	1700	**Water**	**1400 - 1600**
		Glacial till (compacted)	1200 - 2100	Air	331.5

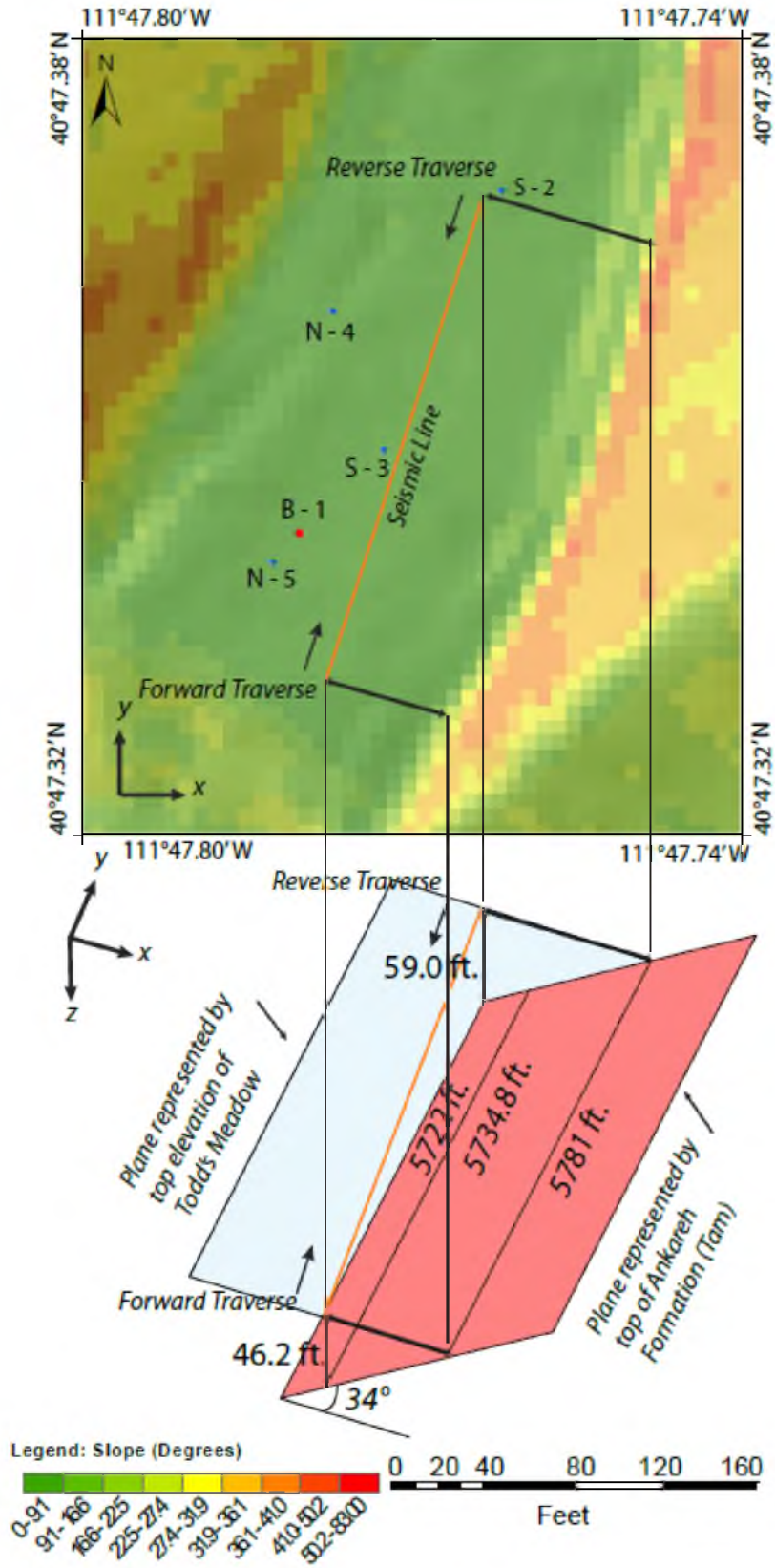

Figure 4.6, Seismic refraction interpretation of Todd's Meadow

APPENDIX A

GEOTECHNICAL DATA

Moisture Content

Moisture content was determined according to ASTM D 2216-90, Method of Laboratory Determination of Water (Moisture) Content of Soil, Rock, and Soil-Aggregate Mixtures. Moisture content is simply defined as the mass of water compared to the mass of solids in a volume of soil simply as follows (Bardet, 1997: 17).

$$w = \frac{W_w}{W_s} \times 100\ (\%) \qquad \text{[Equation A.1]}$$

Laboratory determination of water content was determined by using Equation A.2 and is presented in Tables A.1 – A.2, where W_w = mass weight of soil + container, W_d = dry mass of soil + container, and W_c = mass of container (Bardet, 1997: 18).

$$w = \frac{W_w - W_d}{W_d - W_c} \times 100\ (\%) \qquad \text{[Equation A.2]}$$

Atterberg Limits

Atterberg limit tests were conducted according to ASTM D 4318-93, Test Method for Liquid Limit, Plastic Limit, and Plasticity Index of soils. Atterberg limit test results are presented in Tables A.3 – A.7. The fundamental relationship used to defined the Atterberg Limits describes the index of plasticity, *PI*, in relation to the liquid limit, *LL*, and plastic limit, *PL* as defined by the following equation (Bardet, 1997: 34). Refer to ASTM D 4318-93 for specifics on determination of the liquid limit and plastic limit.

$$PI = LL - PL \qquad \text{[Equation A.3]}$$

Specific Gravity

Specific Gravity tests were conducted according to ASTM D 854-92, Standard Test Method for Specific Gravity of Soils. Equation A.4 is the laboratory equation for Specific Gravity where G_s = specific gravity, W_s = mass of solids, W_{fw} = mass of flask + mass of flask filled with de-aired water only, W_{fs} = mass of flask filled with deaired water + mass of solids in flask (Bardet, 1997: 47). Specific Gravity data is shown in Table A.8.

$$G_s = \frac{W_s}{W_s + W_{fw} - W_{fs}} \qquad \text{[Equation A.4]}$$

Grain Size Distribution Tests

Grain size distribution tests were conducted according to ASTM D 422-63 and ASTM 2217-85, Test Method of Particle Size Analysis of Soil (Bardet, 1997: 2). A total of 20 grain size distribution tests were performed. Data is presented in Tables A.9 – A.14.

Table A.1, Moisture content data 1

Date:	2/8/2012									
Boring #	Depth (ft)	Mass Container 1 , MC_1 (g)	Mass Container 2 , MC_2 (g)	Mass Soil 1 wet , MW_1(g)	Mass Soil 2 wet, MW_2 (g)	Mass Soil 1 dry , MD_1 (g)	Mass Soil 2 dry , MD_2(g)	w_1	w_2	Average w
B-6	19.5	0.7	0.7	41.3	46.4	31.8	35.6	23.4	23.6	23.5
	18.5	0.7	0.6	40.1	35.9	30.6	27.4	24.1	24.1	24.1
	17.3	0.7	0.7	47.2	51.2	34.1	37.0	28.2	28.1	28.1
	13.3	0.6	0.7	49.4	37.7	37.9	28.7	23.6	24.3	23.9
	9.9	0.6	0.6	42.1	34.9	32.3	26.6	23.6	24.2	23.9
	8.8	0.6	0.6	39.0	35.6	29.4	26.9	25.0	24.9	24.9
	7.8	0.8	0.7	39.5	42.2	29.7	31.5	25.3	25.8	25.6
	5.2	0.8	0.7	34.0	47.5	27.1	37.8	20.8	20.7	20.8
	3.7	0.7	0.8	36.3	48.8	29.3	39.4	19.7	19.6	19.6
	1.8	0.7	0.8	38.4	38.7	28.3	28.7	26.8	26.4	26.6

Date:	2/9/2012									
Boring #	Depth (ft)	Mass Container 1 , MC_1 (g)	Mass Container 2 , MC_2 (g)	Mass Soil 1 wet , MW_1(g)	Mass Soil 2 wet, MW_2 (g)	Mass Soil 1 dry , MD_1 (g)	Mass Soil 2 dry , MD_2(g)	w_1	w_2	Average w
B-5	14.2	0.8	0.9	44.0	56.4	34.5	44.2	22.0	22.0	22.0
	13.0	0.8	0.9	55.0	42.3	40.9	31.5	26.0	26.1	26.1
	11.5	0.8		41.5		31.6		24.3		24.3
	10.0	0.6		50.9		40.1		21.5		21.5
	8.8	0.7	0.7	39.1	45.6	29.5	34.4	25.0	24.9	25.0
	8.0	0.7	0.7	54.3	46.2	40.4	34.7	25.9	25.3	25.6
	6.3	0.7	0.7	45.7	48.6	35.3	37.2	23.1	23.8	23.5
	5.1	0.8	0.8	51.1	40.1	40.0	31.6	22.1	21.6	21.8
	4.6	0.9	0.8	50.7	43.6	42.5	36.2	16.5	17.3	16.9
	3.2	0.8	0.9	52.8	40.0	41.8	31.7	21.2	21.2	21.2
	1.3	0.9	0.9	48.7	41.3	38.1	32.1	22.2	22.8	22.5

Date:	2/10/2012									
Boring #	Depth (ft)	Mass Container 1 , MC_1 (g)	Mass Container 2 , MC_2 (g)	Mass Soil 1 wet , MW_1(g)	Mass Soil 2 wet, MW_2 (g)	Mass Soil 1 dry , MD_1 (g)	Mass Soil 2 dry , MD_2(g)	w_1	w_2	Average w
B-7	14.8	0.9	0.9	71.0	78.5	57.1	62.7	19.8	20.4	20.1
	10.0	0.8	0.8	78.3	37.2	62.9	30.0	19.9	19.8	19.8
	8.8	0.9	0.9	44.1	34.7	35.7	28.3	19.4	18.9	19.2
	6.0	0.9	0.8	37.8	47.2	31.2	39.3	17.9	17.0	17.5
	5.0	0.9	0.9	47.0	37.9	40.3	32.1	14.5	15.7	15.1
	3.8	0.8	0.9	36.0	32.9	31.7	29.2	12.2	11.6	11.9
	2.0	0.9	1.0	38.6	47.8	33.7	41.5	13.0	13.5	13.2
	1.0	0.9		38.8		31.5		19.3		19.3

Date:	2/13/2012									
Boring #	Depth (ft)	Mass Container 1 , MC_1 (g)	Mass Container 2 , MC_2 (g)	Mass Soil 1 wet , MW_1(g)	Mass Soil 2 wet, MW_2 (g)	Mass Soil 1 dry , MD_1 (g)	Mass Soil 2 dry , MD_2(g)	w_1	w_2	Average w
B-8	6.0	1.0	1.0		38.5	31.3	33.4	-	13.6	13.6
	4.8	0.9	1.1	40.1	30.7	34.3	26.3	14.8	14.9	14.8
	2.5	0.9	0.8	43.5	34.5	38.8	30.9	11.0	10.7	10.9

Table A.2, Moisture content data 2

Date:	2/14/2012									
Boring #	Depth (ft)	Mass Container 1 , MC_1	Mass Container 2 , MC_2	Mass Soil 1 wet , MW_1(g)	Mass Soil 2 wet, MW_2 (g)	Mass Soil 1 dry , MD_1 (g)	Mass Soil 2 dry , MD_2(g)	w_1	w_2	Average w
B-2	2.0	0.8		34.5		27.5		20.8	0.0	10.4
	2.5	0.9	0.8	27.0	30.0	22.6	25.1	16.9	16.8	16.8
	3.0	1.0	0.9	28.3	33.9	23.1	28.1	19.0	17.6	18.3
	4.3	0.8		25.7		21.2		18.1		18.1
	5.0	1.1	1.0	37.1	27.8	29.4	22.5	21.4	19.8	20.6
	6.2	0.8	0.9	33.2	30.6	25.5	23.6	23.8	23.6	23.7
	7.5	0.9	1.0	34.5	33.5	25.4	24.7	27.1	27.1	27.1
	8.2	0.9	0.8	36.3	35.1	27.1	26.3	26.0	25.7	25.8
	9.3	1.0	0.9	39.8	36.7	28.8	26.6	28.4	28.2	28.3
	10.0	1.0	0.9	37.7	30.2	28.0	22.3	26.4	27.0	26.7
	11.3	1.1		37.3		24.2		36.2		36.2
	11.9	1.0	1.0	33.6	32.9	23.4	22.0	31.3	34.2	32.7
	14.5	1.0	1.0	35.8	31.4	21.8	19.8	40.2	38.2	39.2
	15.1	1.0	1.0	31.6	34.9	19.8	21.6	38.6	39.2	38.9

Date:	2/15/2012									
Boring #	Depth (ft)	Mass Container 1 , MC_1	Mass Container 2 , MC_2	Mass Soil 1 wet , MW_1(g)	Mass Soil 2 wet, MW_2 (g)	Mass Soil 1 dry , MD_1 (g)	Mass Soil 2 dry , MD_2(g)	w_1	w_2	Average w
B-1	1.0	0.9		31.8		26.4		17.5		17.5
	2.5	1.0		32.4		28.7		11.8		11.8
	3.5	1.2		34.4		29.8		13.9		13.9
	4.5	1.2		31.7		26.3		17.7		17.7
	5.5	1.2		35.1		30.4		13.9		13.9
	6.0	1.2		35.2		28.7		19.1		19.1
	7.5	1.3		32.9		27.2		18.0		18.0
	8.0	1.2		34.5		28.9		16.8		16.8
	8.5	1.1		33.6		26.7		21.2		21.2
	9.5	1.0		36.0		26.3		27.7		27.7
	10.0	1.2		33.1		25.6		23.5		23.5
	11.5	1.0	1.1	41.3	37.6	32.1	29.7	22.8	21.6	22.2
	12.1	1.1	1.1	31.1	35.1	24.1	27.2	23.3	23.2	23.3
	13.3	1.1	1.1	40.4	29.8	28.7	21.2	29.8	30.0	29.9
	14.8	1.1	1.1	30.9	30.6	22.7	21.6	27.5	30.5	29.0
	16.1	1.1		29.5		20.0		33.5		33.5
	17.5	1.0	1.0	39.1	32.2	28.2	23.3	28.6	28.5	28.6
	18.0	1.0	1.1	49.6	36.6	34.3	25.6	31.5	31.0	31.2
	19.2	1.1	1.1	60.7	45.4	42.3	32.1	30.9	30.0	30.4

Date:	2/16/2012									
Boring #	Depth (ft)	Mass Container 1 , MC_1	Mass Container 2 , MC_2	Mass Soil 1 wet , MW_1(g)	Mass Soil 2 wet, MW_2 (g)	Mass Soil 1 dry , MD_1 (g)	Mass Soil 2 dry , MD_2(g)	w_1	w_2	Average w
B-4	1.1	0.8	0.8	41.8	45.7	35.2	38.5	16.1	16.0	16.1
	1.8	0.9	1.0	31.1	34.9	26.7	30.1	14.6	14.2	14.4
	2.5	1.0	1.2	39.8	34.6	34.2	30.0	14.4	13.8	14.1
	3.0	1.0	1.0	31.9	45.9	27.6	39.3	13.9	14.7	14.3
	3.7	0.9	0.9	34.8	31.6	29.4	26.9	15.9	15.3	15.6
	4.2	0.9	0.9	28.7	39.5	23.5	32.8	18.7	17.4	18.0

Table A.3, Summary of Atterberg limits data 1

B - 1		*Liquid Limit Test*						*Plastic Limit Test*					Liquid Limit (%) *L.L.*	Plastic Limit (%) *P.L.*	Index of Plasticity (%) *I.P.*
Depth (ft)	Set #	Tare Mass (g) W_c	Tare Mass with Wet Soil, W_w	Tare Mass with Dry Soil, W_d	Blow Count, N	Water Content, *w*	Water Content, fitted, *w*	Tare Mass (g), W_c	Tare Mass with Wet Soil, W_w	Tare Mass with dry Soil, W_d	Water Content, *w*	Plastic Limit Comment			
0.5-1.3	1	0.5	8.4	5.4	5	61.2%	61.4%	0.4	1.4	1.11	40.8%	At	53.8%	40.0%	13.8%
	2	0.5	13.5	8.7	10	58.5%	58.5%	0.4	3.6	2.5	52.4%	Above			
	3	0.5	12.4	8.2	21	54.5%	54.7%	0.4	3.3	2.4	45.0%	Above			
	4	0.5	8.2	5.5	25	54.0%	53.8%	-	-	-	-	-			
2.5-3.5	1	0.5	15.2	10.2	-	-	-	0.4	2.9	2.3	31.6%	Below	48.9%	30.0%	18.9%
	2	0.5	8.5	5.7	19	53.8%	53.8%	0.4	1.5	1.1	57.1%	At			
	3	0.5	15.5	10.5	23	50.0%	50.4%	0.4	1.8	1.4	40.0%	Below			
	4	0.5	12.2	8.3	24	50.0%	49.7%	-	-	-	-	-			
4.6-5.1	1	0.0176	0.49	0.36	8	38.0%	38.3%	0.0176	0.11	0.095	18.4%	At	31.3%	18.0%	13.3%
	2	0.0176	0.38	0.285	14	35.5%	34.9%	0.0176	0.095	0.085	14.8%	Below			
	3	0.0176	0.435	0.335	23	31.5%	31.9%	0.0176	0.065	0.06	11.8%	Below			
	4	-	-	-	-	-	-	-	-	-	-	-			
5.0 - 5.5	1	0.5	9.2	6.5	13	45.0%	43.9%	0.4	2.1	1.7	30.8%	Above / At	41.8%	28.0%	13.8%
	2	0.5	9.8	7.1	19	40.9%	42.7%	0.4	2.2	1.8	28.6%	At			
	3	0.5	10.4	7.5	34	41.4%	40.9%	-	-	-	-	-			
	4	0.5	12.3	8.9	40	40.5%	40.4%	-	-	-	-	-			
13.6-14.1	1	0.5	8.2	6	13	40.0%	-	0.4	4.4	3.4	33.3%	Above	39.4%	25.0%	14.4%
	2	0.5	9.3	6.7	16	41.9%	-	0.4	2.7	2.2	25.4%	At			
	3	0.5	8.9	6.4	16	42.4%	42.4%	0.4	3.3	2.6	31.8%	Above			
	4	0.5	8.8	6.5	30	38.3%	38.2%	0.4	2.4	1.9	33.3%	Above			
	5	0.5	9.8	7.2	27	38.8%	38.9%	-	-	-	-	-			
19.2-19.8	1	0.5	12.9	9.6	13	36.3%	-	0.4	2.4	1.9	33.3%	Above	40.2%	20.0%	20.2%
	2	0.5	12.9	9.65	13	35.5%	35.3%	0.4	2.5	2.1	20.5%	At			
	3	0.5	11.8	8.9	16	34.5%	35.0%	0.4	5.6	4.4	30.0%	Above			
	4	0.5	7.2	5.55	35	32.7%	32.6%	0.5	-	-	-	-			

Table A.4, Summary of Atterberg limits data 2

B - 2		*Liquid Limit Test*						*Plastic Limit Test*					Liquid Limit (%) *L.L.*	Plastic Limit (%) *P.L.*	Index of Plasticity (%) *I.P.*
Depth (ft)	Set #	Tare Mass (g) W_c	Tare Mass with Wet Soil, W_w	Tare Mass with Dry	Blow Count, N	Water Content, *w*	Water Content, fitted, *w*	Tare Mass (g), W_c	Tare Mass with Wet	Tare Mass with dry	Water Content, *w*	Plastic Limit Comments			
0.8 - 2.0	1	0.5	5.7	3.83	15	56.2%	58.1%	0.5	2	1.5	50.0%	Above	55.4%	40.0%	15.4%
	2	0.5	7.2	4.67	13	60.7%	58.9%	0.5	1.8	1.3	62.5%	Above			
	3	0.5	4.7	3.2	24	55.6%	55.6%	0.5	3	2.2	40.1%	Above			
	4	0.5	7.5	5.103	48	52.1%	51.8%	0.5	1.1	0.9	50.0%	Above			
7.8 - 8.2	1	0.5	5.3	3.9	14	41.2%	41.2%	0.5	2.1	1.7	33.3%	Above	38.4%	20.0%	18.4%
	2	0.5	6.5	4.8	19	39.5%	39.7%	0.5	1.9	1.6	27.3%	Above			
	3	0.5	6.7	5	33	37.8%	37.1%	0.5	2.5	2.1	20.4%	At			
	4	0.5	7	5.3	42	35.4%	35.9%	0.5	2.9	2.4	26.3%	Above			
9.3 - 10.0	1	0.5	4.5	3.2	74	48.1%	48.1%	0.5	1.6	1.2	57.1%	Above	58.2%	28.0%	30.2%
	2	0.5	5.3	3.7	62	50.0%	49.8%	0.5	1.6	1.3	28.3%	At			
	3	0.5	5.9	4.2	93	45.9%	46.0%	0.5	1.9	1.5	40.0%	Above			
	4	0.5	5.8	4.0	51	51.4%	51.6%	0.5	2.5	1.9	42.9%	Above			
13.9 - 14.5	1	0.5	8.9	5.7	52	61.5%	61.6%	0.5	3.4	2.8	26.1%	At	65.5%	26.1%	39.4%
	2	0.5	10.2	6.4	31	64.4%	64.4%	0.5	3.7	2.5	60.0%	Above			
	3	0.5	7.4	4.6	14	68.3%	68.6%	0.5	5.7	3.8	57.6%	Above			
	4	0.5	7.9	4.9	16	68.2%	67.9%	-	-	-	-	-			

Table A.4, Summary of Atterberg limits data 3

B - 5		*Liquid Limit Test*						*Plastic Limit Test*					Liquid Limit (%) *L.L.*	Plastic Limit (%) *P.L.*	Index of Plasticity (%) *I.P.*
Depth (ft)	Set #	Tare Mass (g) W_c	Tare Mass with Wet Soil,	Tare Mass with Dry Soil, W_d	Blow Count, N	Water Content, *w*	Water Content, fitted, *w*	Tare Mass (g), W_c	Tare Mass with Wet Soil, W_w	Tare Mass with dry Soil, W_d	Water Content, *w*	Plastic Limit Comment			
1.3 - 1.9	1	0.5	12.2	8.4	12	48.1%	48.7%	0.5	1.8	1.5	30.0%	At	45.6%	30.0%	15.6%
	2	0.5	13.9	9.6	21	47.3%	46.3%	0.5	1.5	1.2	42.9%	above			
	3	0.5	10.4	7.3	28	45.6%	45.1%	0.5	2.2	1.8	30.8%	At			
	4	0.5	11.8	8.4	37	43.0%	43.9%	0.5	3.5	2.8	30.4%	At			
	5	-	-	-	-	-	-	0.4	2.8	2.2	33.3%	Above			
2.5 - 3.2	1	0.5	11.8	8.6	16	39.5%	39.2%	0.5	2.8	2.3	24.8%	At	38.1%	24.8%	13.2%
	2	0.5	14.5	10.6	18	38.6%	38.9%	0.5	2.9	2.3	33.3%	Above			
	3	0.5	13.2	9.8	48	36.6%	36.4%	0.5	2.3	2	20.0%	Below			
	4	0.5	11.2	8.3	33	37.2%	37.4%	0.5	1.8	1.6	18.2%	Below			
3.8 - 4.6	1	0.5	12.3	9.5	15	31.1%	31.6%	0.5	2.7	2.4	18.4%	At	29.6%	18.0%	11.6%
	2	0.5	16.9	12.9	14	32.3%	31.8%	0.5	2.5	2.1	25.0%	Above			
	3	0.5	18.4	14.4	32	28.8%	28.7%	0.5	2	1.7	25.0%	Above			
	4	0.5	12	9.5	40	27.8%	27.8%	0.5	-	-	-	-			
5.6 - 6.3	1	0.5	12.8	9.2	19	41.4%	41.1%	0.5	1	0.9	25.0%	Above	40.4%	15.0%	25.4%
	2	0.5	13	9.4	22	40.4%	40.7%	0.5	1.4	1.2	28.6%	Above			
	3	0.5	11.8	8.5	17	41.3%	41.3%	0.5	1.3	1.2	14.3%	At			
	4	0.5	22.1	16	40	39.4%	39.3%	0.5	1.4	1.3	12.5%	Below			
8.0 - 8.8	1	0.5	11.2	7.9	6	44.6%	44.7%	0.5	4.4	3.6	25.8%	Above	37.0%	20.0%	17.0%
	2	0.5	10.4	7.5	12	41.4%	41.0%	0.5	2.2	1.9	20.6%	At			
	3	0.5	10.1	7.4	16	39.1%	39.4%	0.5	2.6	2.2	23.5%	Above			
	4	0.5	11.1	8.3	35	35.9%	35.2%	0.5	1.7	1.4	33.3%	Above			
	5	0.5	11.2	8.4	29	35.4%	36.2%	-	-	-	-	-			
13.7 - 14.3	1	0.5	7.6	5.9	8	31.5%	31.6%	0.5	1.5	1.3	25.0%	Above	29.9%	20.0%	9.9%
	2	0.5	7.2	5.6	11	31.4%	31.2%	0.5	2.5	2.2	17.6%	Below			
	3	0.5	10	7.8	23	30.1%	30.1%	0.5	2.3	2	20.0%	At			
	4	0.5	11.7	9.1	20	30.2%	30.3%	-	-	-	-	-			
	5	0.5	7.8	6.3	20	25.9%	29.0%	-	-	-	-	-			

Table A.5, Summary of Atterberg limits data 4

B - 6		*Liquid Limit Test*						*Plastic Limit Test*					Liquid Limit (%) $L.L._*$	Plastic Limit (%) $P.L._*$	Index of Plasticity (%) $I.P._*$
Depth (ft)	Set #	Tare Mass (g) W_c	Tare Mass with Wet Soil, W_w	Tare Mass with Dry Soil,	Blow Count, N	Water Content, *w*	Water Content, fitted,	Tare Mass (g), W_c	Tare Mass with Wet Soil,	Tare Mass with dry Soil, W_d	Water Content, *w*	Plastic Limit Comments			
1.2 - 1.8	1	0.5	7.2	4.5	10	67.5%	67.0%	0.5	1.0	0.9	25.0%	At	60.8%	25.0%	35.8%
	2	0.5	8.1	5.2	18	61.7%	63.1%	0.5	1.5	1.2	42.9%	Below			
	3	0.5	9.4	6.0	25	61.8%	60.8%	0.5	2.1	1.7	33.3%	Below			
	4	0.5	7.4	4.9	45	56.8%	56.9%	0.5	0.9	0.72	81.8%	Above			
5.3 - 6.0	1	0.5	5.9	4.4	17	38.5%	39.3%	0.5	1.8	1.5	30.0%	Above	38.8%	23.0%	15.8%
	2	0.5	7.1	5.2	24	40.4%	38.9%	0.5	2.3	1.8	38.5%	Above			
	3	0.5	5.6	4.2	32	37.8%	38.5%	0.5	2.1	1.8	23.1%	At			
	4	0.5	8.2	6.1	68	37.5%	37.6%	0.5	2	1.6	36.4%	Above			
9.0 - 9.8	1	0.4	8.5	6.3	28	37.3%	36.8%	0.4	1.6	1.4	20.0%	Below	38.6%	25.0%	13.6%
	2	0.3	10.2	7.5	32	37.5%	36.3%	0.3	1.4	1.2	22.2%	At			
	3	0.4	6.7	5.1	45	34.0%	34.9%	0.4	1.3	1.1	25.2%	At			
	4	0.3	10.6	7.8	20	37.3%	38.1%	0.4	1.8	1.5	27.3%	Above			
12.8-13.3	1	0.5	9.1	6.8	45	36.5%	39.4%	0.5	1.3	1.1	33.3%	Above	35.7%	17.0%	18.7%
	2	0.5	8.9	6.7	35	36.6%	36.0%	0.5	2.0	1.7	25.0%	Below			
	3	0.5	6.6	5.0	25	35.6%	31.4%	0.5	1.2	1.1	16.7%	At			
	4	0.5	8.3	7.1	11	18.2%	20.0%	0.5	1.1	1.0	20.0%	Above			
16.5-17.3	1	0.5	4.5	3.2	17	48.1%	46.9%	0.5	1.3	1.1	33.3%	Above	45.8%	19.0%	26.8%
	2	0.5	4.1	3	24	44.0%	45.9%	0.5	2.0	1.7	25.0%	Below			
	3	0.5	6	4.3	47	44.7%	44.1%	0.5	1.2	1.1	16.7%	Below			
	4	0.5	4.5	3.3	77	42.9%	42.8%	0.5	1.1	1.0	19.5%	At			
18.9-19.5	1	0.5	6.7	5.0	23	37.8%	37.9%	0.5	1	0.9	25.0%	At	36.9%	25.0%	11.9%
	2	0.5	6.2	4.6	22	39.0%	38.3%	0.5	1.1	1	20.0%	Below			
	3	0.5	6.3	5.0	44	28.9%	32.5%	0.5	1.6	1.3	37.5%	Above			
	4	0.5	8.3	6.3	50	34.5%	31.4%	0.5	2.3	1.8	38.5%	Above			

Table A.6, Summary of Atterberg limits data 5

B - 7		*Liquid Limit Test*						*Plastic Limit Test*					Liquid Limit (%)	Plastic Limit (%)	Index of Plasticity (%)
Depth (ft)	Set #	Tare Mass (g) W_c	Tare Mass with Wet Soil, W_w	Tare Mass with Dry Soil, W_d	Blow Count, N	Water Content, w	Water Content, fitted, w	Tare Mass (g), W_c	Tare Mass with Wet Soil, W_w	Tare Mass with dry Soil, W_d	Water Content, w	Plastic Limit Comments	*L.L.*	*P.L.*	*I.P.*
4.2 - 5.0	1	13.6	18.2	17.1	61	31.43%	32.84%	13.8	14.5	14.4	16.67%	At	34.04%	17.00%	17.04%
	2	13.7	17.9	16.8	36	35.48%	33.55%	13.8	15.2	14.8	40.00%	Above			
	3	13.7	17.3	16.4	18	33.33%	34.48%	13.8	14.8	14.5	42.86%	Below			
	4	13.8	18.5	17.3	33	34.29%	33.66%	13.9	15.0	14.7	37.50%	Above			
9.0 - 9.9	1	13.8	19.6	18.3	58	28.89%	28.73%	13.9	15.0	14.7	37.50%	Above	31.29%	15.00%	16.29%
	2	13.6	17.2	16.3	19	33.33%	32.13%	13.9	14.8	14.65	20.00%	Below			
	3	13.8	17.6	16.7	28	31.03%	30.95%	14.0	14.7	14.6	15.30%	At			
	4	13.6	19.2	17.9	22	30.23%	31.68%	13.9	14.2	14.2	20.00%	Below			
13.3 - 14.1	1	13.9	21.7	19.9	52	30.00%	29.30%	13.7	15.5	15.2	20.00%	Above	31.33%	15.00%	16.33%
	2	13.8	22.5	20.5	34	29.85%	30.36%	14.0	14.8	14.6	33.33%	Above			
	3	13.8	23.8	21.3	15	33.33%	32.85%	13.9	14.9	14.8	11.11%	Below			
	4	13.9	18.6	17.5	24	30.56%	31.42%	13.8	15.1	14.9	15.04%	At			
B - 8		*Liquid Limit Test*						*Plastic Limit Test*					Liquid Limit (%)	Plastic Limit (%)	Index of Plasticity (%)
Depth (ft)	Set #	Tare Mass (g) W_c	Tare Mass with Wet Soil, W_w	Tare Mass with Dry Soil, W_d	Blow Count, N	Water Content, w	Water Content, fitted, w	Tare Mass (g), W_c	Tare Mass with Wet Soil, W_w	Tare Mass with dry Soil, W_d	Water Content, w	Plastic Limit Comments	*L.L.*	*P.L.*	*I.P.*
2.0 - 2.5	1	0.5	11.2	8.7	40	0.30487805	30.55%	0.5	1.4	1.2	28.57%	Below	31.87%	29.00%	2.87%
	2	0.5	11.3	8.7	27	0.31707317	31.65%	0.5	1.2	1	40.00%	Above			
	3	0.5	11	8.4	16	0.32911392	33.13%	0.5	1.6	1.35	29.41%	At			
	4	-	-	-	-	-	-	0.5	1.8	1.6	18.18%	Below			
5.5 - 6.0	1	0.5	16.6	12.7	10	0.31967213	32.00%	0.5	4.3	3.3	35.71%	Above	24.79%	20.00%	4.79%
	2	0.5	9.5	7.5	16	0.28571429	28.30%	0.5	2	1.8	20.00%	At			
	3	0.5	15.3	12.1	17	0.27586207	27.83%	0.5	2.9	2.4	26.32%	Above			
	4	0.5	8.2	6.1	68	37.50%	37.59%	0.5	2	1.6	36.36%	Above			

Table A.7, Summary of liquid limit, plastic limit, index of plasticity

Boring #	Depth (ft)	Liquid Limit ***L.L.***	Plastic Limit ***P.L.***	Index of Plasticity ***I.P.***
B -1	0.5-1.3	53.8%	40.0%	13.8%
	2.5-3.5	48.9%	30.0%	18.9%
	4.6-5.1	31.3%	18.0%	13.3%
	5.0 - 5.5	41.8%	28.0%	13.8%
	13.6-14.1	39.4%	25.0%	14.4%
	19.2-19.8	40.2%	20.0%	20.2%
B - 2	0.8 - 2.0	55.4%	40.0%	15.4%
	7.8 - 8.2	38.4%	20.0%	18.4%
	9.3 - 10.0	58.2%	28.0%	30.2%
	13.9 -14.5	65.5%	26.1%	39.4%
B - 5	1.3 - 1.9	45.6%	30.0%	15.6%
	2.5 - 3.2	38.1%	24.8%	13.2%
	3.8 - 4.6	29.6%	18.0%	11.6%
	5.6 - 6.3	40.4%	15.0%	25.4%
	8.0 - 8.8	37.0%	20.0%	17.0%
	13.7 - 14.3	29.9%	20.0%	9.9%
B - 6	1.2 - 1.8	60.8%	25.0%	35.8%
	5.3 - 6.0	38.8%	23.0%	15.8%
	9.0 - 9.8	38.6%	25.0%	13.6%
	12.8-13.3	35.7%	17.0%	18.7%
	16.5-17.3	45.8%	19.0%	26.8%
	18.9-19.5	36.9%	25.0%	11.9%
B - 7	4.2 - 5.0	34.0%	17.0%	17.0%
	9.0 - 9.9	31.3%	15.0%	16.3%
	13.3-14.1	31.3%	15.0%	16.3%
B - 8	2.0 - 2.5	31.9%	29.0%	2.9%
	5.5 - 6.0	24.8%	20.0%	4.8%

Table A.8, Summary of specific gravity data

Boring #	Depth (ft)	M_{fw} (oz)	M_{fs} (oz)	M_c (oz)	M_d (oz)	G_s
B-1	1	24.120	25.610	0.485	3.005	2.447
	3.5	24.120	25.725	0.485	3.080	2.621
	5.1	24.120	24.810	0.500	1.610	2.643
	7.5	24.120	25.845	0.485	3.260	2.643
	14.3	24.120	25.505	0.480	2.675	2.710
	17.5	24.120	26.415	0.490	4.160	2.669
	19.5	24.120	25.930	0.485	3.380	2.668
B-2	4	24.120	25.130	0.485	2.145	2.554
	6.2	24.120	24.120	25.175	0.485	2.551
	8.1	24.120	24.660	0.485	1.400	2.440
	11.9	24.120	25.185	0.485	2.225	2.578
	15.1	24.120	25.110	0.495	2.335	2.165
B-5	1.3	24.120	25.860	0.500	3.280	2.673
	4.6	24.120	24.120	26.270	0.500	2.693
	6.3	24.120	25.875	0.500	3.265	2.738
	8.8	24.120	25.725	0.480	3.080	2.613
	14.3	24.120	26.585	0.500	4.450	2.660
B-6	1.8	24.120	25.080	0.490	2.030	2.655
	3.8	24.120	25.600	0.495	2.900	2.600
	5.8	24.120	25.610	0.485	2.875	2.656
	9.1	24.120	26.170	0.485	3.750	2.687
	12.3	24.120	25.995	0.495	3.510	2.645
	17.3	24.120	25.795	0.490	3.195	2.626
B-7	5	24.120	25.850	0.485	3.520	2.326
	9.9	24.120	27.430	0.485	5.745	2.697
	14.1	24.120	26.350	0.490	4.035	2.696
B-8	0.6	24.120	25.755	0.485	3.125	2.627
	2	24.120	26.535	0.485	4.315	2.707
	6	24.120	25.875	0.485	3.255	2.729

Table A.9, B – 1Grain size distributions

B-1 17.5'	Sieve Number	Diameter (mm)	Percent Finer by Weight	USCS Soil Type
		16	96.90%	**SC Clayey Sand**
	10	2	80.17%	
	20	1	69.24%	
	30	0.6	65.78%	
	40	0.425	61.64%	
	80	0.19	51.46%	
	100	0.15	49.11%	
	170	0.09	42.62%	
	200	0.075	39.93%	
B-1 6.0' - 8.5'	Sieve Number	Diameter (mm)	Percent Finer by Weight	USCS Soil Type
		16	100.00%	**CL Sandy Lean Clay**
	10	2	94.80%	
	20	1	87.73%	
	30	0.6	83.90%	
	40	0.425	79.59%	
	80	0.19	70.76%	
	100	0.15	68.60%	
	170	0.09	59.53%	
	200	0.075	56.13%	
B-1 2.0' - 5.5'	Sieve Number	Diameter (mm)	Percent Finer by Weight	USCS Soil Type
		16	98.56%	**CL Sandy Lean Clay**
	10	2	94.13%	
	20	1	87.70%	
	30	0.6	84.31%	
	40	0.425	80.22%	
	80	0.19	69.03%	
	100	0.15	66.43%	
	170	0.09	59.14%	
	200	0.075	56.48%	

Table A.10, B – 2 Grain size distributions

B-2 14.5'-15.9'	Sieve Number	Diameter (mm)	Percent Finer by Weight	USCS Soil Type
		16	98.20%	**CH Sandy Fat Clay**
	10	2	92.52%	
	20	1	88.06%	
	30	0.6	86.11%	
	40	0.425	83.56%	
	80	0.19	74.98%	
	100	0.15	72.97%	
	170	0.09	66.15%	
	200	0.075	63.59%	
B-2 9.0'-10.0'	Sieve Number	Diameter (mm)	Percent Finer by Weight	USCS Soil Type
		16	100.00%	**CH Sandy Fat Clay**
	10	2	93.13%	
	20	1	86.07%	
	30	0.6	83.24%	
	40	0.425	79.94%	
	80	0.19	71.61%	
	100	0.15	70.22%	
	170	0.09	64.57%	
	200	0.075	62.68%	
B-2 5.8' - 7.5'	Sieve Number	Diameter (mm)	Percent Finer by Weight	USCS Soil Type
		16	100.00%	**CL Sandy Lean Clay**
	10	2	91.63%	
	20	1	84.33%	
	30	0.6	81.13%	
	40	0.425	77.27%	
	80	0.19	65.59%	
	100	0.15	63.21%	
	170	0.09	55.29%	
	200	0.075	51.92%	
B-2 0.8' - 3.0'	Sieve Number	Diameter (mm)	Percent Finer by Weight	USCS Soil Type
		16	98.81%	**CL Sandy Lean Clay**
	10	2	88.09%	
	20	1	79.42%	
	30	0.6	75.95%	
	40	0.425	71.73%	
	80	0.19	60.50%	
	100	0.15	58.68%	
	170	0.09	52.18%	
	200	0.075	49.64%	

Table A.11, B – 4, B – 5 Grain size distributions

B-4 3.7' - 4.2'	Sieve Number	Diameter (mm)	Percent Finer by Weight	USCS Soil Type
		16	96.00%	**SC Clayey Sand**
	10	2	73.38%	
	20	1	61.96%	
	30	0.6	58.63%	
	40	0.425	55.50%	
	80	0.19	43.10%	
	100	0.15	41.92%	
	170	0.09	31.94%	
	200	0.075	29.10%	

B-5 14.5'	Sieve Number	Diameter (mm)	Percent Finer by Weight	USCS Soil Type
		16	100.00%	**CL Lean Clay with Sand**
	10	2	96.71%	
	20	1	93.67%	
	30	0.6	92.67%	
	40	0.425	91.55%	
	80	0.19	88.71%	
	100	0.15	87.89%	
	170	0.09	80.42%	
	200	0.075	77.60%	
B-5 7.3' - 8.5'	Sieve Number	Diameter (mm)	Percent Finer by Weight	USCS Soil Type
		16	98.56%	**CL Sandy Lean Clay**
	10	2	94.13%	
	20	1	87.70%	
	30	0.6	84.31%	
	40	0.425	80.22%	
	80	0.19	69.03%	
	100	0.15	66.43%	
	170	0.09	59.14%	
	200	0.075	56.48%	
B-5 3.8' - 5.1'	Sieve Number	Diameter (mm)	Percent Finer by Weight	USCS Soil Type
		16	96.51%	**CL Sandy Lean Clay**
	10	2	87.47%	
	20	1	79.98%	
	30	0.6	76.01%	
	40	0.425	71.15%	
	80	0.19	63.37%	
	100	0.15	61.87%	
	170	0.09	57.07%	
	200	0.075	54.42%	

Table A.12, B – 6 Grain size distributions

B-6 18.5' - 19.5'	Sieve Number	Diameter (mm)	Percent Finer by Weight	USCS Soil Type
		16	98.15%	SC Clayey Sand
	10	2	78.37%	
	20	1	66.30%	
	30	0.6	61.20%	
	40	0.425	55.49%	
	80	0.19	42.36%	
	100	0.15	39.97%	
	170	0.09	34.25%	
	200	0.075	32.79%	
B-6 12.2' - 13.3'	Sieve Number	Diameter (mm)	Percent Finer by Weight	USCS Soil Type
		16	93.81%	SC Clayey Sand
	10	2	72.26%	
	20	1	59.18%	
	30	0.6	53.91%	
	40	0.425	48.37%	
	80	0.19	36.27%	
	100	0.15	33.95%	
	170	0.09	28.69%	
	200	0.075	27.07%	
B-6 7.9' - 9.10'	Sieve Number	Diameter (mm)	Percent Finer by Weight	USCS Soil Type
		16	97.13%	SC Clayey Sand
	10	2	82.89%	
	20	1	72.50%	
	30	0.6	68.24%	
	40	0.425	63.61%	
	80	0.19	53.34%	
	100	0.15	51.25%	
	170	0.09	46.29%	
	200	0.075	44.49%	
B-6 1.8' - 3.9'	Sieve Number	Diameter (mm)	Percent Finer by Weight	USCS Soil Type
		16	97.24%	SC Clayey Sand
	10	2	76.66%	
	20	1	60.94%	
	30	0.6	54.72%	
	40	0.425	48.03%	
	80	0.19	32.86%	
	100	0.15	29.65%	
	170	0.09	22.95%	
	200	0.075	20.80%	

Table A.13, B – 7 Grain size distributions

B-7 14.1'	Sieve Number	Diameter (mm)	Percent Finer by Weight	USCS Soil Type
		16	97.18%	**CL Sandy Lean Clay**
	10	2	73.75%	
	20	1	63.74%	
	30	0.6	59.62%	
	40	0.425	55.58%	
	80	0.19	53.86%	
	100	0.15	53.25%	
	170	0.09	50.83%	
	200	0.075	48.82%	
B-7 8.2' - 9.9'	Sieve Number	Diameter (mm)	Percent Finer by Weight	USCS Soil Type
		16	96.91%	**CL Sandy Lean Clay**
	10	2	73.69%	
	20	1	65.43%	
	30	0.6	62.26%	
	40	0.425	59.18%	
	80	0.19	53.91%	
	100	0.15	53.34%	
	170	0.09	50.62%	
	200	0.075	49.42%	
B-7 5.0' -6.0'	Sieve Number	Diameter (mm)	Percent Finer by Weight	USCS Soil Type
		16	97.53%	**CL Sandy Lean Clay**
	10	2	77.22%	
	20	1	69.05%	
	30	0.6	65.48%	
	40	0.425	62.63%	
	80	0.19	57.30%	
	100	0.15	56.34%	
	170	0.09	53.39%	
	200	0.075	51.84%	
B-7 1.1' - 2.1'	Sieve Number	Diameter (mm)	Percent Finer by Weight	USCS Soil Type
		16	98.24%	**CL Sandy Lean Clay**
	10	2	78.70%	
	20	1	68.21%	
	30	0.6	65.08%	
	40	0.425	63.06%	
	80	0.19	53.53%	
	100	0.15	52.37%	
	170	0.09	48.95%	
	200	0.075	47.27%	

Table A.14, B – 8 Grain size distributions

B-8 5.3' - 6.0'	Sieve Number	Diameter (mm)	Percent Finer by Weight	USCS Soil Type
		16	100.00%	**CL -ML Silty Sandy Clay**
	10	2	95.17%	
	20	1	88.51%	
	30	0.6	86.09%	
	40	0.425	82.93%	
	80	0.19	76.25%	
	100	0.15	74.95%	
	170	0.09	68.01%	
	200	0.075	65.98%	

APPENDIX B

DRAINED AND UNDRAINED SHEAR STRENGTH

Drained Strength

The drained shear strength angle, ϕ', and cohesive strength, c', has been determined from the Mohr-Coulomb strength criterion in Equation B.1 (Duncan & Wright, 2005: 22). CU tests typically are presented in terms of the Mohr-Coulomb strength criterion with Mohr circles. However, due to unusual test results, the CU test results have been plotted in $p' - q$ space.

$$s = c' + \sigma' tan\phi' \qquad \text{[Equation B.1]}$$

The drained shear strength of the soils was identified through the effective stress paths in $p' - q$ space from CU tests. The drained shear strength is observed from the effective stress path where the point of maximum shear stresses occur, typically associated with the point of maximum stress in $p' - q$ space (Abramson et. al, 2002: 249). The critical failure line, *Kf*, is also determined from the point of maximum stress, where the drained shear friction angle corresponds to the angle ψ. Figures B.1 - B.3 show the drained friction angle as well as cohesive strength is $p' - q$ space, *a*. The factors ψ and a are then related back to the original $p' - q$ space with the following equations.

CU Test results for B – 1, B – 6, and B – 8 are shown in Figures B.1 to B.2. Relevant equations relating the typical σ' – τ space to $p'-q$ space are shown in Equations B.2 to B.6 (Abramson et. al, 2002: 249).

$$p' = \frac{1}{2}(\sigma'_1 + \sigma'_3) \qquad \text{[Equation B.2]}$$

$$q = \frac{(\sigma'_1 - \sigma'_3)}{2} \qquad \text{[Equation B.3]}$$

$$q = a + p' \tan\psi \qquad \text{[Equation B.4]}$$

$$a = c'\cos\phi'; c' = \frac{a}{\cos\phi'} \qquad \text{[Equation B.3]}$$

$$\tan\psi = \sin\phi';\ \phi' = \sin^{-1}(\tan\psi) \qquad \text{[Equation B.6]}$$

A sample calculation follows for B – 1:

$\psi = 35°;\ \phi' = \sin^{-1}(\tan\psi) = \sin^{-1}(\tan(35°)) = 44.4°;\ \boldsymbol{\phi' = 44.4°}.$

$a = 132\ PSF;\ c' = \frac{a}{\cos\phi'} = \frac{132\ PSF}{\cos(35°)} = 184.9\ PSF;\ \boldsymbol{c' = 184.9\ PSF}.$

The drained shear strength in terms of $p'-q$ space and ψ and a in addition to the equivalent shear strength in terms of σ' – τ space and c' and ϕ' are shown in Table B.1.

Undrained Shear Strength and Normalization Approach

The undrained shear strengths for the soil samples was evaluated through a normalization approach with the following methodology. The concept is that a hypothetical factor, *N*, relating the undrained shear strength to the initial confining stress used in the tests can be obtained for each CU test with B – 1, B – 6, and B – 8. Next, this factor is plotted against the effective stress at depth in order to determine an appropriate undrained shear strength.

The factor N is described as:

$$N = \frac{\tau_{failure}}{\sigma_o{}'} \qquad \text{[Equation B.7]}$$

Table B.2 summarizes the undrained shear strengths and initial confining stresses for each of the CU tests. The factor, *N* relating the undrained shear strength at failure to the initial confining stress is also shown. The average value between each of the tests has taken for the factor *N*.

The undrained shear strength angle, ϕ_u, and cohesive strength, *c*', s = s_u is the undrained shear strength and has been determined from the Mohr-Coulomb strength criterion (Duncan & Wright, 2005: 22).

$$s = s_u = c' + \sigma' tan\phi' \qquad \text{[Equation B.8]}$$

The next step in the approach is to develop a plot of the normalized factor at depth against the effective stress profile at depth to determine the undrained shear strength at

depth and the undrained shear angle. Plots representing the effective stress vs. depth and normalized shear strength vs. depth in addition to plots representing Mohr circle space have then been constructed and are shown in Figures B.4 to B.6. Figure B.4 outlines the results from the normalized approach for B – 1. A clear trend for the slope of the line has been established and the undrained shear angle, ϕ_u, for all soil samples and is found using the Mohr-Coulomb strength criterion. Table B.4 summarizes the undrained strength parameters for each slope.

DCP Data and Undrained Strength for Slope # 2

The undrained shear strength of soils for Slope # 2 was obtained using the DCP data. A series of empirical correlations and equations were used to translate the DCP into ultimate bearing capacity, and then from bearing capacity into undrained shear strength.

The first step was to evaluate the penetration rate (PR). The penetration rate is simply the increment of length that the cone penetrometer rod advances per blow. This data was then used with empirical correlations with what is known as the California Bearing Ratio (CBR). The CBR is an empirical ratio that is used to estimate the potential strength and bearing capacity of subsurface soils (ASTM, 2005). The CBR is expressed as a percentage and different soils types have empirical correlations to the CBR.

The CBR is calculated for a variety of soil types including CL and CH soils and has specific equations for each soil type. Equations B.9 to B.11 show the respective equations. The penetration rate, PR, is expressed in terms of millimeters/blow.

The ultimate bearing capacity, q_c, is determined from the CBR values. Equation B.12 shows the equation for bearing capacity. The undrained shear strength of soils for Slope # 2 was obtained using the DCP data.

Finally, the ultimate bearing capacity is then related to another empirical equation for the determination of the undrained shear strength outlined in Equation B.13. Equations presented below are for the empirical correlations between the CBR and the ultimate bearing capacity. Equations have been developed by the United States Army Corp of Engineers (Kessler Soil Engineering Products, 2010).

For CL Soils:

$$CBR = \frac{292}{PR^{1.12}} \qquad \text{[Equation B.9]}$$

For CL soil types with CBR < 10%:

$$CBR = \frac{1}{(0.017019 \cdot PR)^2} \qquad \text{[Equation B.10]}$$

For CH soil types:

$$CBR = \frac{1}{(0.002871 \cdot PR)} \qquad \text{[Equation B.11]}$$

Next, the ultimate bearing capacity, q_c, is correlated to the CBR in the following relationship:

$$q_c = 3.794 \cdot CBR^{0.664} \quad \text{[Equation B.12]}$$

The ultimate bearing capacity is then related to the undrained shear strength of the soil and effective stresses acting on the soil in the following equation (Duncan & Wright, 2005: 48):

$$s_u = \frac{q_c - \sigma_{vo}}{N^*_k} \quad \text{[Equation B.13]}$$

N^*_k is known as the cone factor and the values are (Duncan & Wright, 2005: 48):

$$N^*_k = 14 \pm 5 \quad \text{[Equation B.14]}$$

A value of N^*_k = 14 was used for all values in the determination of the undrained shear strength. Fourteen in this case resides in the middle of the N^*_k = 14 to N^*_k = 19 range and represents an average value.

The undrained shear strength was averaged over the appropriate soil type. In Slope # 2, a CL soil type was used for values from 0 to 7.7 ft. and a CH soil type was taken for 7.7 ft. to 16.0 ft. The values were averaged of the specified depths and are shown in Table B.4.

A corresponding friction angle was assigned to each soil type based on characteristics from the soil type's Atterberg Limits. The CL soil had similar properties to CL soil type in B – 1, so the undrained value of 37° was assigned to this soil type from the CU tests. The CH soil on the other was not encountered in other borings and a

correlation based on the Atterberg Limits was used. A value of 25° was assumed for the CH soil. Finally, a general form of the equation for shear strength was used to calculate the cohesive strength, *c'*, used a model input in the slope stability models.

Figure B.7 shows the incremental undrained shear strength for these DCP runs. Figure B.8 shows the slope profile for Slope # 2 where the DCP runs were operated in the slope profile.

The undrained shear strength regions have been correlated according to the subsurface geology from boring B – 2. CH soils from 0 ft. to 1.7 ft. were ignored for modeling purposes and have been lumped with a CL soil type ranging from 0 ft. to 7.6 ft., a CH soil type from 7.6 ft. to 16.0 ft., and landslide material at depths exceeding 16.0 ft.

The average undrained shear strengths have been calculated by the average of the undrained shear strength per depth according to the geology and soil type. Values for the undrained friction angle, ϕ_u, and undrained cohesive strength, c_u, have been calculated using Equation B.14. Undrained condition parameters are summarized in Table B.4.

A total of four changes are noted within B – 2. The DCP runs correlate to the four logs. B-2-1 shows a weak upper surface soil and change at 1.7 ft. and a distinct increase in shear strength at 7.6 ft., which could represent the CH soil type. B-2-2 shows similar characteristics. The 0 ft. to 2 ft. could correlate to the upper surface CH soil type because of the low undrained shear strength in the unconsolidated materials. A change from 2 ft. to 3.5 ft. at this location could actually represent the CL soil type. A distinct change is noted from 3.5 ft. to 8 ft. and likely represents the CH soil type. Finally, 8 ft. to 10.5 ft. likely represents boulders from landslide material. The undrained shear strengths for soils from B – 1, B – 2, B – 6, and B – 8 in summarized in Table B.4.

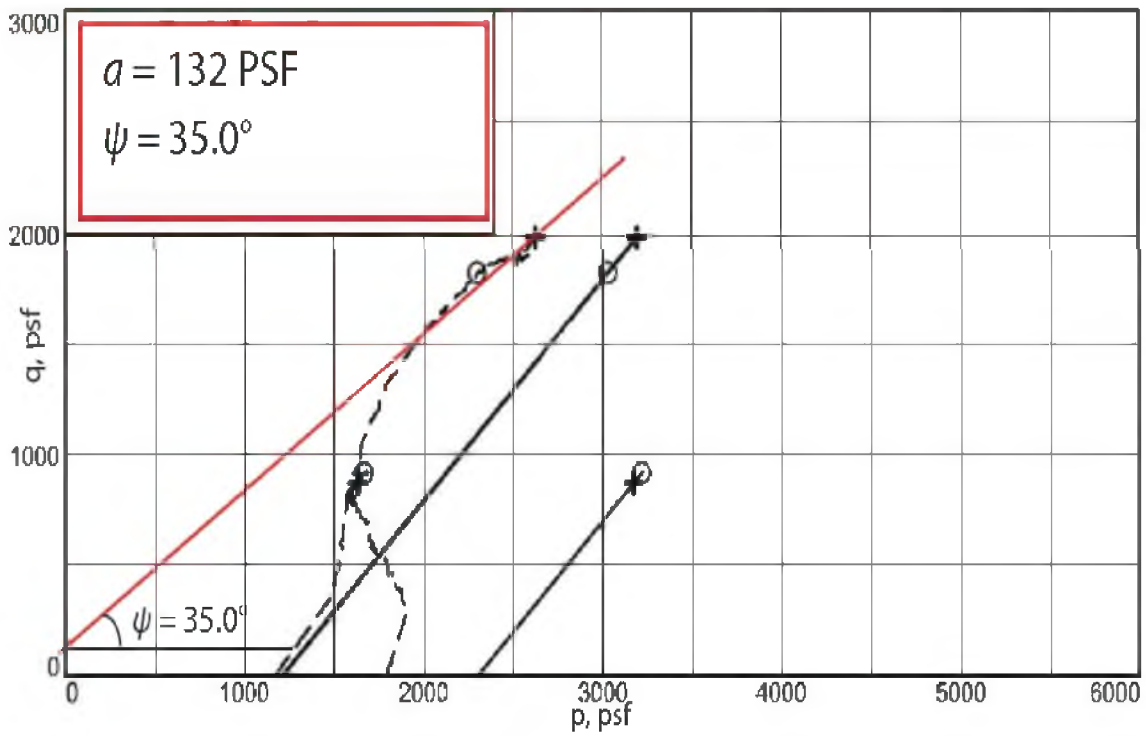

Figure B.1, B – 1 Drained CU test results

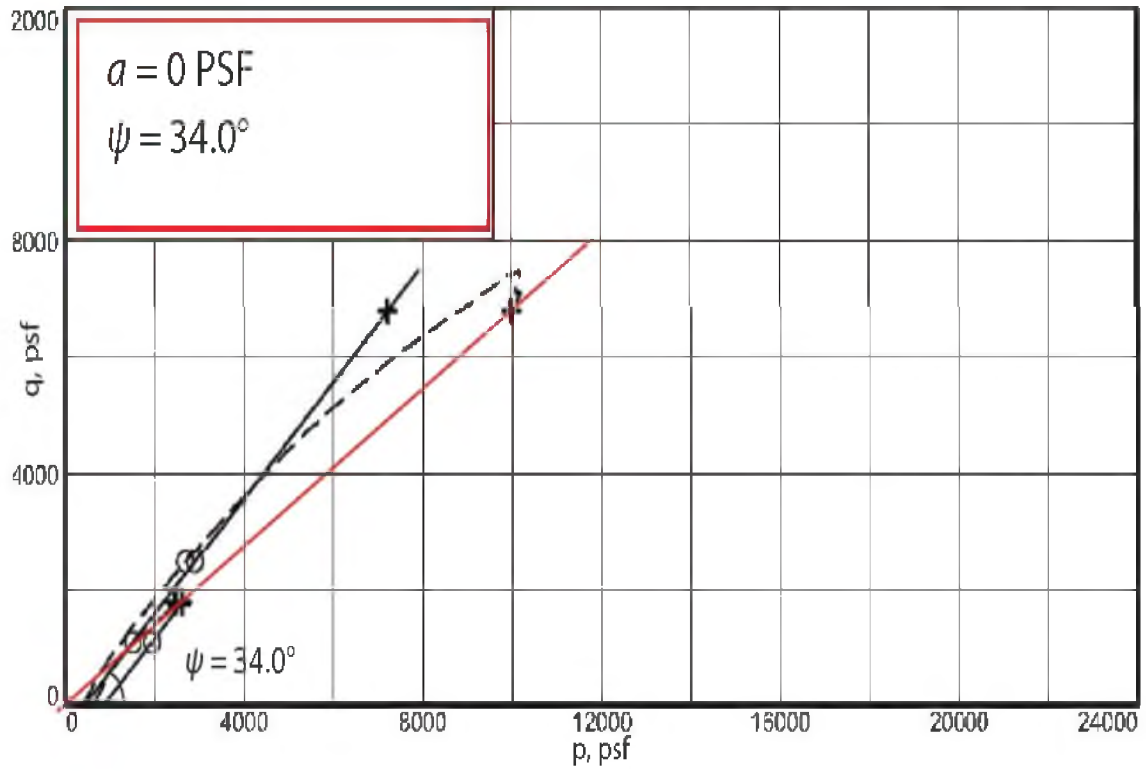

Figure B.2, B – 6 Drained CU test results

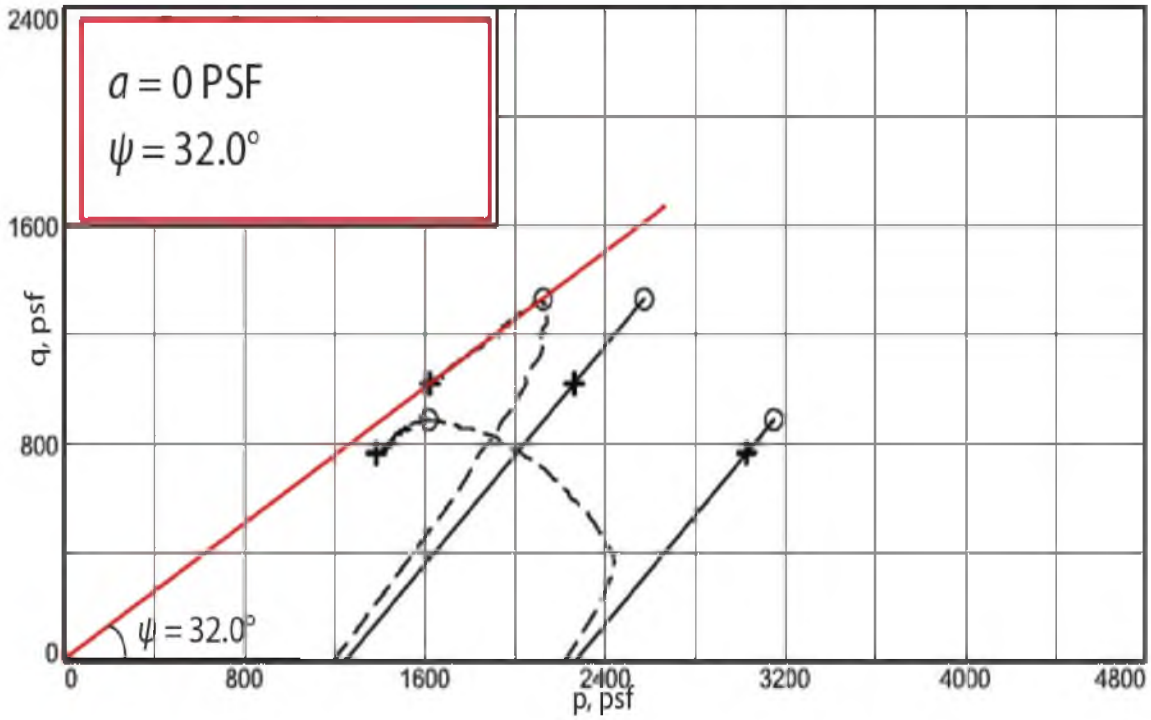

Figure B.3, B – 8 drained CU test results

Table B.1, Drained strength parameters

Slope Stability Model	Boring #	Layer #	γ (lb/ft^3)	USCS Soil Type	Effective Stress Cohesion, *a*, (lb/ft^2)	Critical Stress friction angle, ψ	Effective Stress Cohesion, *c'*, (lb/ft^2)	Effective Stress friction angle, ϕ'
Slope # 2	B-1	1	99.4	-	-	-	-	-
Slope # 1	B-2	1	99.4	CL	132.0	35.0	184.9	44.4
Slope # 3	B-6	1	108.8	SC	0.0	35.0	0.0	42.4
Infinite Slope	B-8	1	93.7	CL - ML	0.0	32.0	0.0	38.7

Table B.2, Normalized approach factors

Soil Sample	Test	$\tau_{failure}$ (PSF)	σ_o (PSF)	N ($\tau F/\sigma_o$)	Average N ($\tau F/\sigma_o$)
B - 1	1	1819	1210	1.503306	0.77
	2	900	2301	0.391134	
B - 6	1	2430	422	5.758294	0.65
	2	1080	857	1.26021	
B - 8	1	1310	1243	1.053902	0.65
	2	970	2262	0.428824	

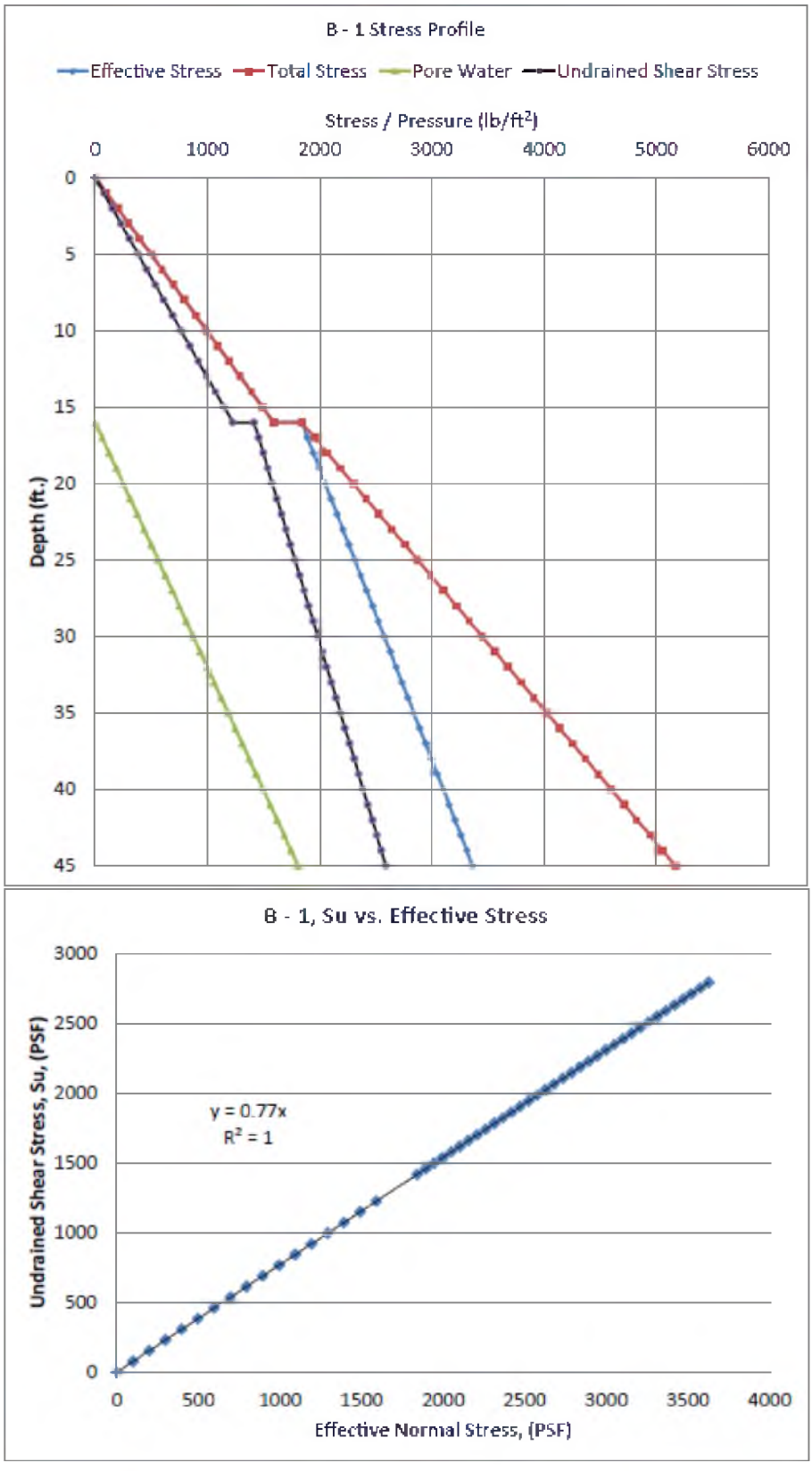

Figure B.4, B – 1 effective stress, normalized shear strength and Mohr circle space

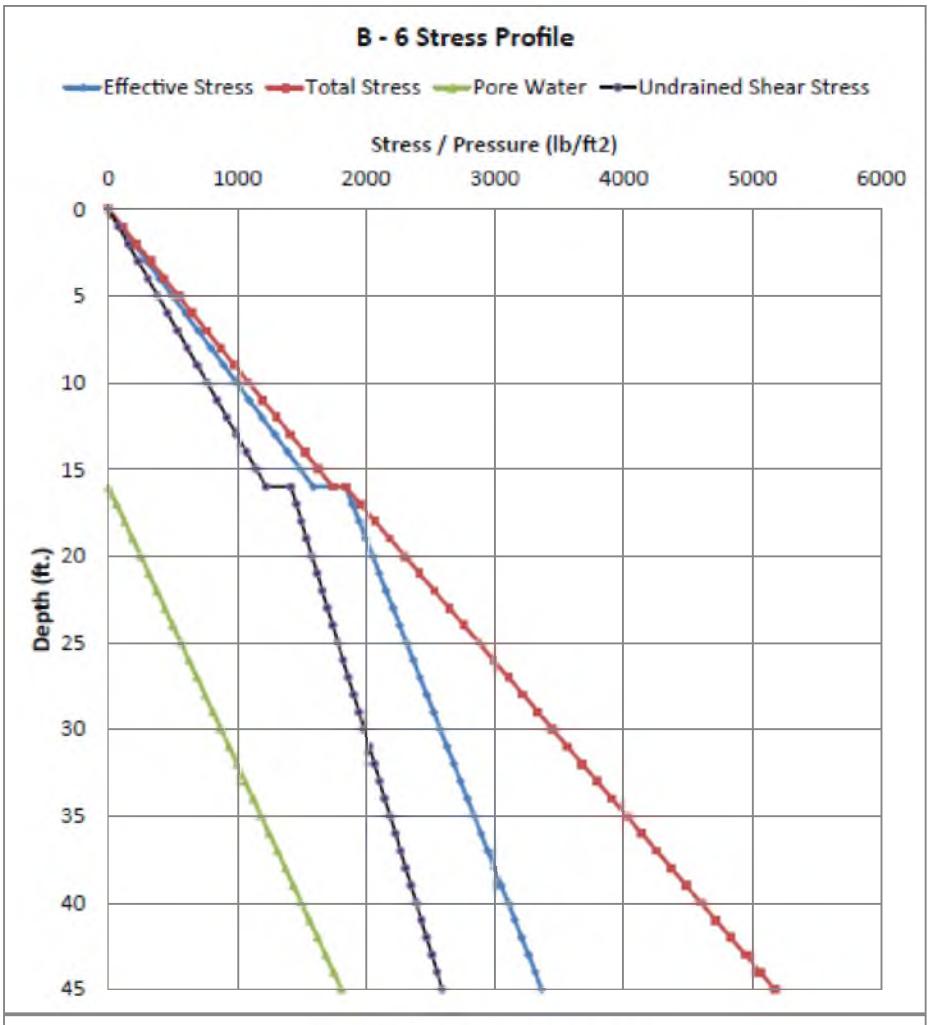

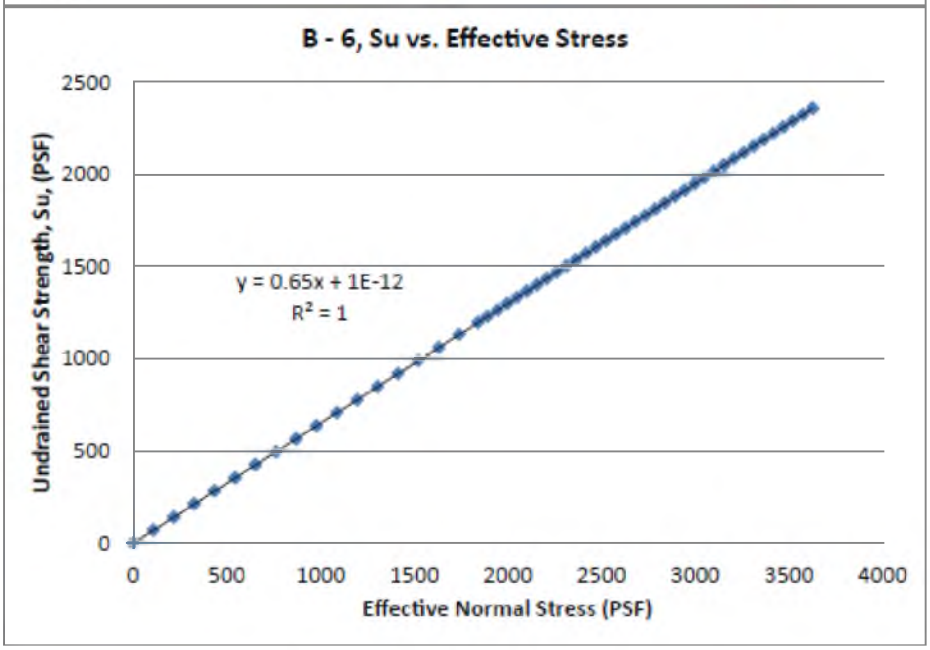

Figure B.5, B – 6 effective stress, normalized shear strength and Mohr circle space

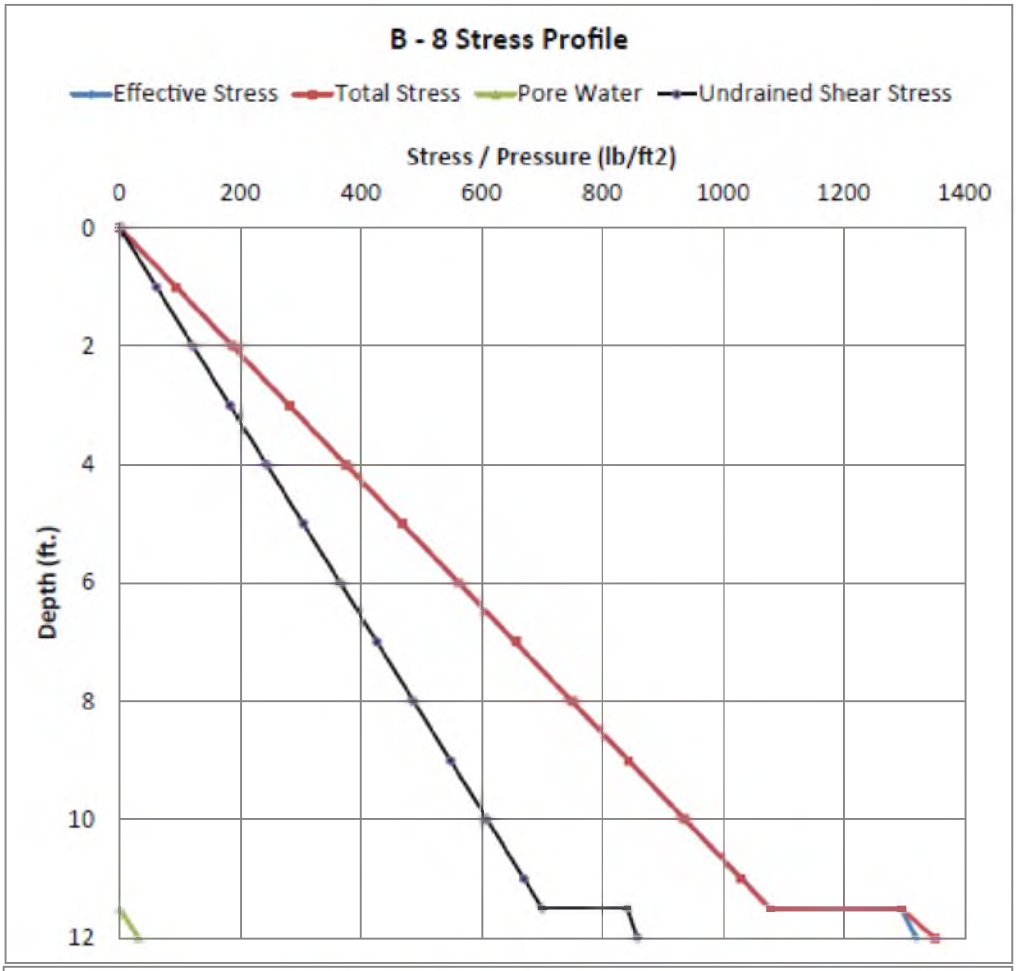

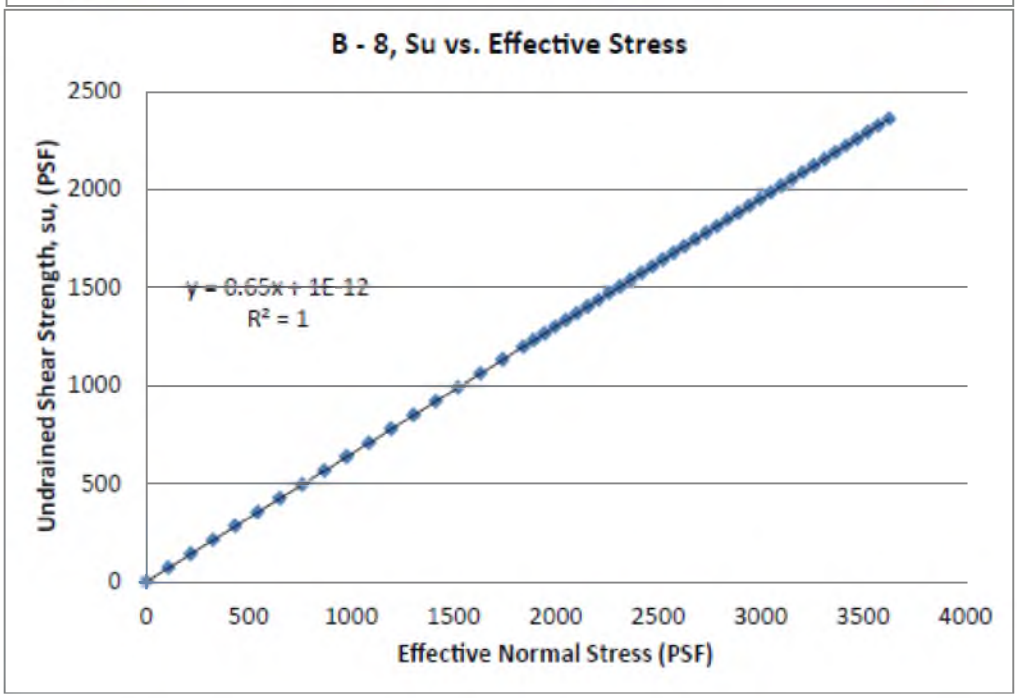

Figure B.6, B – 8 effective stress, normalized shear strength and Mohr circle space

Table B.3, Undrained strength parameters

Slope Stability Model	Boring #	Layer #	γ (lb/ft^3)	USCS Soil Type	Total Stress Cohesion, c_u, (lb/ft2)	Total Stress friction angle, ϕ_u
Slope # 2	B-1	1	99.4	CL	0	37.6
Slope # 1	B-2	1	99.4	CL	25	33
	B-2	2	110	CH	150	25
	B-2	3	120	GW-GC	0	40
Slope # 3	B-6	1	108.8	SC	0	33
Infinite Slope	B-8	1	93.7	CL - ML	0	33

Table B.4, Slope # 2 Soil properties

SOIL TYPE	*Su*, (lb/ft^2)	c_u (lb/ft^2)	ϕ_u	Reference
CL	96	18.5	37.6	Duncan & Wright, 2005 & B-1 properties
CH	175	123.7	25	Duncan & Wright, 2005

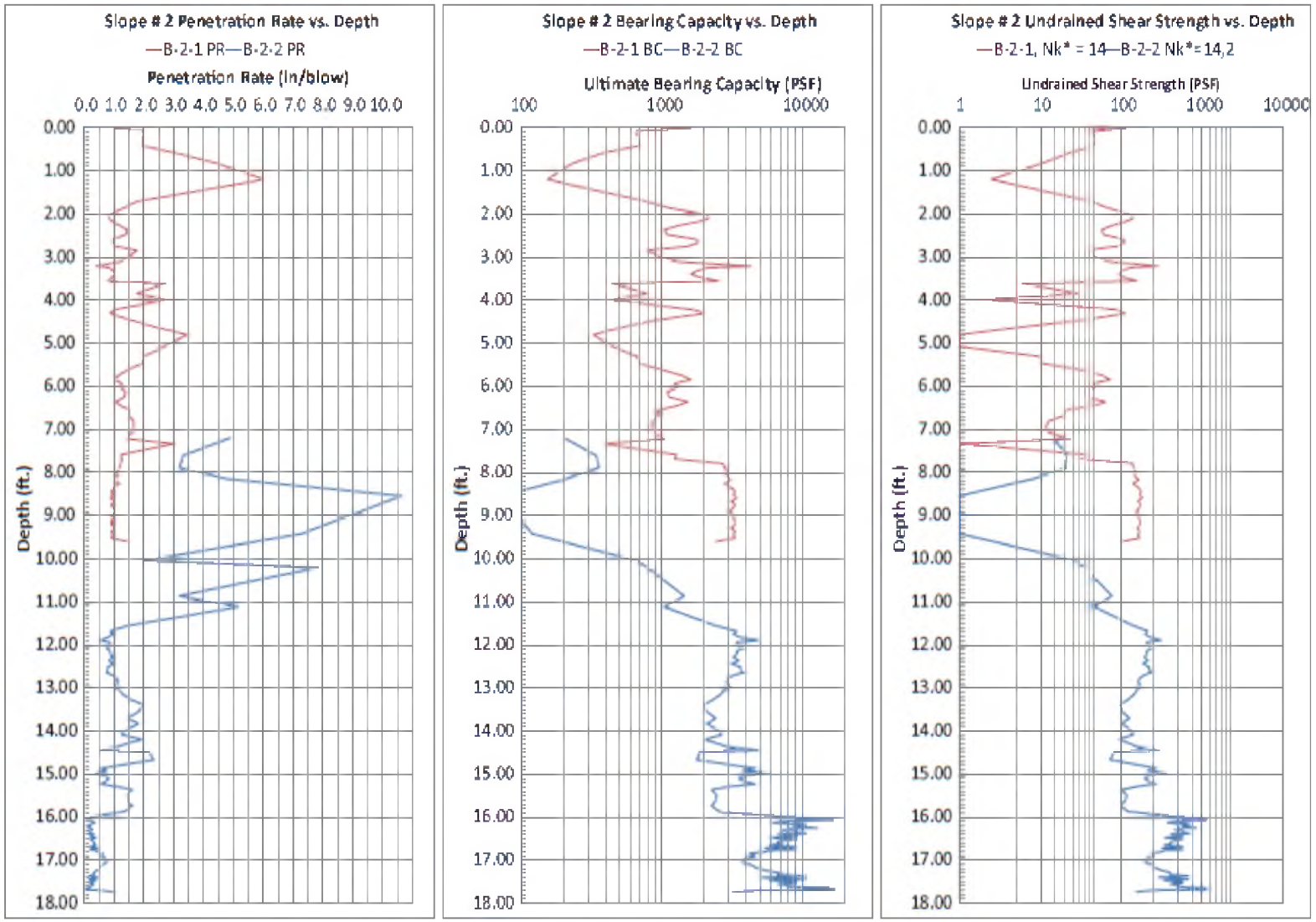

Figure B.7, DCP Data through Slope # 2

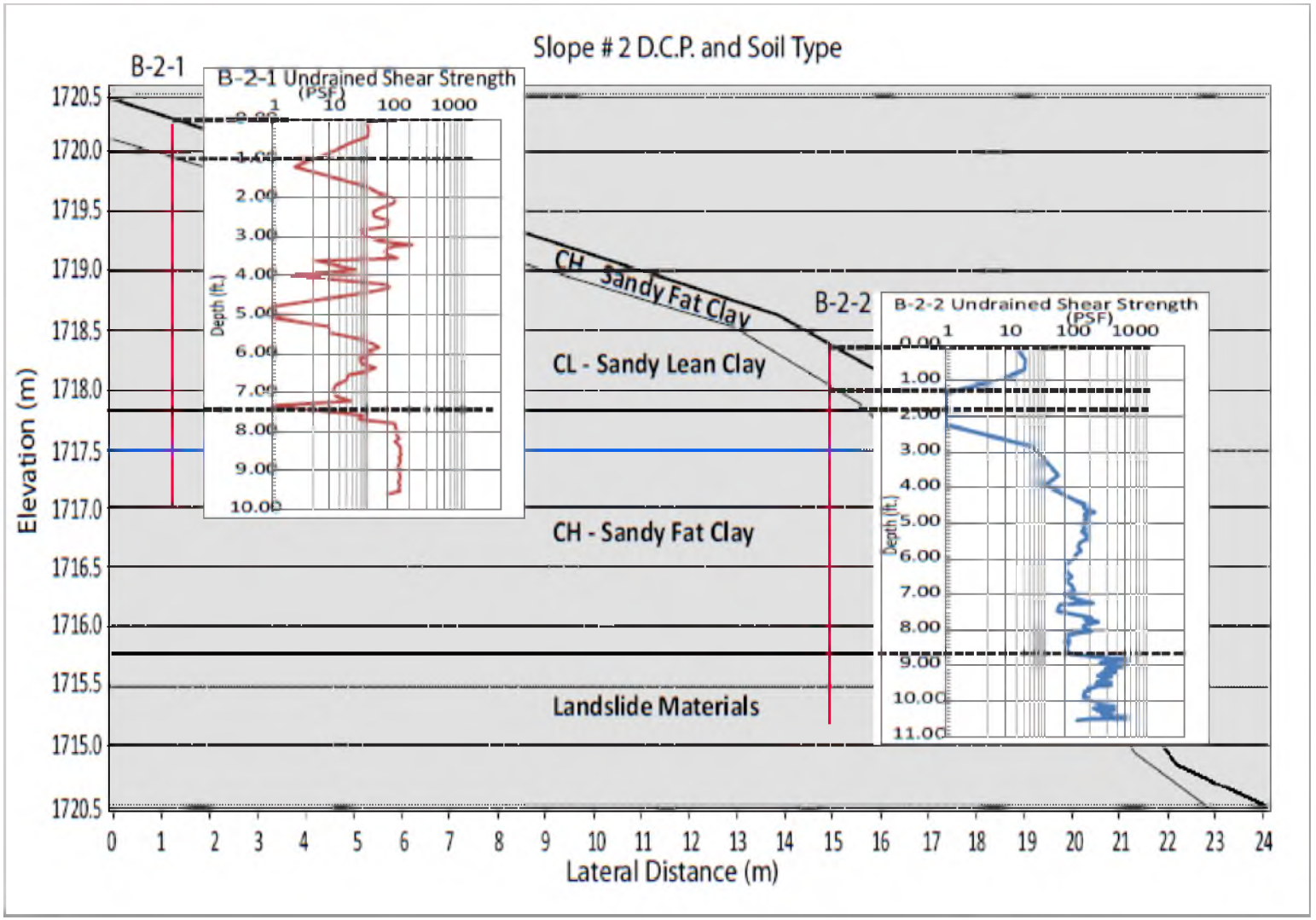

Figure B.8, Slope # 2 cross-Section with soil types and DCP undrained shear strengths

APPENDIX C

GOVERNING GEOTECHNICAL ENGINEERING EQUATIONS FOR SLOPE STABILITY ANALYSIS

Limit Equilibrium Methods

The concept of shear strength, *s*, is derived from the Mohr-Coulomb strength criterion as was previously defined in Equation B.14. The Factor of Safety Principle: *F.S.* >1.0 required for stability (Duncan & Wright, 2005: 60):

$$F.S. = \frac{s}{\tau} \qquad \text{[Equation B.13]}$$

Limit-equilibrium methods are based on free body diagrams shown in Figures C.1 – C.2 where driving and resisting forces are resolved in into shear strengths of moments.

Factor of Safety, Ordinary Method of Slices (Duncan & Wright, 2005: 65):

$$F.S. = \frac{\sum[c'\Delta l + (\gamma h cos^2\alpha - u)\Delta l \, tan\phi']}{\sum W \sin\alpha} \qquad \text{[Equation C.1]}$$

Factor of Safety, Bishop's Simplified Method (Duncan & Wright, 2005: 74):

$$F.S. = \frac{\sum \left[\frac{c'\Delta l \cos\alpha + (W - u\,\Delta l\ \cos\alpha)\ tan\phi'}{\cos\alpha + \frac{(\sin\alpha\ tan\phi')}{F.S.}} \right]}{\sum W \sin\alpha} \qquad \text{[Equation C.2]}$$

The Pseudostatic Method

The pseudostatic method is a relatively simple method in evaluating slope stability in earthquake regions (Abramson et. al, 2002: 394). The method is implemented by including the horizontal and static seismic forces used to simulate inertial forces due to ground accelerations from an earthquake where the seismic forces are assumed to be proportional to the weight of any potential sliding mass multiplied by horizontal and vertical seismic coefficients, k_v and k_h (Abramson et. al, 2002: 394). The seismic coefficients are expressed as a percentage of the acceleration of gravity, g, and in most analyses $k_v = 0$. The seismic force is assumed to act only in the horizontal direction, which ultimately induces an inertial force k_hW within the slope where W represents the weight of the potential sliding mass (Abramson et. al, 2002: 395). In terms of additional forces from seismic loads, loads are added in the force balance in the interslice forces, kW Figure C.3 shows an illustration of the seismic coefficient multiplied by the mass of interslice, W.

Bishop's Method is coded into the software program Slope/W and includes analyses for the pseudostatic procedure from seismic loads. The details of the calculations and coding of Slope/W from Bishop's Method are not shown in this text.

Infinite Slope Stability Analysis Principles

The infinite slope stability analysis method assumes that the slope is of infinite extent and that sliding occurs on a plane parallel to the face of the slope (Duncan & Wright, 2005: 62). Figure C.4 demonstrates equilibrium analysis with a rectangular block element of slope and assumes that forces perpendicular to the slope are exactly equal, opposite, and collinear to one another and hence cancel out (Duncan & Wright, 2005).

The sum of forces is simplified by using the unit weight of soil and the above considerations for the shear forces along the base of the rectangular block element. Ultimately, the sum of forces is related to the Mohr-Coulomb strength criterion and substitutions are made to the definition of the factor of safety, the ratio of the shear strength to the equilibrium shear stress, and the following equation is derived.

Factor of safety, infinite slopes with pore water pressure and static loads (Duncan & Wright, 2005):

$$F.S. = \frac{c' + (\gamma z cos^2\beta - \mu) tan\phi'}{\gamma z cos\beta sin\beta} \qquad \text{[Equation C.4]}$$

For the slope adjacent to where B – 8 is with: Table C.1, Infinite slope stability parameters:

$$F.S. = \frac{\frac{0lb}{ft^2} + \left(\frac{94lb}{ft^3} * 11.2ft.* cos^2(35) - 0.5ft.* \frac{62.4lb}{ft^3}\right)\tan(32)}{\frac{94lb}{ft^3} * 11.2ft.* \cos(35)\sin(35)} = \mathbf{1.11}$$

Drained condition *F.S.* for slight increase in groundwater elevation:

$$F.S.=\frac{\frac{0lb}{ft^2}+\left(\frac{94lb}{ft^3}*11.2ft.*cos^2(35)-2.1ft.*\frac{62.4lb}{ft^3}\right)\tan(32)}{\frac{94lb}{ft^3}*11.2ft.*\cos(35)\sin(35)}=\mathbf{1.00}$$

Factor of Safety, Infinite Slopes with Pseudo-Static Seismic Loads (Duncan & Wright, 2005: 64):

$$F.S.=\frac{c'+(\gamma zcos^2\beta-k\gamma zcos\beta sin\beta-\mu)tan\phi'}{\gamma zcos\beta sin\beta+k\gamma zcos^2\beta} \qquad \text{[Equation C.5]}$$

where k is the horizontal seismic coefficient caused by an earthquake.

For the slope adjacent to B – 8 with the same parameters in Table C.2 with a horizontal seismic load, $k = 0.1\ g$:

$$F.S.=\frac{\frac{460lb}{ft^2}+\left(\frac{94lb}{ft^3}*11.5ft.*cos^2(35)-0.1*\frac{94lb}{ft^3}*11.2ft.*\cos(35)\sin(35)-0.5ft.*\frac{62.4lb}{ft^3}\right)\tan(32)}{\frac{94lb}{ft^3}*11.5ft.*\cos(35)\sin(35)+0.5*\frac{94lb}{ft^3}*11.2ftcos^2(35)}$$

$$=\mathbf{1.02}$$

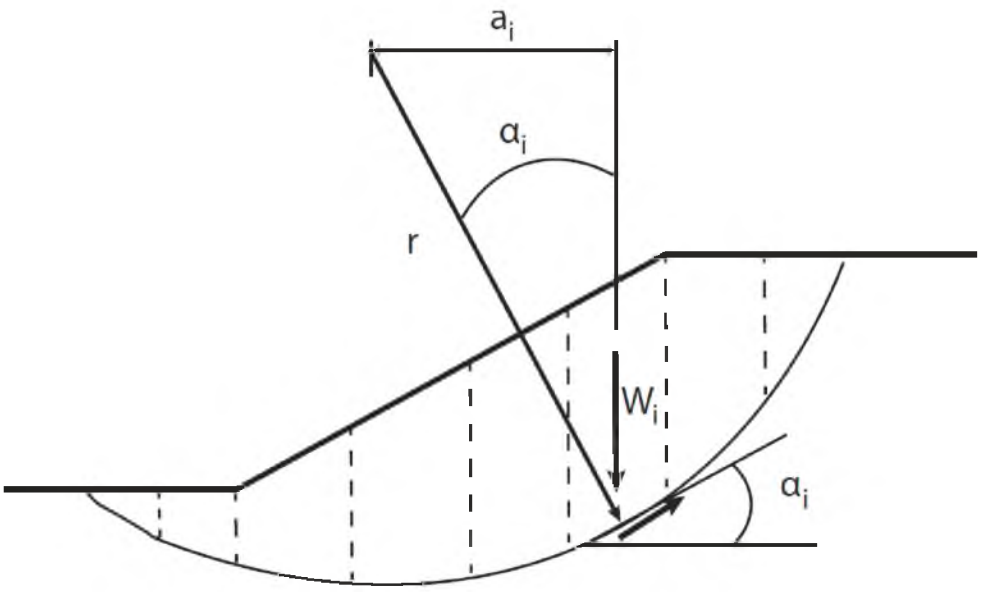

Figure C.1, Principles of limit equilibrium methods. (Adapted from Duncan & Wright, 2005)

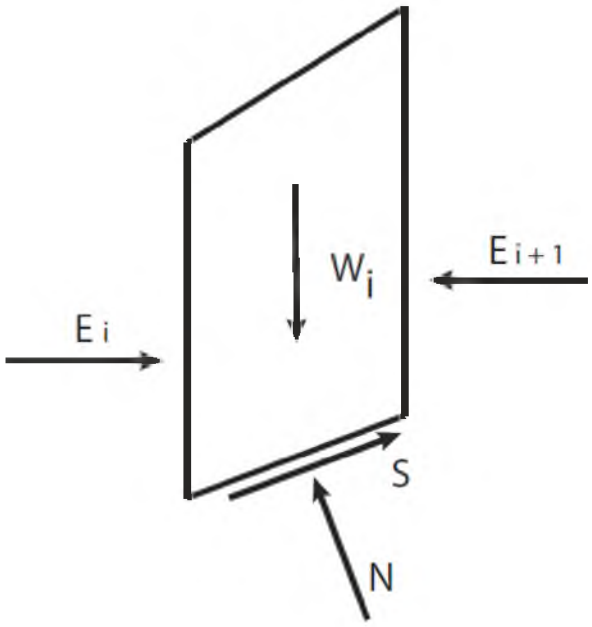

Figure C.2, Method of slices concept. (Adapted from Duncan & Wright, 2005)

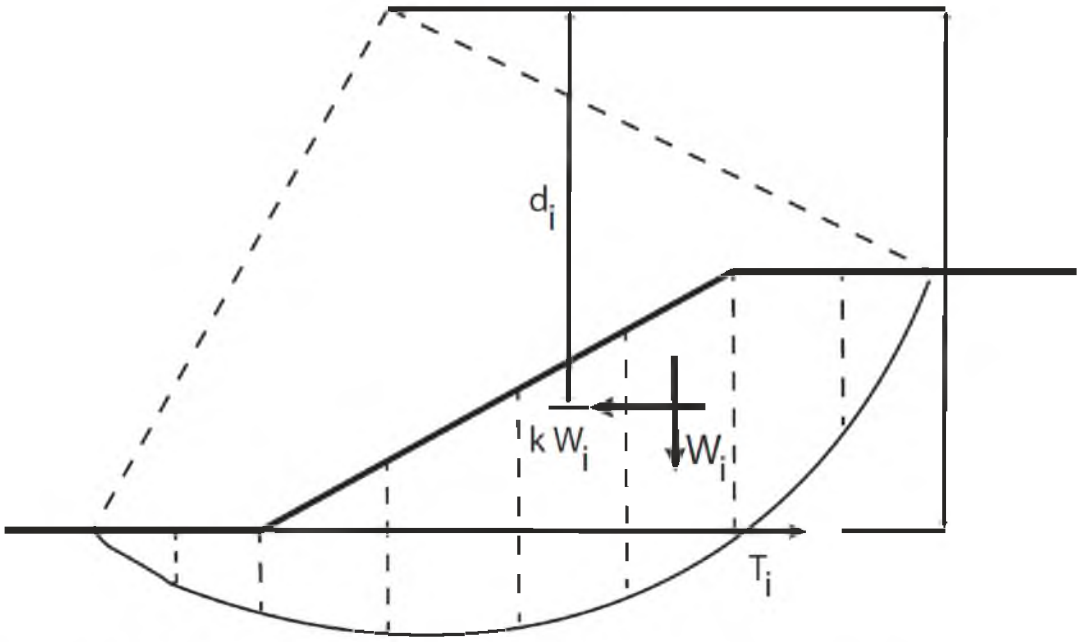

Figure C.3, Pseudostatic method. (Adapted from Duncan & Wright, 2005)

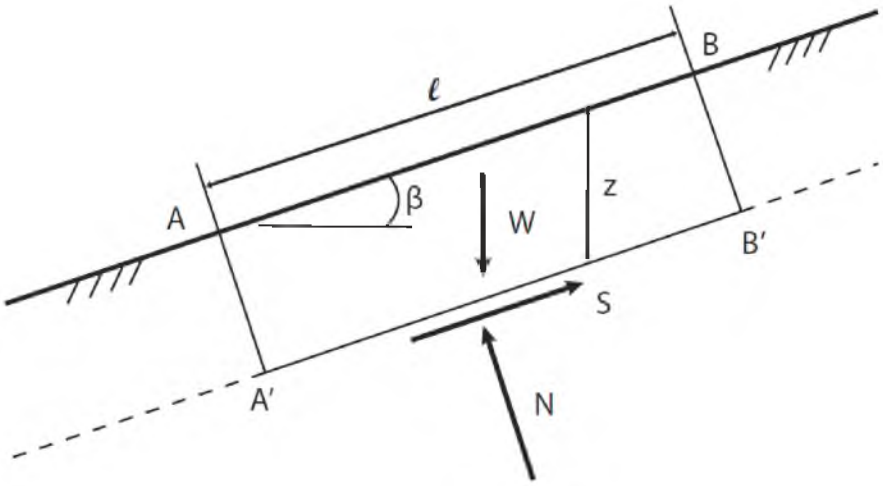

Figure C.4, Infinite slope diagram. (Adapted from Duncan & Wright, 2005)

Table C.1, B – 8 drained condition parameters

c' (lb/ft^2)	0
γ (lb/ft^3)	94
γ_w (lb/ft^3)	62.4
D (ft)	11.2
Z_w (ft)	0.5
α (deg)	35
ϕ' (deg)	32

Table C.2, B – 8 undrained condition parameters

c' (lb/ft^2)	0
γ (lb/ft^3)	94
γ_w (lb/ft^3)	62.4
D (ft)	11.2
Z_w (ft)	2.1
α (deg)	35
ϕ' (deg)	32

APPENDIX D

SEISMIC REFRACTION

Seismic Refraction Survey and Principles

Processed seismic data was first analyzed using standard seismic refraction methods. To accomplish this, the field data was plotted in Linux-based GNU ® plotting software and field seismograms of distance vs. time were constructed. The first breaks in each geophone trace were then selected for the forward and reverse traverses of the surveys. Figures D.1 and D.2 show the field seismograms for Survey # 1 and Survey # 2.

Using this method, plots of distance vs. time were made for seismic refraction analysis using the premise of the inverse of the slopes of the plots to determine seismic velocities in the subsurface. The concept is simple and is summarized shown by Dr. Anne Sheehan et. al to be (2006: 68),

$$velocity = \frac{distance}{time} \rightarrow v = \frac{x}{t} \rightarrow t = \frac{x}{v} \rightarrow \frac{dt}{dx} = \frac{1}{v}. \qquad \text{[Equation D.1]}$$

The thickness of the layers in the subsurface were calculated using the following considerations using Survey # 2 Forward Traverse data. The data show that velocities increase sequentially with and with each layer, so standard equations can be used.

Two Layer System

For a given two layer system where v2 > v1 that has multiple layers or only two layers, the thickness of the first layer can be found as (Sheehan et. al, 2006: 73)

$$h_1 = \frac{t_i}{2}\left(\frac{v_2 v_1}{(v_2^2 - v_1^2)^{1/2}}\right) \qquad \text{[Equation D.2]}$$

For layer one, v_1 = 391 m/s, v_2 = 1403 m/s, ti = 0.0422 s,

$$h_1 = \frac{0.0422s}{2}\left(\frac{(1403m/s)(391m/s)}{(1403m/s^2 - 391m/s^2)^{1/2}}\right) = 8.6\,m = 28.2\,ft$$

Three Layer System

For a given three layer system where v3 > v2 > v1, the thickness of the second layer can be calculated as (Sheehan et. al, 2006: 74)

$$h_2 = \left(ti_2 - \frac{2h_1(v_3^2 - v_1^2)^{1/2}}{v_3 v_1}\right)\frac{v_3 v_2}{2(v_3^2 - v_2^2)^{1/2}} \qquad \text{[Equation D.3]}$$

For layer two, v_1 = 391 m/s, v_2 = 1403 m/s, v_3 = 3230 m/s, t_{i2} = 0.0482 s

$$h_2 = \left(0.0482s - \frac{(2 * 8.6m)\left(\left(3230\frac{m}{s}\right)^2 - \left(391\frac{m}{s}\right)^2\right)^{\frac{1}{2}}}{\left(\left(3230\frac{m}{s}\right)\left(391\frac{m}{s}\right)\right)}\right)\frac{\left(3230\frac{m}{s}\right)\left(1403\frac{m}{s}\right)}{2\left(\left(3230\frac{m}{s}\right)^2 - \left(1403\frac{m}{s}\right)^2\right)^{\frac{1}{2}}}$$

$$= 3.6\,m\,, or\ 11.7\,ft.$$

Total thickness to bedrock = h1 + h2 = 28.2 ft. + 11.7 ft. = **39.9 ft**.

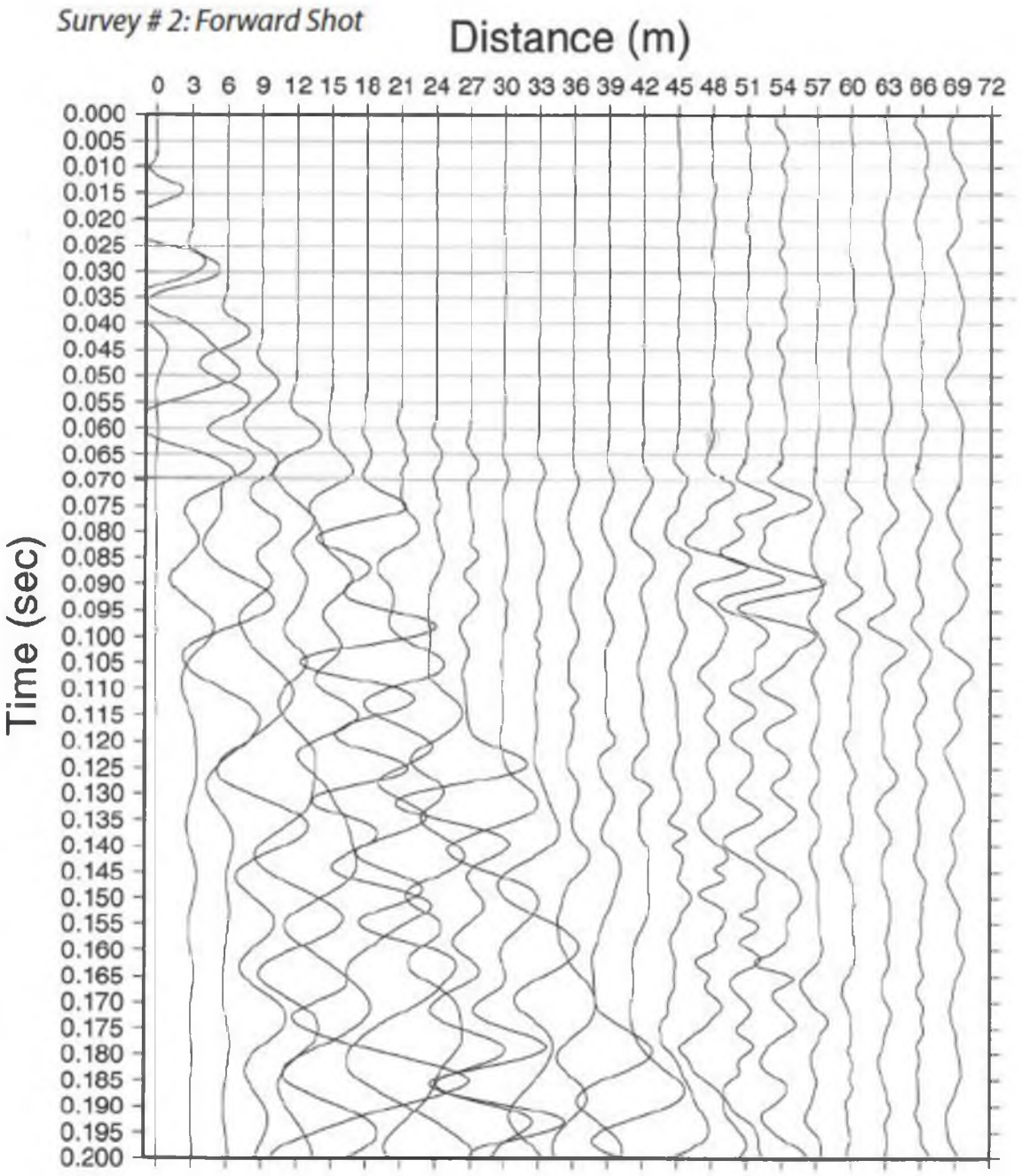

Figure D.1, Forward traverse seismogram

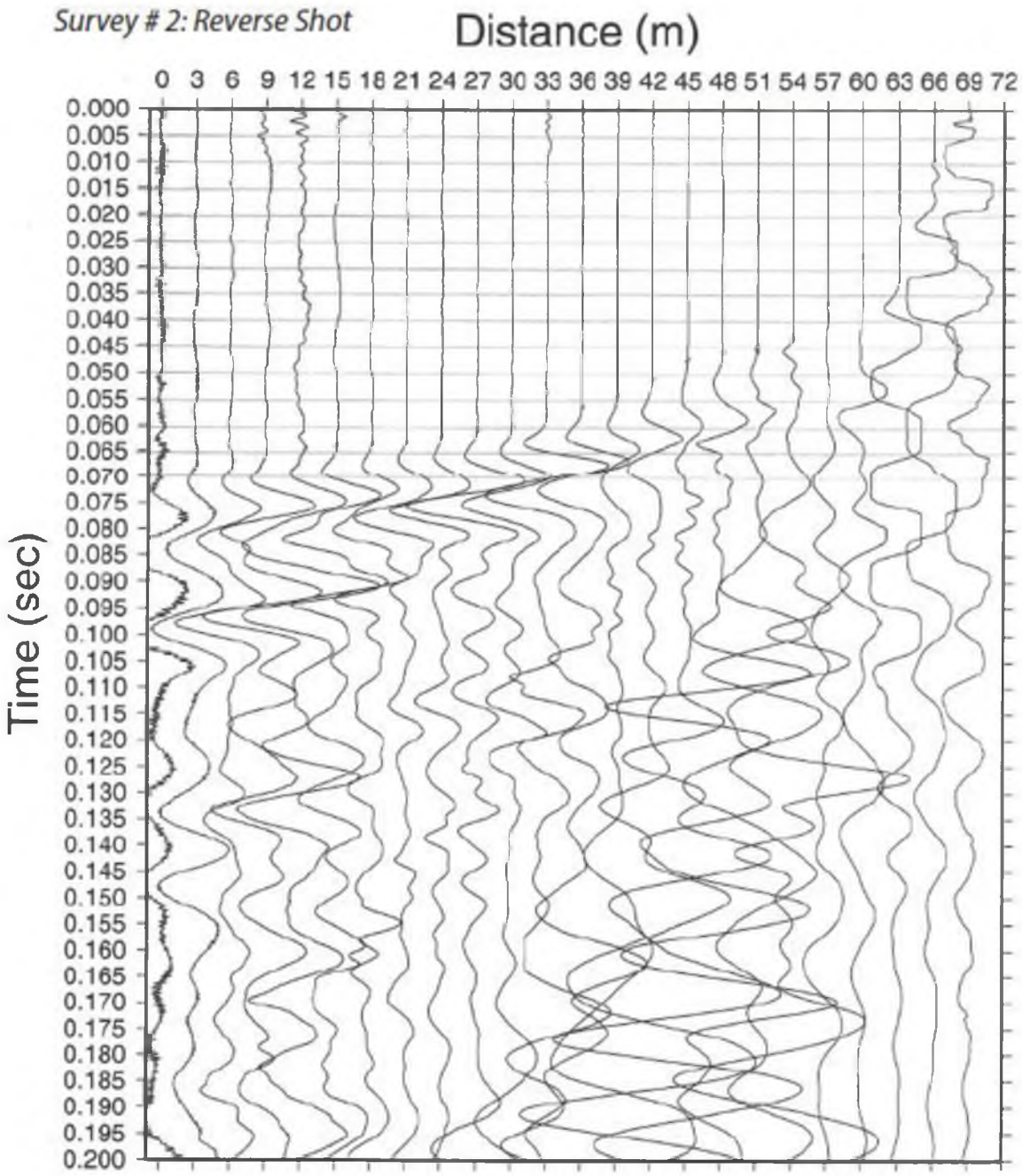

Figure D.2, Reverse traverse seismogram

APPENDIX E

RADIOCARBON DATING RESULTS

Charcoal was found frequently within all borings in the field site and selected samples were sent to Beta Analytic for C-14 radiocarbon. As of 7/3/2012, two samples have been analyzed, B – 2 at 15.5 ft. & B – 5 at 14.5 ft., with precisely the same conventional radiocarbon age as 4370 ± 30 BP. Both samples ages were double-checked by Beta Analytic for accuracy.

Samples were prepared in accordance with Beta Analytic laboratory recommendations. The specific recommendations adhered to were 10 – 50 mg of charcoal sample and separated from the soils by water flotation and stored at temperatures less than 70° C and stored in Ziploc ® Bags (Beta Analytic)

Figure E.1, B – 2 15.5 ft. charcoal sample

Figure E.2, B – 5 14.5 ft. charcoal sample

CALIBRATION OF RADIOCARBON AGE TO CALENDAR YEARS

(Variables: C13/C12=-24.6:lab. mult=1)

Laboratory number:	**Beta-321714**
Conventional radiocarbon age:	**4370±30 BP**
2 Sigma calibrated results: (95% probability)	**Cal BC 3090 to 3060 (Cal BP 5040 to 5010) and Cal BC 3030 to 2910 (Cal BP 4980 to 4860)**

Intercept data

Intercepts of radiocarbon age with calibration curve:	Cal BC 3000 (Cal BP 4950) and Cal BC 2990 (Cal BP 4940) and Cal BC 2930 (Cal BP 4880)
1 Sigma calibrated result: (68% probability)	Cal BC 3020 to 2920 (Cal BP 4970 to 4870)

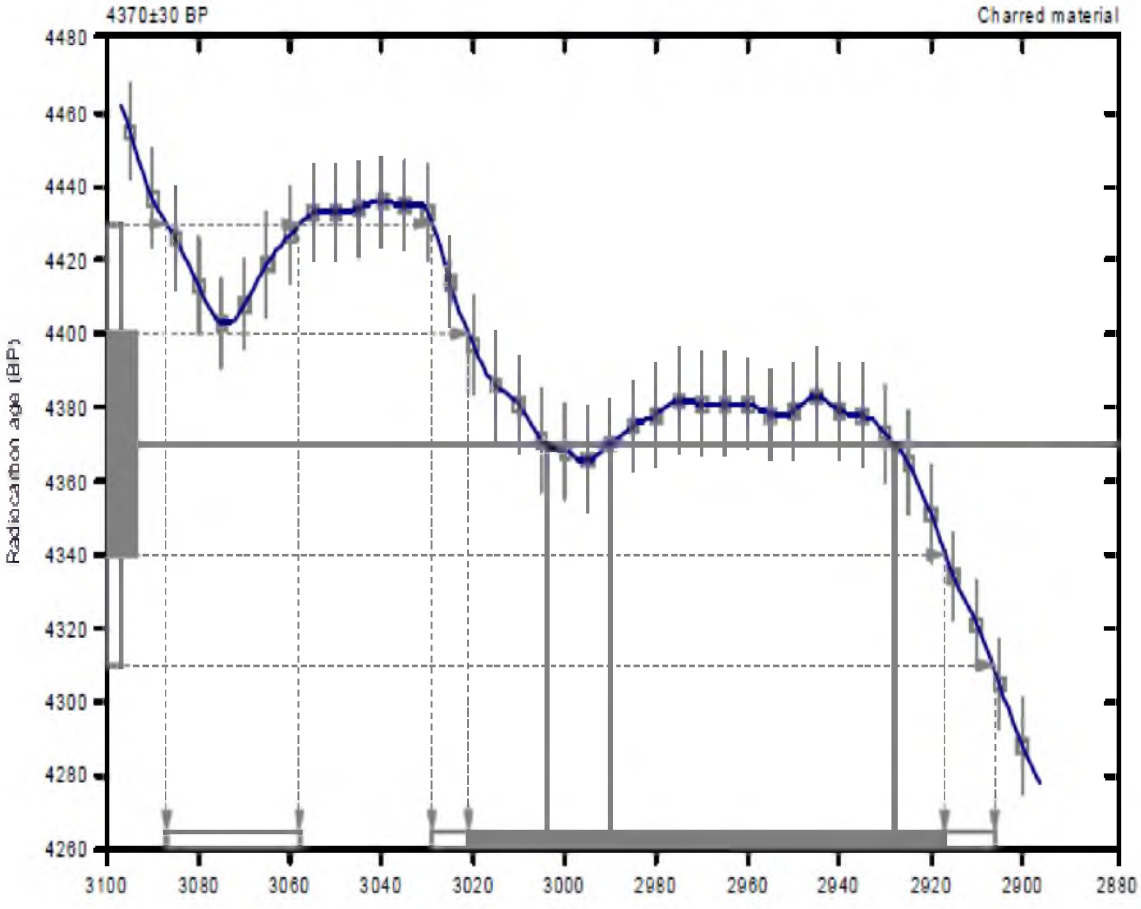

Figure E.3, B – 2 15.5 ft. C-14 results

CALIBRATION OF RADIOCARBON AGE TO CALENDAR YEARS

(Variables: C13/C12=-24.6:lab. mult=1)

Laboratory number:	Beta-322558
Conventional radiocarbon age:	4370±30 BP
2 Sigma calibrated results: (95% probability)	Cal BC 3090 to 3060 (Cal BP 5040 to 5010) and Cal BC 3030 to 2910 (Cal BP 4980 to 4860)

Intercept data

Intercepts of radiocarbon age with calibration curve:	Cal BC 3000 (Cal BP 4950) and Cal BC 2990 (Cal BP 4940) and Cal BC 2930 (Cal BP 4880)
1 Sigma calibrated result: (68% probability)	Cal BC 3020 to 2920 (Cal BP 4970 to 4870)

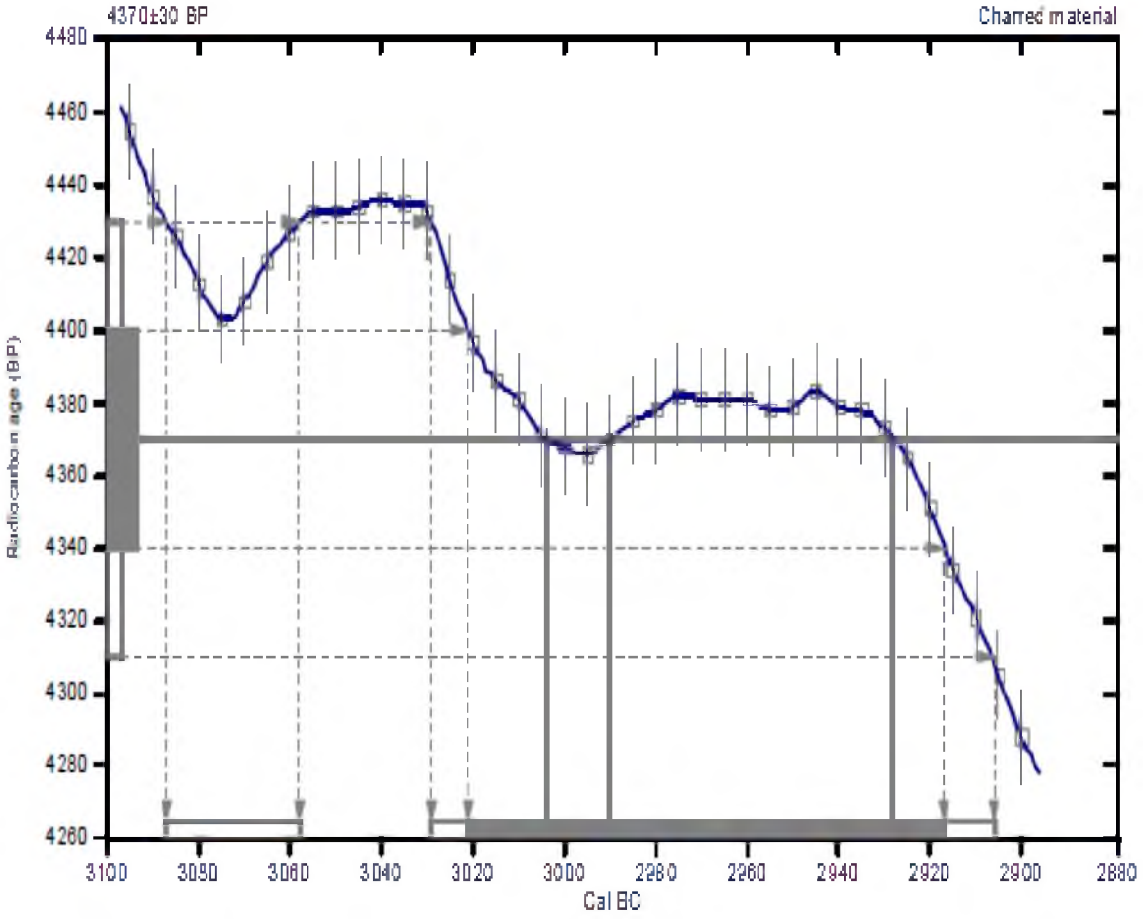

Figure E.4, B – 5 14.5 ft. C-14 results

REFERENCES

Abramson, L., Boyce, G., Thomas, S., and Sharma, S., 2002. Slope Stability and Stabilization Methods. New York City, NY: John Wiley & Sons, Inc.

AMS Sampling Equipment, 2011. Soil Sampling Kits.
< http://www.ams-samplers.com/category.cfm?CNum=25 > [02 Nov. 2011]

Anderson, Mary P. and Woessner, William W., 2002. Applied Groundwater Modeling: Simulation of Flow and Advective Transport. California: Academic Press.

Anderson, Robert S. and Anderson, Suzanne, P., 2010. Geomorphology: The Mechanics and Chemistry of Landscapes. Cambridge, United Kingdom: Cambridge University Press.

Bardet, Jean Pierre, 1997. Experimental Soil Mechanics. Upper Saddle River, NJ: Prentice Hall.

Boggs, Samuel J., 2006. Principles of Sedimentology and Stratigraphy: Fourth Edition. Upper Saddle River, NJ: Pearson – Prentice Hall.

Brand, E.W., Premchitt, J., and Phillipson, H.B., 1984. Relationship Between Rainfall and Landslides in Hong Kong. Canadian Geotechnical Society Proceedings. 4th International Symposium on Landslides, 377-384.

Burger, H., Jones, C., and Sheehan, A., 2006. Introduction to Applied Geophysics: Exploring the Shallow Subsurface. New York: W.W. Norton & Company.

Canton, Jasmin Chamney, 2009. Environmental Controls on the formation and isotopic composition of a laminated tufa in Red Butte Canyon, Utah. M.S. Thesis. Salt Lake City, UT: University of Utah.

Carlson, D., Plummer, C., McGeary, D., 2003. Physical Geology: Ninth Edition. New York, N.Y: McGraw Hill.

Coduto, Donald P., 1999. Foundation Design: Principles and Practices: 2nd Edition. Upper Saddle River, NJ: Prentice Hall.

Coduto, Donald P., 1999. Geotechnical Engineering: Principles and Practices. Upper Saddle River, NJ: Prentice Hall.

Christenson, Gary E 1994. Earthquake Groundshaking in Utah. Public Information Series 29. Salt Lake City, UT: Utah Geological Survey.

Crittenden, M.D. and Van Horn, R., 1987. Map showing surficial units and bedrock geology of the Fort Douglas quadrangle and parts of the Mountain Dell and Salt Lake City North quadrangles, Davis, Salt Lake, and Morgan Counties, Utah. 1:24,000. Denver, CO: United States Geological Survey.

DuRoss, C.B. and Hylland, M.D., 2012, Paleoseismic investigation to compare surface faulting chronologies of the West Valley fault zone and Salt Lake City segment of the Wasatch Fault zone, Salt Lake County, Utah: Final technical report to the U.S. Geological Survey, National Earthquake-Hazards Reduction Program, award no. G10AP00068, 61 p., 2 plates.

Elliot, Ashley H. and Harty, Kimm M., 2010. Landslide Maps of Utah: Salt Lake City 30 × 60 Quadrangle. Salt Lake City, UT: Utah Geological Survey.

Ehleringer, J.R and Sperry, J., 2010. Red Butte Canyon Research Natural Area. < http://www.redbuttecanyon.net > [5 Jul. 2010]

Ehleringer, J.R., L.A. Arnow, T. Arnow, I.B. McNulty, and Negus, N.C., 1992 Red Butte Canyon Research Natural Area – History, flora, geology, climate, and ecology. Great Basin Naturalist, 52 95 – 121.

GEO-SLOPE International, Ltd., 2004. Geostudio 2004: Slope/W, Basic License. Computer software. Calgary, AB: Geoslope International, Ltd.

Hill, Stephen Scott, 2006. A groundwater flow path delineation and an analysis of the stable isotopic climate response of a layered tufa in Red Butte Canyon, Utah. M.S. Thesis. Salt Lake City, UT: University of Utah.

Kessler Soils Engineering Products, Inc., 2010 KSE DCP Dynamic Cone Penetrometers: K – 100 Models with Quick Connect Pin Users' Manual. Broadlands, VA: Kessler Soil Engineering Products, Inc.

Lewis, Gary and Veissman, Warren, 2003. Introduction to Hydrology: Fifth Edition. Upper Saddle River, NJ: Prentice Hall.

Lysne, Steve 2009. A Guide to Southern Idaho's Freshwater Mollusks. Idaho: U.S. Fish and Wildlife Service.

Marshak, S. and Mitra, G., 1989. Basic Methods of Structural Geology. Upper Saddle River, NJ: Prentice Hall.

National Ecological Observatory Network, 2012. National Ecological Observatory Network Website. < http://www.neoninfo.org > [29 Jun. 2012]

Pack, R.T., 1984. Debris Flow Initiation in Davis County, Utah, During the Spring Snowmelt Period of 1983. Proceedings of the 21st Engineering Geology and Soils Engineering Symposium. 59 – 77.

Rogers, David J. and Watkins, Conor, 2004. Landsliding and Channel Diversion at Fishtail Canyon. Missouri University of Science and Technology. < http://web.mst.edu/~rogersda/cp_megalandslides/fishtail_canyon.htm > [10 May 2012]

Solomon, Douglas, K., 2001. Water Levels Parleys 2000 - 2001. Microsoft Excel Spreadsheet. [21 Apr. 2012]

Solomon, Douglas, K., 2010. GEO 5350/6350 Assignment # 6: Red Butte Canyon Field Trip 2010 and Groundwater Map. Proprietary Assignments for GEO 5350/6350. Salt Lake City, UT: University of Utah.

Utah Automated Geographic Reference Center AGRC, 2006. Utah 2 meter LIDAR Data 2006. < http://gis.utah.gov/data/elevation-terrain-data/2-meter-lidar/ > [10 Oct. 2011]

Utah Field Station Network, 2009. Red Butte Canyon Natural Research Area. < http://www.utahfieldstations.org/stations/11-redbutte.html > [29 Jun. 2012].

Utah Geological Survey, 1996. The Wasatch Fault. Public Information Series 40. Salt Lake City, UT: Utah Geological Survey.

United States Geological Survey: Earth Resources and Observation Science EROS Center, 2012. Utah: High Resolution Orthoimagery. < http://earthexplorer.usgs.gov/ > [2012. 17 Feb 2011]

Wong, I. et al., 2002. Ground-Shaking Map for a Magnitude 7.0 Earthquake on the Wasatch Fault Salt Lake City, Utah Metropolitan Area. Public Information Series 76. Salt Lake City, UT: Utah Geological Survey.

Wright, S. and Duncan, M., 2005. Soil Strength and Slope Stability. Hoboken, NJ: John Wiley & Sons.